Dissertation
submitted to the
Combined Faculties for the Natural Sciences and for Mathematics
of the Ruperto-Carola University of Heidelberg, Germany
for the degree of
Doctor of Natural Sciences

presented by
M.Sc. Asrar Ali Khan
born in: Cuddapah (India)
Oral-examination: 03.02.16

Comparative secretome study of brown adipocytes and the role of ITIH4 in adipose biology

Referees:
PD Dr. Karin Müller-Decker
Prof. Dr. Stephan Herzig

Summary

Adipose tissues in mammals can be broadly classified into two main types: white and brown adipose tissue. Although both are defined as adipose tissues, they differ drastically in their function. The main function of white adipose tissues (WAT) is the storage of fat. Unlike its white counterpart, brown adipose tissue (BAT) specializes in burning fat via thermogenesis and is known to play an important role in non-shivering thermogenesis especially in hibernating animals and newborn babies. Recent evidence of functional BAT in adult humans and its ameliorating effect on metabolic disorders has brought BAT under the spotlight for treatment of metabolic diseases like obesity and type 2 diabetes mellitus.

WAT also acts as an endocrine organ by secreting signaling molecules called adipokines such as leptin and adiponectin. Adipokines constitute the secretome of WAT and not only play an important role in WAT function but also affect whole-body energy homeostasis. Various studies have investigated the role of adipose tissue secretome in metabolic disorders like obesity and insulin resistance. The WAT secretome has also been extensively characterized in various settings such as in whole WAT, mature white adipocyte etc. However, the BAT secretome and its adipokines (‘batokines’) have not yet been investigated.

Thus, the main aim of this dissertation work was a comparative study of the white and brown adipocyte secretomes using a combination of Click-iT® AHA labeling and pulsed-SILAC (stable isotope labeling by amino-acid in cell culture). In total 1013 proteins were detected and a subset of these proteins was selected based on their secretion with norepinephrine stimulation. An in vitro assay was developed and optimized to test their putative effect on insulin secretion. In addition, one of the secretome candidates, inter-alpha-trypsin inhibitor heavy chain H4 (ITIH4) was investigated as a potential batokine and BAT activity marker. Although, the serum levels of ITIH4 did not correlate with BAT activity under cold stimulation, its expression was found to increase with adipogenesis and browning of white adipocytes. Using in vitro knockdown studies, a reduction in differentiation was observed which was characterized by reduction in mature adipocyte functions such as lipolysis, lipid and intracellular triglyceride storage, glucose uptake and lipogenesis. Therefore, rather than being a batokine, ITIH4 was shown to be important for adipogenesis and adipocyte biology.

In summary, this dissertation sheds light on BAT secreted proteins and also introduces a new player in field of adipogenesis, both of which might have a significant impact in BAT biology and in the treatment of metabolic disorders like obesity.

Zusammenfassung

In Säugetieren existieren zwei Arten von Fett: das weiße und das braune Fettgewebe. Obwohl beide als Fettgewebe bezeichnet werden, gibt es bedeutende funktionelle Unterschiede. Während das weiße Fettgewebe (white adipose tissue, WAT) hauptsächlich eine Speicherfunktion besitzt, ist das braune Fettgewebe (brown adipose tissue, BAT) darauf spezialisiert, Energie zur Wärmegewinnung zu verbrauchen. Dieser Thermogenese genannte Prozess dient vor allem bei Säuglingen und Winterschläfern zur Regulation der Körpertemperatur. Neuere Erkenntnisse haben gezeigt, dass aktives BAT auch bei erwachsenen Menschen existiert. Sein Potential zur Steigerung des Energieumsatzes hat dieses Gewebe in den Fokus neuer Therapien gegen metabolische Erkrankungen wie Adipositas und Typ 2 Diabetes gestellt.

Neben seiner Speicherfunktion, fungiert WAT als endokrines Organ, welches sogenannte Adipokine sezerniert, die nicht nur lokal im Fettgewebe, sondern auch systemisch wirken. Bekannte Beispiele sind die Peptidhormone Leptin und Adiponektin. In ihrer Gesamtheit bilden die Adipokine das Sekretom des WAT. Während das WAT Sekretom auf der Ebene von Gewebe und einzelnen Adipozyten bereits gut untersucht ist, wurde das Sekretom des BAT und seine spezifischen Adipokine („Batokine“) bislang nicht systematisch analysiert.

Das Hauptziel der vorliegenden Arbeit war deshalb die Durchführung einer vergleichenden Studie der Sekretome von WAT und BAT. Mittels einer Kombination von Click-iT® AHA Markierung und Pulsed-SILAC (stable isotope labeling by amino-acid in cell culture) konnten insgesamt 1013 sezernierte Proteine nachgewiesen werden. Ein Teil davon wurde selektiv in Abhängigkeit von Noradrenalin-Stimulation sezerniert. Es wurde ein in vitro Assay entwickelt, um die Effekte der Sekretome auf die Insulinsekretion von Betazellen darzustellen. Der Noradrenalin-abhängig sezernierte Faktor inter-alpha-trypsin inhibitor heavy chain H4 (ITIH4) wurde als beispielhaftes Batokin und potentieller BAT Aktivitätsmarker eingehend untersucht. Obwohl die ITIH4 Serumlevel nicht mit der Aktivität des BAT nach Kälteexposition korrelierten, konnte gezeigt werden, dass seine Expression während der Adipogenese sowie des „browning“ von weißen Adipozyten gesteigert war. Adipozyten mit Knockdown von ITIH4 zeigten eine Reduktion typischer Fettzellfunktionen, wie beispielsweise Lipolyse, Einlagerung von Triglyzeriden und anderen Lipiden, Glukoseaufnahme und Lipogenese. Folglich kann ITIH4 eine wichtige Rolle in der Entwicklung und Funktion von Fettzellen zugewiesen werden, es scheint aber kein spezifisches Batokin zu sein.

Zusammengefasst, leistet die vorliegende Arbeit einen wichtigen Beitrag zum Verständnis des BAT als endokrines Organ und identifiziert eine neue Komponente in der Adipogenese. Beide Aspekte sind von enormer Bedeutung für das Verständnis der Biologie des BAT und können Ansatzpunkte für zukünftige Therapien gegen Adipositas und seine Folgeerkrankungen liefern.

Acknowledgements

First and foremost, I would like to thank Prof. Dr. Stephan Herzig for giving me the opportunity to carry out this dissertation in his lab. I am grateful for his constant support, guidance and mentorship. I would also like to thank Prof. Dr. Karin Müller-Decker for being my TAC member and 1st referee. In addition, I would like to thank Dr. Jeroen Krijgsveld (EMBL) for being my 3rd TAC member and also for collaborating with us for the secretome screen. I would also like to thank Dr. Jenny Hansson and Sophia Foehr from the Krijgsveld lab for performing the screen. This project would not have been possible without their help. I would also like to thank Prof. Dr. Rüdiger Hell and Prof. Dr. Peter Angel for accepting to be part of my defense committee.

My deepest thanks go to my colleagues and friends from the A170 lab for their support, helpful discussions, useful inputs and amiable working environment. I am grateful to Dr. Anke Sommerfeld for guiding and teaching me when I first started my PhD and for the useful inputs and discussions for my projects. I would also like to thank Dr. Mauricio Berriel Diaz for taking over this role and for his helpful input and discussions during our meetings. My gratitude goes to Dr. Tobias Schafmeier for his impeccable lab management, for translating the summary and for being one of the driving forces behind the DIABAT EU consortium. I would also like to thank Dr. Karin Mössenböck, Dr. Roldan Medina de Guia, Dr. Dasa Medrikova and Dr. Milen Kirilov for sharing their experimental samples with me. I am also very grateful for the constant professional and person support from Aishwarya Sundaram, Dr. Frits Mattijssen and Dr. Adriano Maida. I would also like to thank Carolina De La Torre, Maria Muciek and Dr. Carsten Sticht for performing and analyzing the microarrays. Very special thanks to Dr. Anja Krones-Herzig, Annika Zota and Daniela Sohn for ordering the mice and helping me with the adipose tissue isolations.

I cannot begin to express my gratitude to my friends who were responsible for some of my fondest memories in Heidelberg: Phivos - my brother; Reinhard – a true friend; Alex - my nutritional support; Oliver - my climbing partner; Elena, Milene and Joana - my muses. My deepest thanks to my pals from my masters and PhD program: Claudia, Teresa, Joschka, Katha, Daniel, Ivo, Irem, Krishna, Paula, Susi and Franzi for all the wonder times together. Thank you one and all. You all made life in Heidelberg an unforgettable experience.

Lastly, I would like express my deepest gratitude to my family without whose support I would not be where I am today. To Abrar, for inspiration and unwavering support and to Mum and Dad, for always believing in me and being there through the highs and lows. I owe it all and then some to you all.

“The only sovereign you can allow to rule you is reason.” – Terry Goodkind, *Faith of the Fallen*

Index

Introduction

Obesity and overweight

Obesity: the modern day pandemic

Obesity and overweight are defined as the excessive and harmful accumulation of fat. The WHO defines obesity in terms of the body mass index (BMI) which is the ratio of a person's weight to their height squared (kg/m^2). A BMI of 25 or greater is classified as overweight while a BMI of 30 or more is obesity. Since 1980 global obesity has doubled and currently most of the world's population lives in countries where obesity and overweight kills more people than underweight and malnutrition (Figure 1). A large number of children are also affected by this disease. In 2013, the WHO estimated that 42 million children globally under the age of 5 years were overweight and obese. Previously considered a 'disease of affluence', obesity is now also prevalent in developing countries with middle or low incomes especially in urban environments (WHO fact sheet 311, 2015).

The main cause of overweight and obesity is the perturbation of energy balance caused by an excessive amount of calories consumed relative to those expended (positive energy balance). This imbalance is becoming more prevalent due to the global increase in the consumption of high-calorie foods and the decrease in physical activity. Obesity is also associated with several severe co-morbidities like cardiovascular diseases (several heart diseases and stroke), diabetes, musculoskeletal diseases (like osteoarthritis), metabolic syndrome and cancer. Childhood obesity is a major risk factor for developing prediabetes (Li, Ford et al. 2009), bone and joint problems, breathing complications (Daniels, Arnett et al. 2005) and hypertension (Freedman, Mei et al. 2007). It also has a serious consequence in adulthood and contributes to increased predisposition to obesity and almost all the associated co-morbidities.

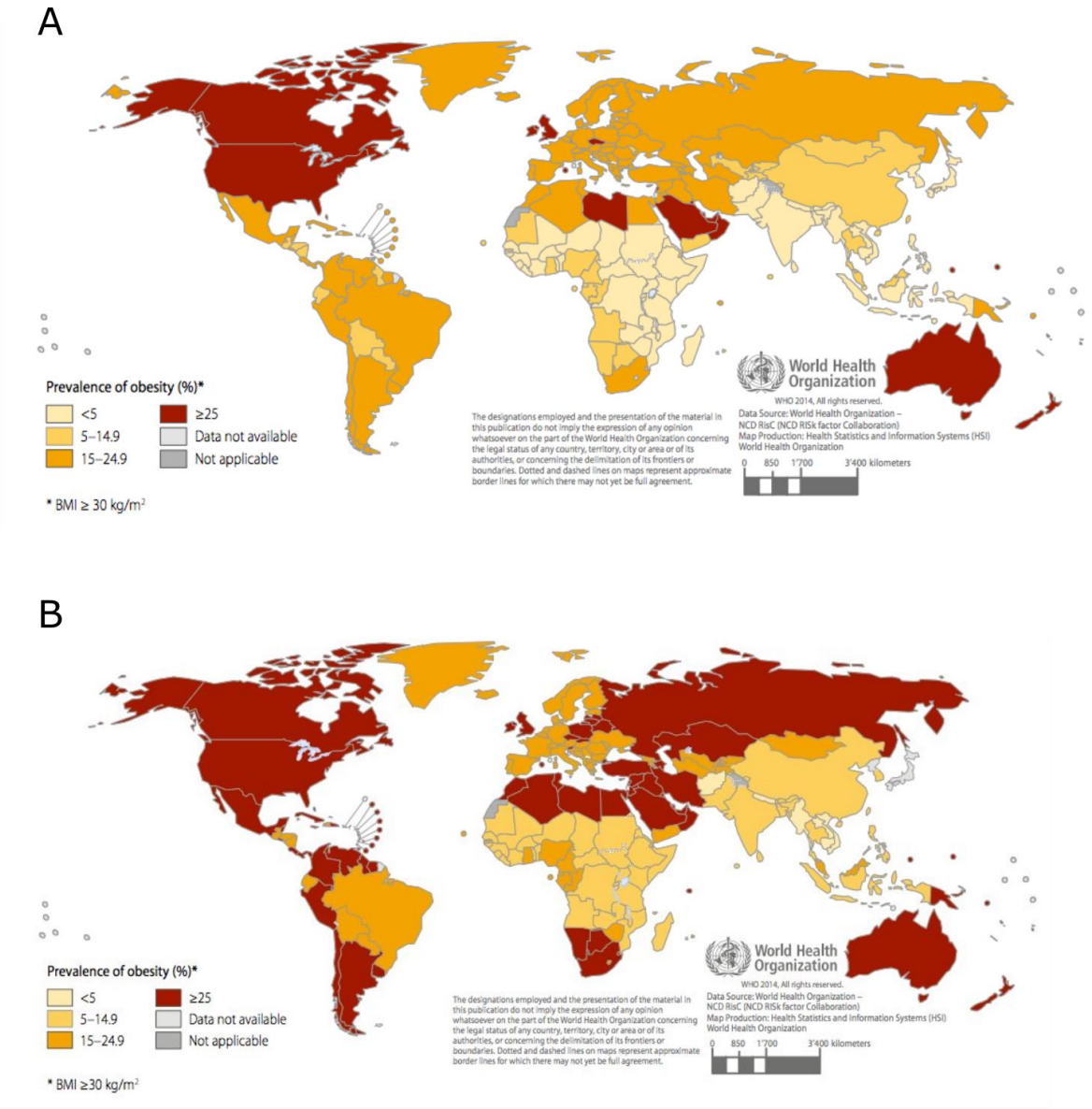

Figure 1: Prevalence of obesity worldwide. Age-standardized prevalence of obesity in men (A) and women (B) aged 18 and over (BMI>30 kg/m2), 2014. Figures obtained from the global status report on non-communicable diseases 2014. © Copyright World Health Organization (WHO), 2014.

Obesity and obesity-related co-morbidities

As mentioned earlier, obesity leads to a number of other metabolic disorders or co-morbidities. A systematic review by Guh, Zhang et al. (2009) identified 18 co-morbities associated with obesity. Statistically significant associations were identified by meta-analysis between obesity and type 2 diabetes, all cancers (with the exception of esophageal and prostate cancer), all cardiovascular diseases, asthma, gallbladder disease, osteoarthritis and chronic back pain.

Metabolic syndrome is a combination of disorders consisting of insulin resistance, obesity, low-grade pro-inflammatory state, hypertension and dyslipidemia (Alberti, Zimmet et al. 2006). Metabolic syndrome in turn further increases the risk of cardiovascular diseases and type 2 diabetes in addition to other disorders like thrombophilia, non-alcoholic fatty liver disease and reproductive disorders (Cornier, Dabelea et al. 2008).

The insulin resistance observed in obesity is generally a consequence of nutritional overload. During nutritional overload, adipose tissue dysfunction occurs which leads to the accumulation of fat in other organs and the release of harmful pro-inflammatory factors (discussed in next section). Both these events lead to obesity-related systemic insulin resistance (Sethi and Vidal-Puig 2007).

Obesity leads to hypertension due to an increase in total blood volume and cardiac output. In general, cardiac workload is higher in obesity which makes obese patients hypertensive (Messerli, Ventura et al. 1982). Wong and Marwick (2007) suggested the existence of a cardiomyopathy of obesity supported by experimental models and epidemiological and clinical studies. The myocardial changes observed in obesity cardiomyopathy cannot be attributed to diabetes, hypertension or coronary heart disease alone and can be considered a direct consequence of obesity. These myocardial changes affect ventricular structures as well as systolic and diastolic function.

The high metabolic and inflammatory environment of obesity is one of the main reasons for the development of osteoarthritis. Adipose-derived pro-inflammatory cytokines affecting joint degradation and local inflammatory processes are another factor in the development of obesity-related osteoarthritis. In addition, obesity-related perturbations in glucose and lipid metabolism and mechanical loads (that activate mechanoreceptors on chondrocytes) are other reasons for the development of osteoarthritis (As reviewed by Sowers and Karvonen-Gutierrez 2010).

Similar to insulin resistance, adipocyte dysfunction is also one of the reasons behind obesity-related carcinogenesis. The insulin resistance, increased levels of secreted factors like leptin and endogenous sex steroids and chronic inflammation caused by obesity promote carcinogenesis and cancer progression by either having a growth-promoting effect on cancer cells or/and by inhibiting apoptosis. For example, the mitogenic and anti-

apoptotic properties of IGF-1, insulin and leptin have shown to promote carcinogenesis (Pollak, Schernhammer et al. 2004, Hoda, Keely et al. 2007).

Therefore, adipose tissue and its dysfunction contribute to the development of obesity and its related disorders and are important facets in the struggle against the global obesity pandemic.

Adipose tissues

Different shades of adipose tissues

There are two main types of adipose tissues in mammals: white and brown (Table 1). White adipose tissue (WAT) is the classical fat storage organ. It has important immune and endocrine functions and also provides thermal insulation and mechanical protection to internal organs. Brown adipose tissue (BAT) on the other hand is adept in burning fuel reserves to produce heat and modulate body temperature through non-shivering thermogenesis. This is accomplished by uncoupling protein 1 (UCP1) that uncouples ATP production from the mitochondrial electrochemical gradient and generates heat. The presence of UCP1 is a defining feature of BAT. Both, white and brown adipose tissues play a vital role in maintaining whole body energy homeostasis and regulating insulin sensitivity and are important for health. For example, disruption of normal white adipose tissue function is associated with insulin resistance (Rosen and Spiegelman 2006) and on the other hand, activation of brown adipose tissue improves insulin sensitivity and weight loss (Cypess, Lehman et al. 2009).

Table 1: Characteristics of white and brown adipose tissues. Adapted and modified form Saely, Geiger et al. (2012)

	White adipose tissue	**Brown adipose tissue**
Function	Energy storage.	Heat production (thermogenesis).
Morphology	Single large lipid droplet, variable amount of mitochondria.	Multilocular lipid droplets, high number of mitochondria.
Development	From Myf5-negative progenitor cells.	From Myf5-positive progenitor cells (some Myf5-negative brown fat cells which are derived from other lineages also exist).
Human data	Large amounts and dysfunction are associated with increased risk of obesity-related disorders.	Large amounts are associated with decreased risk of obesity-related disorders.
Impact of aging on fat mass	Increases with age relative to total body weight.	Decreases with age.

One of the pivotal discoveries in the field of adipose tissue biology was the detection of functional brown adipose tissue in adult humans (Nedergaard, Bengtsson et al. 2007). Until this discovery, BAT was only thought to be present in human infants where it contributed to non-shivering thermogenesis. Morphologically, brown adipocytes differ from white adipocytes by having smaller multilocular lipid droplets (in contrast to a large unilocular lipid droplet in white adipocytes) and higher number and larger mitochondria (Cinti 2002). The large number of mitochondria confers the darker brown color to these adipocytes.

Adipocyte differentiation or adipogenesis for both white and brown adipocytes consists of first commitment to a preadipocyte lineage and subsequent differentiation. The

white and brown adipocytes arise from different mesenchymal precursor cells: Myf5-negative, for white adipocytes and Myf5-positive (myogenic precursor) for brown adipocytes. Despite their different developmental origins, both white and brown adipocytes share some common core adipogenic components like the transcription factor peroxisome proliferator-activated receptor gamma (PPARγ), CCAAT/enhancer-binding proteins (C/EBPs) like C/EBPα, C/EBPβ and C/EBPδ and bone morphogenic proteins (BMPs) (Farmer 2006). Other adipogenic factors are unique to brown adipocyte differentiation. These include PR domain–containing protein-16 (PRDM16) that induces brown adipocyte specific gene induction (Seale, Kajimura et al. 2007) and peroxisome proliferator–activated receptor γ-coactivator-1α (PGC-1α) (Puigserver, Wu et al. 1998) that regulates oxidative metabolism, mitochondrial biogenesis and thermogenesis (As reviewed by Lin, Handschin et al. 2005).

As mentioned earlier, UCP1 is responsible for BAT thermogenesis. There are several different means by which the thermogenic program, and in turn UCP1, can be activated in BAT (As reviewed by Villarroya and Vidal-Puig 2013). The most well characterized activation of BAT is via the sympathetic nervous system (SNS) in response to thermogenic stimuli. In this case norepinephrine binds to adrenergic receptors and activates protein kinase A (PKA). PKA in turn activates p38 MAP kinase and thyroxine 5'-dediodinase (5'-D), ultimately leading to the induction of the thermogenic genes. The liver can also activate BAT via the release of bile acids and fibroblast growth factor 21 (FGF21) that interact with TGR5 receptors and FGF receptor/b-Klotho (KLB) complexes respectively. On the other hand, natriuretic peptides (NPs) released by the heart activate BAT via interaction with NP receptors (NPRs) and activation of protein kinase G and p38 MAP kinase.

In addition to brown and white adipocytes, a third type of adipocytes called 'beige' or 'brite' adipocytes are also present (Loncar 1991). These cells are brown-like adipocytes in white adipose tissues and resemble white adipocytes in their basal characteristics and origin but upregulate the expression of UCP1 upon cAMP stimulation (Wu, Bostrom et al. 2012). This phenomenon is called 'browning'. There are several mediators of browning known like COX2, SIRT1, BMP7, Irisin etc. but all of them act via three core transcriptional regulators: PPARγ, PRDM16 and PGC-1α (As reviewed by Lo and Sun 2013). All browning agents known so far bind, interact, activate or inhibit these core factors. The most commonly used browning agents for *in vitro* studies are rosiglitazone (a PPARγ agonist) and carbaprostacyclin or $cPGI_2$ (a stable analog of PGI_2 that also activates PPARγ). The browning process and brite adipocytes are important in combating obesity as mouse strains with a higher predisposition to browning show a lower tendency for becoming obese and vice versa (Guerra, Koza et al. 1998). In addition, it is also speculated that browning increases the plasticity of the white adipose depots by allowing a functional switch from energy storage to energy consumption (Wu, Cohen et al. 2013).

Although brite adipocytes are functionally similar to classical brown adipocytes, there are a few key differences that set them apart. They are formed from Myf5-negative

precursor cells (Seale, Bjork et al. 2008) and also have distinct gene signature profiles compared to brown adipocytes (Wu, Bostrom et al. 2012). Moreover, the expression of *Ucp1* and other thermogenic genes is upregulated upon activation in brite adipocytes (for example with β-adrenergic receptor agonists) while brown adipocytes express high levels of these genes at the basal conditions.

Adipose tissue in health and disease

Adipose tissues play a very important role in metabolic health. WAT is crucial for the maintenance of normal glucose and serum triglyceride levels and insulin sensitivity. Mice lacking WAT were found to suffer from severe metabolic abnormalities like insulin resistance, hyperglycemia, hyperlipidemia and fatty liver (Gavrilova, Marcus-Samuels et al. 2000). BAT, due to its thermogenic capacity, is a promising candidate for counter-acting nutrient overload, obesity and diabetes. In humans, the activity of BAT inversely correlates with adiposity and the activation of BAT clears glucose at a systemic level thereby improving insulin sensitivity (Orava, Nuutila et al. 2011). In addition, it has been shown that BAT in mice can also clear triglyceride rich proteins from circulation and reduce hyperlipidemia (Bartelt, Bruns et al. 2011). It is estimated that BAT in humans could contribute as much as 20% daily energy expenditure (Stock and Rothwell 1983). In a recent review, Betz and Enerback (2015) have highlighted the importance of human BAT in diabetes and obesity as well as the possibility of BAT being a potential drug target to treat these maladies.

Dysfunctional adipose tissues are now considered one of the main contributing factors to obesity and obesity-related metabolic disorders like the metabolic syndrome, type 2 diabetes and cardiovascular diseases (Goossens 2008, Bluher 2013). A positive energy balance, wherein the amount of calories ingested is higher than required, leads to obesity and increase in adipocyte size (hypertrophy). This leads to adipocyte dysfunction when the hypertrophic adipocytes are limited in their expansion due to factors like hypoxia and extracellular matrix (ECM) mechanics. Adipocyte dysfunction disrupts normal adipose tissue lipid metabolism and leads to release of pro-inflammatory factors (called adipokines, discussed in the next section). These factors not only impair adipocyte differentiation but also increase the infiltration of immune cells into the adipose tissue which further exacerbates the inflammation. In addition to changes in lipid metabolism and release of pro-inflammatory secreted factors, adipose tissue dysfunction also leads to spillover of lipids in to the circulation and subsequent accumulation in to other non-adipose organs like liver and muscle (Figure 2). This ectopic fat storage is thought to lead to lipotoxicity and causes low-grade systemic inflammation thereby accelerating the development of obesity and related metabolic disorders (Goossens 2008).

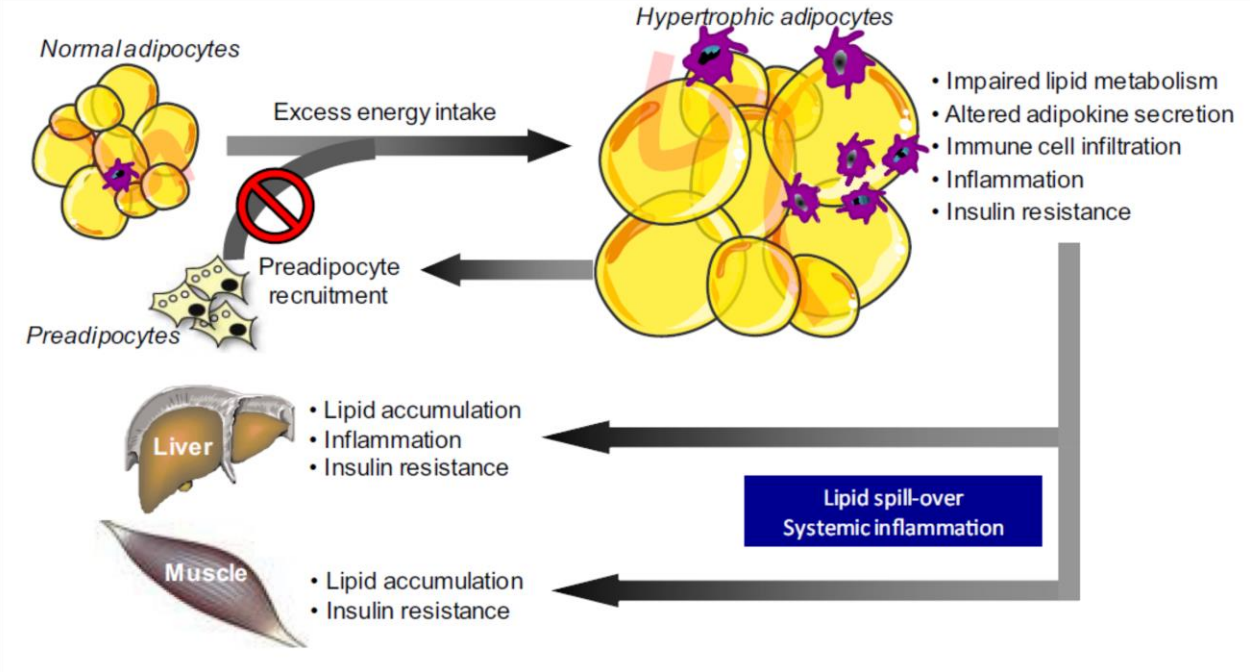

Figure 2*:* The dysfunction of adipose tissues and consequence on metabolic health. A positive-energy balance because of excess energy intake leads to hypertrophic adipocytes. This impairs adipose tissue function and causes lipid spill-over and increased release of pro-inflammatory cytokines. Subsequently, this leads to ectopic lipid accumulation in other organs and low-grade systemic inflammation. Adapted from Goossens (2008).

Adipose tissue as an endocrine organ.

As mentioned before, white adipose tissues are the primary site for fat storage in the body. They mobilize these stored fats to meet the energy demands of the body. Owing to recent advancement in obesity research, it is now widely appreciated now that white adipose tissues are also endocrine organs and secrete a wide range of hormones and signaling factors called adipokines.

Some of the important adipokines are chemokines that are closely related to adipose tissue inflammation. As mentioned in the previous section, changes in the production of these adipokines occur because of the expansion and subsequent dysfunction of adipose tissues during obesity. TNF-α, a pro-inflammatory cytokine, was the first adipokine to be described (Hotamisligil, Shargill et al. 1993). Apart from being expressed in adipocytes, TNF-α is also expressed in macrophages. Similar to TNF-α, interleukin-6 (IL-6) is also an important adipokine secreted by adipocytes and skeletal muscle (Keller, Keller et al. 2003). Another pro-inflammatory cytokine is monocyte chemotactic protein 1 (MCP-1) that plays a role in macrophage recruitment to the adipose tissue (Sartipy and Loskutoff 2003).

In addition, there are adipokines that are solely produced by adipocytes. Leptin is one such important adipokine controlling satiety and body weight (Fruhbeck 2002).

Adiponectin is another adipocyte-derived adipokine that influences insulin sensitivity and exhibits anti-inflammatory properties (Yamauchi, Kamon et al. 2001).

Adipokines are important mediators of organ cross-talk between white adipose tissues and different organs of the body like the brain, muscles, liver etc. They can also act in an autocrine or paracrine manner and influence energy homeostasis, insulin sensitivity and the immune system (Figure 3). Thus, via adipokines, white adipose tissues not only control their own metabolism but also affect the systemic metabolism by acting on other organs. Due to their important role in metabolic health, several adipokines have been implicated in the pathogenesis of metabolic disorders like obesity and type 2 diabetes. Some of the important adipokines are described in the next section.

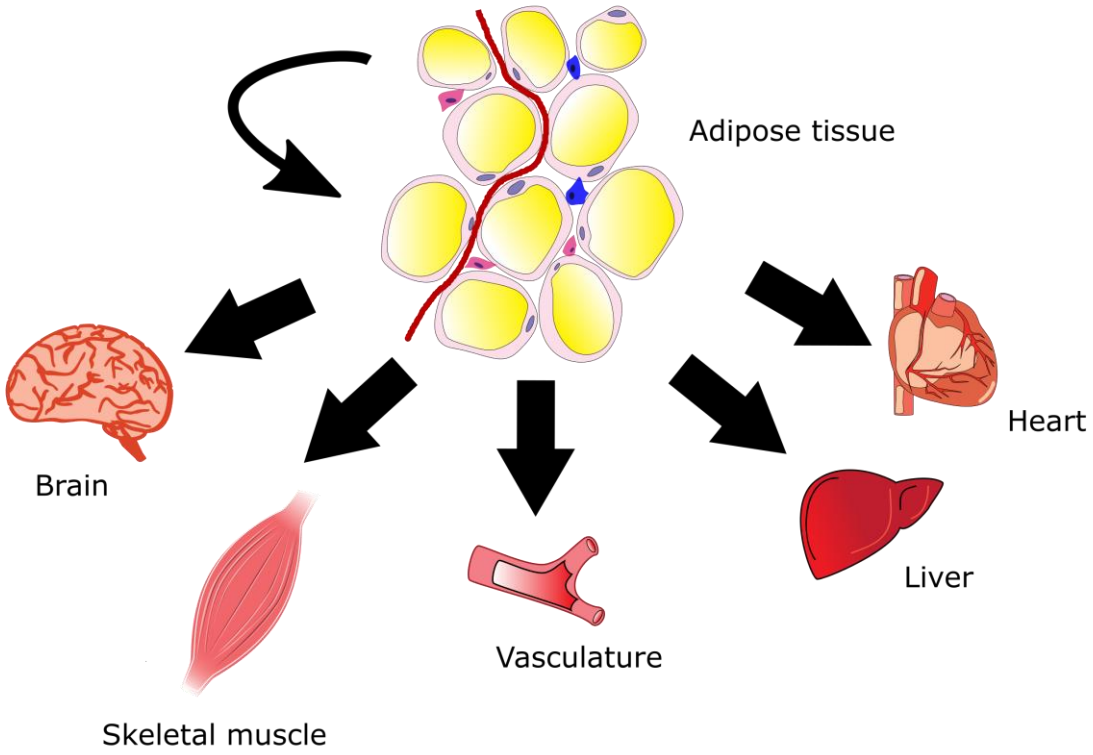

Figure 3: Adipose tissue and multi-organ cross talk. Adipose tissues secrete factors called adipokines that act in an autocrine, paracrine and endocrine manner affecting various different organs. Via adipokines, adipose tissues are able to influence important systemic attributes like systemic insulin sensitivity, energy homeostasis, inflammation and the immune system.

Overview of some important adipokines

Leptin

Leptin is a 16 kDa peptide hormone produced by adipocytes, encoded by the obese (*ob*) gene in mice and *LEP* gene in humans. Circulating plasma levels of leptin correlate with adiposity (i.e. white adipose tissue mass). The main function of leptin is to increase energy expenditure and decrease food intake by acting on distinct neural cell populations in the hypothalamus. However, leptin is also considered to be a 'pleiotropic' hormone because of its involvement in a variety of different functions like angiogenesis, reproduction, cytokine production, phagocytosis etc. (Fietta 2005).

The receptor for leptin is encoded by the diabetes gene (*db*) which is a class I cytokine receptor. It is subjected to alternative splicing and gives rise to six different isoforms out of which only the Ob-Rb (long form) participates in signal transduction. The extracellular leptin signal is received by this isoform and in turn activates the JAK-STAT pathway (Fruhbeck 2006). The most common mutations affect the tyrosine residue Y1138 on the intracellular domain of Ob-Rb in mice, preventing STAT3 activation. However, such mutations occur rarely in humans (Farooqi and O'Rahilly 2006).

Ob/ob and *db/db* mice exhibit a host of different metabolic phenotypes like increased body weight due to increased adiposity and hyperphagia, lower energy expenditure, hyperglycemia, hyperinsulinemia and dyslipidemia (Campfield 2000). Obesity, independent of mutations in leptin or its receptor, is usually characterized with partial leptin resistance and hyperleptinemia. In leptin resistance, the high levels of leptin are not able to modulate energy homeostasis which results in excessive weight gain and development of metabolic diseases like type 2 diabetes mellitus. Selectivity is another aspect of leptin resistance. The concept of selective leptin resistance describes the phenomenon of leptin resistance with intact leptin sympathoexcitatory functions like its effect on arterial blood pressure but resistance to its metabolic functions like satiety and weight reduction. (Mark, Correia et al. 2002). Hyperleptinemia on the other hand is sometimes considered a consequence of aging, unrelated to changes in fat mass and suggested to play a causative role in age-related metabolic decline (Gabriely, Ma et al. 2002, Ma, Muzumdar et al. 2002).

Adiponectin

Adiponectin (also called apM1, Acrp30, GBP28, and AdipoQ) is a 30 kDa protein produced in mature adipocytes. Adiponectin is structurally similar to collagen VIII and X. It makes up

0.01% of the total plasma protein and circulates in the blood in its oligomeric forms, which include its multimeric (high molecular weight, HMW), hexameric (middle molecular weight, MMW) and trimeric (low molecular weight, LMW) isoforms.

Unlike other adipokines, adiponectin is the only known adipokine that is reduced during obesity and has an insulin sensitizing effect. Low levels of plasma adiponectin are indicative of insulin resistance and diabetes (Tschritter, Fritsche et al. 2003). Adiponectin acts in an autocrine/paracrine manner within the adipose tissues and has been shown to regulate pro-inflammatory adipokine secretion in human adipocytes thereby preventing insulin resistance (Dietze-Schroeder, Sell et al. 2005). In addition, over-expression of human adiponectin in Apolipoprotein E-deficient mice, a mouse model that spontaneously develops atherosclerotic lesions on a standard chow diet, suppresses the development of atherosclerosis. (Okamoto, Kihara et al. 2002).

Adiponectin acts via two receptors: AdipoR1 (skeletal muscle) and AdipoR2 (liver). Adiponectin signaling involves AMPK, PPAR α and PPAR γ. The stimulation of AdipoR2 leads to increased β-oxidation and reduced gluconeogenesis in liver while in skeletal muscle, AdipoR1 signaling leads to increased β-oxidation and glucose uptake. This leads to lowering of blood glucose, increased insulin sensitivity and reduced fat content in tissues

The most widely characterized effects of adiponectin include the improvement in insulin sensitivity and its anti-inflammatory and anti-atherosclerotic properties. The insulin sensitizing effect of adiponectin is due to the activation of AMPK which increases glucose uptake, glycolysis and fatty acid oxidation. Another mechanism through which adiponectin reduces inflammation is by promoting phagocytosis of early apoptotic cells by macrophages (Takemura, Ouchi et al. 2007). Adiponectin reduces atherosclerosis by protecting the vascular endothelium against inflammation (Kadowaki and Yamauchi 2005), reducing monocyte adhesion to the endothelium and lowering NFκB levels (Tan, Xu et al. 2004).

In contrast to leptin, there is an inverse relationship of fat mass and adiponectin levels. Increased visceral adiposity decreases adiponectin levels more strongly than subcutaneous adiposity. Adiponectin gene expression is also inhibited by pro-inflammatory cytokines like TNF-α and IL-6 (Bruun, Lihn et al. 2003). Insulin reduces the expression of the adiponectin receptors and leads to a state of adiponectin resistance during hyperinsulinemia (Kadowaki and Yamauchi 2005). Hypoadiponectinemia has been linked to insulin resistance, type 2 diabetes and cardiovascular complications like hypertension, progressive ventricular hypertrophy and diastolic dysfunction and therefore, considered an independent risk factor in the development of cardiovascular and metabolic abnormalities.

Resistin

Resistin is a cysteine-rich protein that is secreted as a dimer. It was discovered while screening for genes that were downregulated in mouse 3T3-L1 adipocytes by thiazolidinedione (TZD) drugs like rosiglitazone (Steppan, Bailey et al. 2001). Resistin is mainly expressed in murine white adipocytes but in humans, it is expressed in macrophages and is induced by TNF-α (Patel, Buckels et al. 2003).

Neither the receptor nor the signaling pathway for resistin has been discovered yet. In mice, resistin inhibits AMPK in liver, skeletal muscle and WAT. It has also been shown to be an important factor in the development of hepatic insulin resistance in high fat diet (HFD) fed mice (Muse, Obici et al. 2004). In addition, resistin also inhibits insulin secretion by inducing the expression of SOCS-3 both *in vitro* and *in vivo* (Steppan, Wang et al. 2005).

Resistin has been extensively studied in rodent models (Summarized by Lazar 2007). Resistin secretion is similar to leptin i.e. levels increase with adiposity and after feeding. High levels of resistin contribute to the development of insulin resistance and type 2 diabetes. Moreover, resistin has a pro-inflammatory effect and stimulates macrophages to release pro-inflammatory cytokines. It also upregulates vascular adhesion molecules like VCAM-1 and ICAM-1 in mice and human endothelial cells. There is also a direct correlation between serum resistin levels and atherosclerosis in humans.

Adipokines in obesity and related disorders

During obesity several pro-inflammatory factors are released by the adipose tissue. These factors include TNF-α, IL-6, MCP-1 and TGF-β1 (Hotamisligil, Shargill et al. 1993, Samad, Yamamoto et al. 1997, Sartipy and Loskutoff 2003). Macrophage infiltration also increases in obesity and leads to the increased circulating and local levels of these pro-inflammatory cytokines. The local adipose tissue expression of both TNF-α and IL-6 were also shown to be higher in patients with obesity-related insulin resistance (Kern, Ranganathan et al. 2001). TNF-α mostly exerts its influence in an autocrine and paracrine manner while the effect of IL-6 is more systemic (endocrine). Both cytokines increase lipolysis and fatty acid oxidation in adipocytes and increase the fatty acids in the blood. As mentioned earlier, this leads to ectopic fat deposition in other organs. It has also been shown that IL-6 can cause hepatic insulin resistance in mice by inhibiting early insulin receptor signaling and downstream insulin action (Klover, Zimmers et al. 2003). Interestingly, it has also been shown that the increase in expression of these cytokines precedes a rise in insulin secretion in obese mice

(Xu, Barnes et al. 2003). This points to the fact that adipose tissue inflammation is an important antecedent to obesity-related insulin resistance.

BAT as an endocrine organ

In relation to its white counterpart, BAT and its role as an endocrine organ has not been extensively studied. It is well documented that the activation of BAT (for example, by cold stimulation) leads to systemic metabolic changes in the body. These changes include decreased blood glucose and increased insulin sensitivity (Bukowiecki 1989). BAT partly contributes to this by an increased glucose uptake and improved insulin sensitivity (Gasparetti, de Souza et al. 2003). WAT and skeletal muscle also increase their catabolic processes (such as lipolysis in WAT) to provide fuel for BAT thermogenesis (Gasparetti, de Souza et al. 2003). These observations beg the question as to whether BAT has an important endocrine function beyond its role in thermogenesis. Another important observation that supports this idea is that mice completely lacking BAT (Lowell, V et al. 1993) were metabolically worse off than mice only deficient in UCP1 and lacking their thermogenic capacity (Enerback, Jacobsson et al. 1997). These studies suggest that BAT can affect whole-body energy homeostasis by UCP1-independent mechanisms.

Adipokines from BAT ('batokines') can be assumed to have the following characteristics: they might have different actions or effects compared to WAT adipokines, their target organs would be different from conventional adipokines and lastly, they would be released upon BAT activation (Villarroya, Cereijo et al. 2013). Recent studies in mice and rats have helped identify several paracrine and autocrine factors released by BAT. Some of them include vascular endothelial growth factor-A (VEGF-A), insulin-like growth factor I (IGF-I), fibroblast growth factor-2 (FGF2), IL-6 and bone morphogenetic protein-8b (BMP8b). These factors have varied functions like promoting angiogenesis (VEGF-A) to increasing sensitivity to noradrenergic stimuli (BMP8a) (As reviewed by Villarroya, Cereijo et al. 2013).

Apart from these paracrine and autocrine factors, there are very few endocrine factors shown to be released from BAT. One of the earliest examples of BAT's endocrine role was triiodinthyronine (T_3) (Silva and Larsen 1983). It is considered a classical BAT endocrine product and has been shown via tracer studies that activated BAT is a major source of T_3 in the body (Silva and Larsen 1985). Another important and well-documented endocrine factor released by BAT is the fibroblast growth factor 21 (FGF21) (Hondares, Iglesias et al. 2011). FGF21 increases glucose oxidation in several tissues and has shown to be protective against obesity and type 2 diabetes (Sarruf, Thaler et al. 2010). Normally, liver is the prime source of FGF21 but upon thermogenic activation BAT contributes to circulating FGF21 levels (Hondares, Iglesias et al. 2011). Studies using BAT transplantation have also shown that FGF21 levels are increased after transplantation and FGF21 could be a major factor in the metabolic improvement seen in transplant-recipient mice (Stanford, Middelbeek et al. 2013). In addition, FGF21 can pass the blood-brain barrier reaffirming the idea that certain

batokines can act on the central nervous system. Lastly, FGF21 has also been shown to be expressed in brite/beige adipocytes, both in mice and humans (Wu, Bostrom et al. 2012, Lee, Werner et al. 2014). The most recent endocrine factor found to be enriched in BAT is neuregulin4 (Nrg4). The expression of Nrg4 was found to increase with brown adipocyte differentiation, adrenergic stimuli and acute cold exposure. Using binding assays on frozen tissue sections, Nrg4 was found to bind to liver most likely through direct binding of its ErbB receptors and reduce *de novo* lipogenesis (Wang, Zhao et al. 2014).

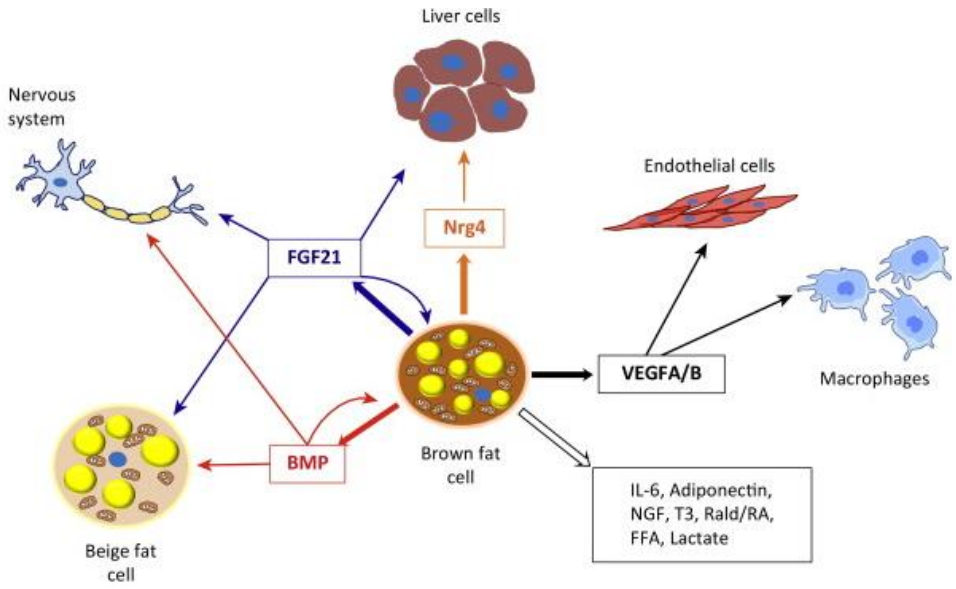

Figure 4: Adipokines released from BAT. Apart from its role in non-shivering thermogenesis, BAT is also known to release its own set of adipokines. Albeit not as extensive as its white counterpart, these adipokines have various different target organs like liver, nervous system, WAT, endothelial cells and immune cells. They also exhibit a wide spectrum of functions like affecting hepatic metabolism, browning of WAT, angiogenesis, sensitization to sympathetic stimuli etc. Abbreviations: BAT, brown adipose tissue; BMP: bone morphogenetic protein, EGF, epidermal growth factor; ErbB, epidermal growth factor receptor; FFA, free fatty acid; FGF, fibroblast growth factor; IL, interleukin; NGF, nerve growth factor; Nrg, neuregulin; RA, retinoic acid; Rald, retinaldehyde; VEGF, vascular endothelial growth factor. Adapted from Wang, Zhao et al. (2015).

Thus, it can be appreciated that BAT possesses an endocrine role in regulating whole-body metabolism (Figure 4). However, further work is needed to uncover the different players in BAT endocrine function. In this direction, a high-throughput screening approach could be vital in identifying several novel batokines.

Aim of the study

The overall aim of this doctoral project was to investigate the secretome of primary brown adipocytes using a high-throughput screening approach involving mass spectroscopy and define the impact of individual mediators on BAT function.

The project is divided into two main parts. The first part comprises the comparative study of the white and brown primary adipocyte secretomes and secretomes from norepinephrine-stimulated and unstimulated primary brown adipocytes. We hypothesized that secreted candidates from the secretome screens can improve the insulin secretion from beta-cells. The optimization of a glucose-stimulated insulin secretion (GSIS) assay was carried out to test this hypothesis. The second part consists of investigating the role of inter-alpha-trypsin inhibitor heavy chain family, member 4 (ITIH4), a candidate obtained from the secretome screening, as a batokine or BAT activity marker and its role in adipocyte biology and differentiation.

Results

Brown adipocyte secretome study

Secretome analysis of adipocytes in complete culture media

A comparative secretome study was carried out to study the secretome of primary brown adipocytes by following the technique described by Eichelbaum, Winter et al. (2012). Briefly, the study technique was a combination of two metabolic pulse labeling methods: Click-iT® AHA labeling (Figure 5A) and stable isotope labeling with amino acids in cell culture (SILAC) (Figure 5B). The Click-iT® AHA labeling involved labeling a cell population with an azide bearing analog of methionine called L-azidohomoalanine (AHA). Labeling with AHA allowed the enrichment (by selective and covalent capture) of newly synthesized AHA-containing proteins using an alkyne-activated resin via click chemistry. A pulsed SILAC on the other hand was used to compare the proteome of two different cell types labeled with either 'intermediate' or 'heavy' labeled arginine and lysine. The resultant secreted proteome obtained by the combination of these two techniques was then qualitatively analyzed using mass spectroscopy (Figure 5B).

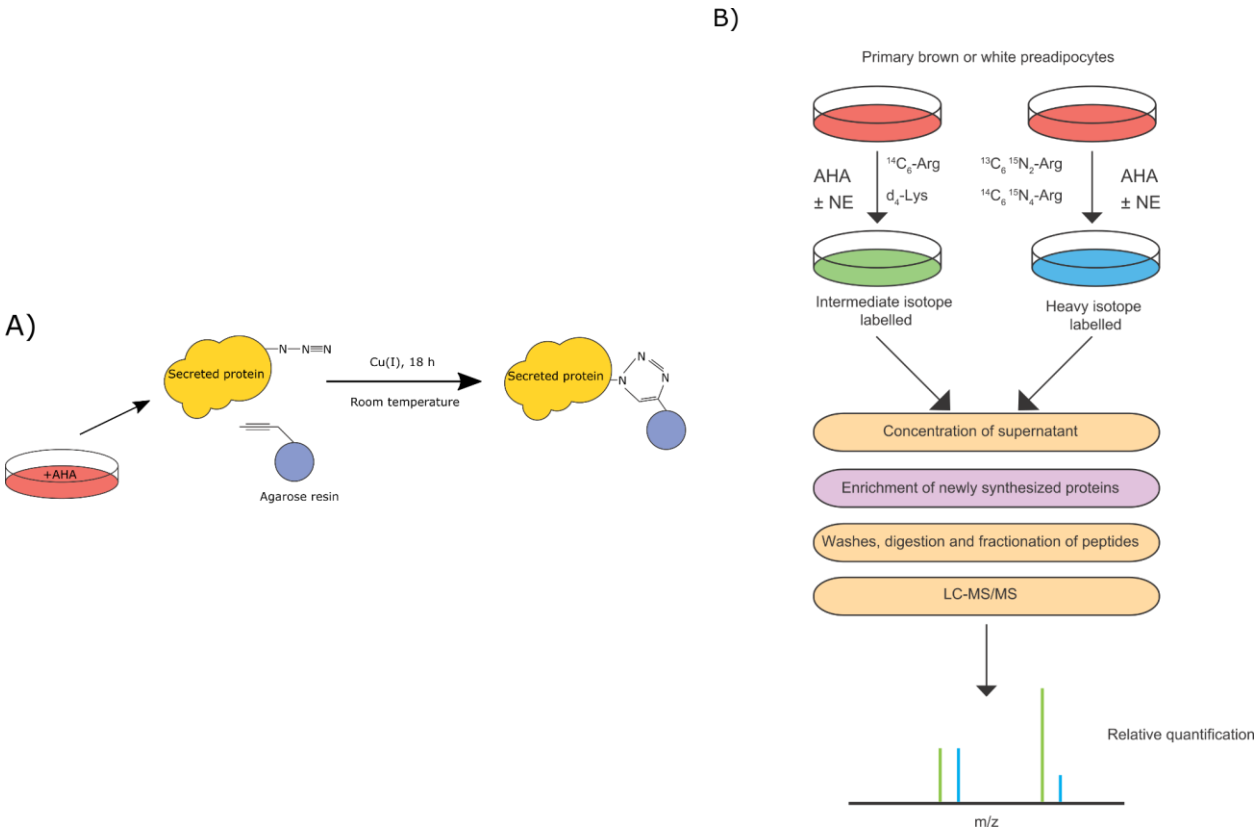

Figure 5: Click-iT® AHA principle and secretome analysis workflow. (A) The desired monolayer culture was incubated with appropriate media (lacking methionine) supplemented with L-Azidohomoalanine (AHA). After an appropriate period of incubation, the media was collected and the newly synthesized secreted proteins were bound to an agarose resin. After washing the resin, the proteins were released from the resin by trypsin digestion. (B) The secretome analysis workflow started with a traditional SILAC setup where two cell populations were incubated with intermediate and heavy isotope labeled amino acids (lysine and arginine). In addition, the cells were incubated with AHA and NE (if stimulation was required). After incubation, the supernatants were collected and the secreted proteins were fished out and enriched using the Click-iT® AHA principle described above. Next, the secreted proteins were washed, digested fractionated and analyzed in a LC-MS/MS setup to obtain a qualitative comparison. The enrichment and LC-MS/MS were carried out in the lab of Dr. Jeroen Krijgsveld (EMBL).

Optimum incubation time with SILAC-Met media was 24 hours

The effect of AHA on cell viability and the optimum secretion of adipokines from primary adipocytes was investigated before the secretome screening. For determining the cytotoxicity of AHA supplemented SILAC-Met media, primary inguinal white and brown preadipocytes from the SVF of C57BL/6J 8 weeks old male mice were differentiated until day 08 and then incubated with either AHA-supplemented, methionine-supplemented, normal

DMEM or methionine-deficient SILAC-Met media for 6, 24 and 48 hours. After the incubation the amount of LDH released was measured in the supernatant. The LDH released was an indication of the amount of cell death. In addition to the cytotoxicity of the SILAC-Met media, the optimum incubation time for maximal detection of secreted adipokines was also determined. To accomplish this, leptin and resistin were detected in the supernatant of primary inguinal white and brown adipocytes after different time points using the MILLIPLEX® MAP Mouse Metabolic Hormone panel on the Luminex xMAP® platform (MAGPIX®).

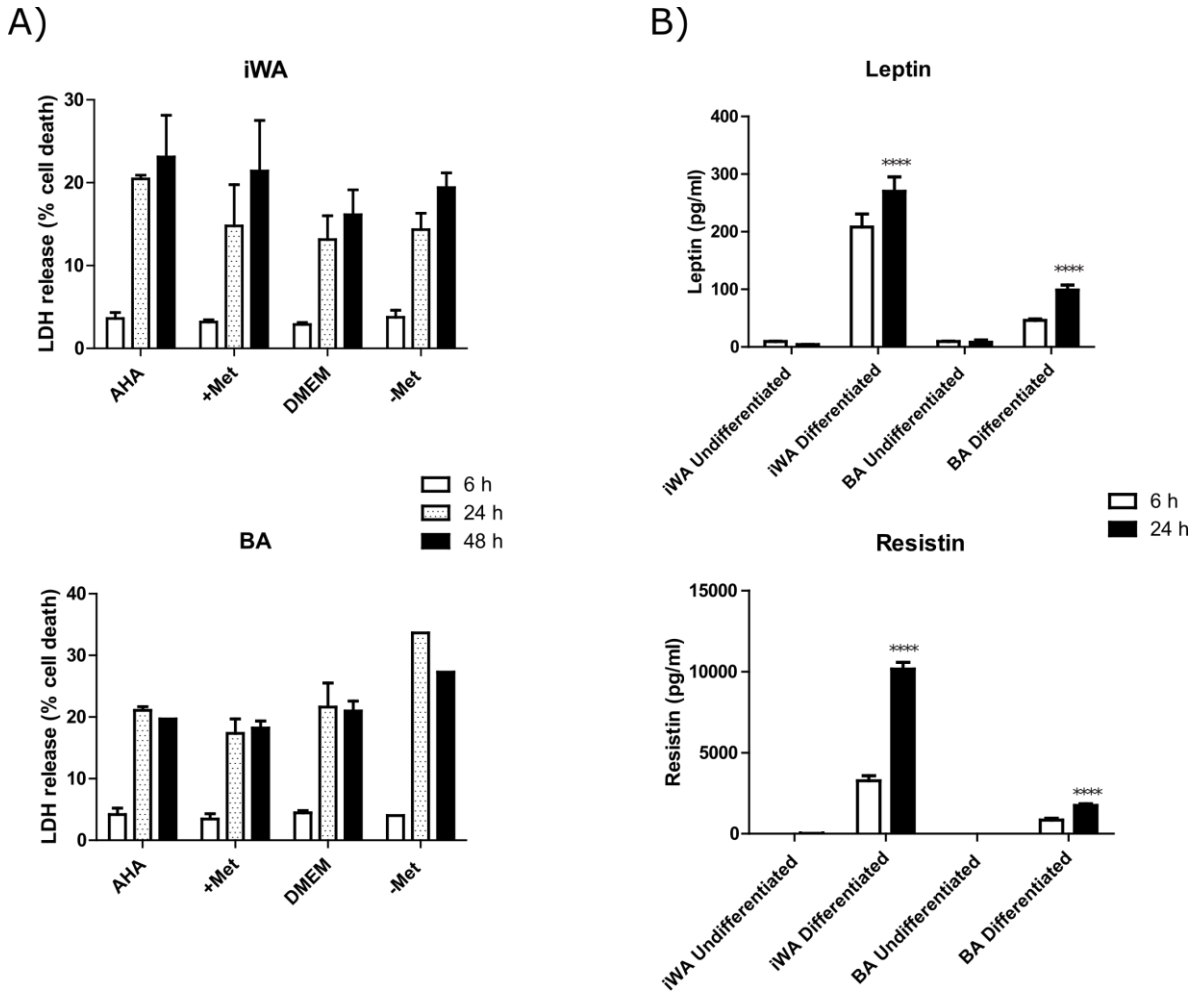

Figure 6: Optimization of secretome conditions. Primary inguinal white and brown adipocytes from the SVF of C57BL/6J 8 weeks old male mice were isolated and differentiated. At day 08, the optimum incubation in SILAC-Met media was determined by measuring the percentage of cell death (measured by LDH release) in the presence of AHA-supplemented, methionine-supplemented, normal DMEM and methionine-deficient SILAC-Met media (A). The optimum time point for maximum secretion of leptin and resistin was also determined in these cells (B) using the MILLIPLEX® MAP Mouse Metabolic Hormone panel. Abbreviations: iWA, inguinal white adipocytes; BA, brown adipocytes; AHA, L-azidohomoalaine; Met, methionine; DMEM, dulbecco's modified eagle medium. n=3, means ±SEM, * indicates significance.

As shown in Figure 6A, the amount of cell death in all of the treatments was significantly higher after 24 and 48 hours of incubation compared to 6 hours. Surprisingly, there was no significant difference between the 24 and 48 hours treatment. It was also observed that primary brown adipocytes were more sensitive to the deficiency of methionine in the growth media. As depicted in Figure 6B the amount of leptin and resistin secreted was significantly higher after 24 hours of incubation compared to 6 hours. As expected, inguinal white adipocytes (iWA) secreted higher amounts of both adipokines compared to brown adipocytes (BA) when compared to their respective undifferentiated states.

Thus, taking together effect of AHA on cell viability and the secretion of leptin and resistin, a 24 hours incubation period was selected for incubation of both iWA and BA in SILAC-Met media for the subsequent secretome studies.

Comparative secretome screening of inguinal white and brown adipocytes

Three secretome studies were conducted using the workflow and incubation time mentioned earlier. Two of the screens compared the secretome of iWA and BA, one with norepinephrine (NE) treatment designated as WA (+NE) vs. BA (+NE) and the other without any stimulation or treatment (basal state) designated as WA (-NE) vs. BA (-NE). The third screen compared the secretome between NE-treated and untreated BA (BA ±NE). The following table contains the details of the three screens.

Table 2: Number of proteins detected in the secretome screens

Screen	Biological replicates	Quantified proteins	In at least 2 replicates	In all 3 replicates	p.adj-value <0.01
BA ±NE	Replicate 1	719	624	275	251
	Replicate 2	279			
	Replicate 3	718			
WA (+NE) vs. BA (+NE)	Replicate 1	478	461	388	69
	Replicate 2	453			
	Replicate 3	485			
WA (-NE) vs. BA (-NE)	Replicate 1	397	353	287	50
	Replicate 2	357			
	Replicate 3	329			

A)

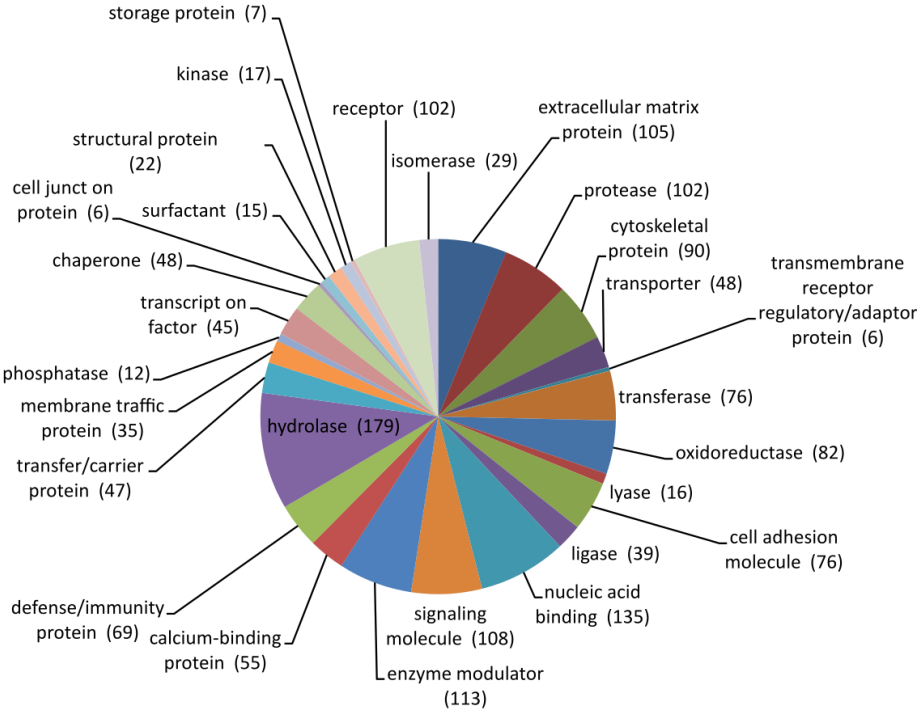

Panther protein classes

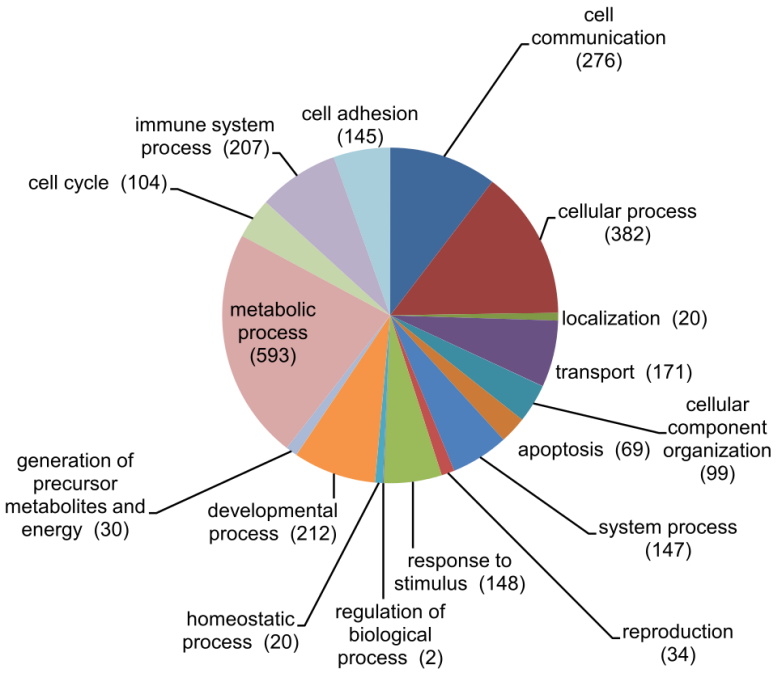

GO biological processes

B)

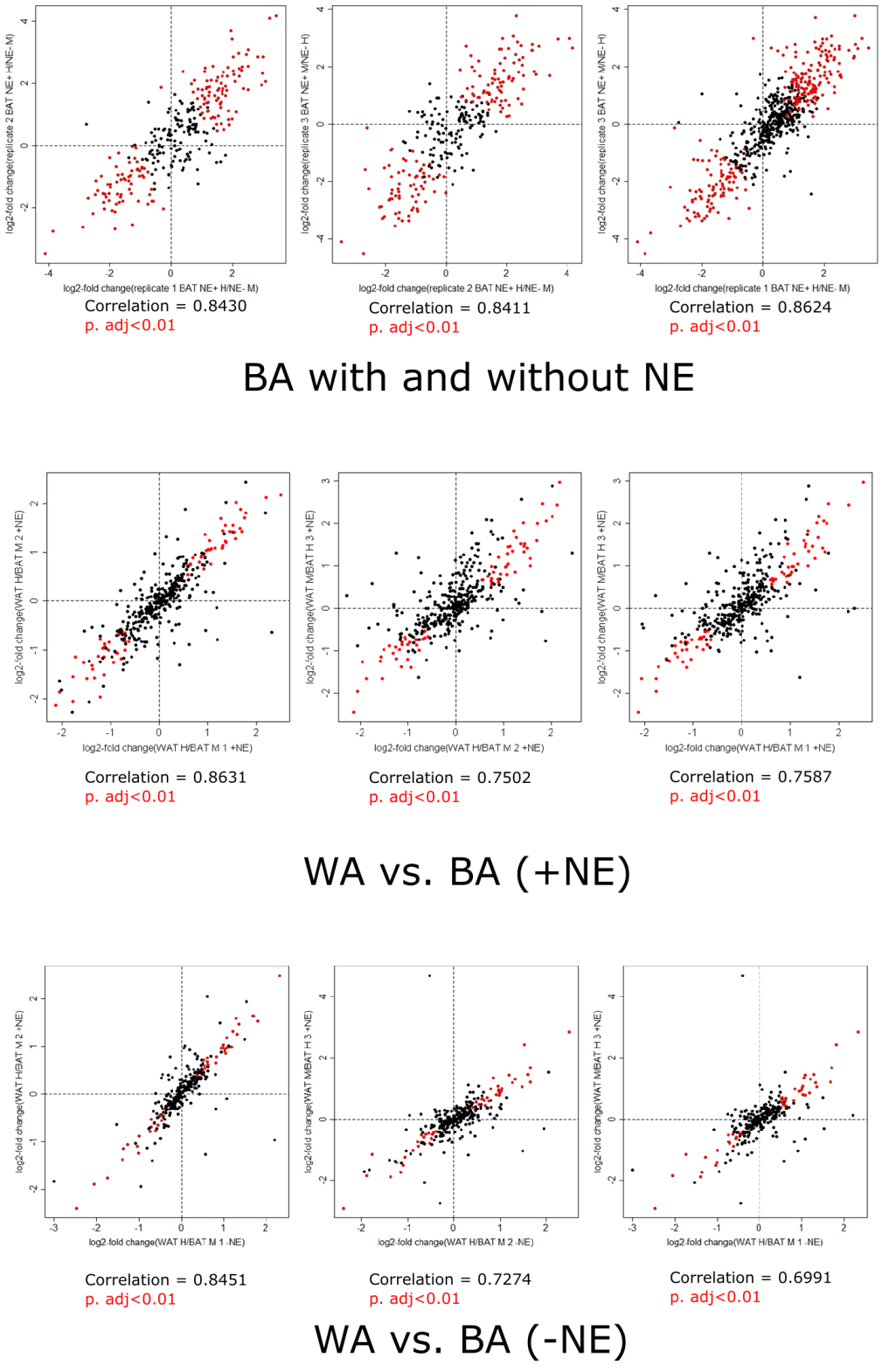

Figure 7: Classification and replicate correlation of the secretome screens. (A) All the proteins identified from the three secretome screens were classified according to the panther protein classes and GO biological processes. (B) The correlation and adjusted p-values between the replicates was determined for each of the three replicates for the three secretome screens. This analysis was carried out in the lab of Dr. Jeroen Krijgsveld (EMBL). Abbreviations: BA, brown adipocytes; WA, white adipocytes; NE, norepinephrine.

In total 1013 proteins were identified in the three secretome screens. Among these proteins, 406 were annotated as secreted. Figure 7A, shows the classification of all the proteins identified based on the Panther protein classes and Gene Ontology biological processes. According to the Panther protein classes, the top five classes represented in the screens were: hydrolases, nucleic acid binding proteins, enzyme modulators, signaling molecules and extracellular proteins. Similarly, according to the GO biological process proteins involved in metabolic process were highly represented, surpassing proteins associated with cellular processes and cell communication by nearly two fold higher representation. These classifications were in accordance to what is reported in other adipocyte secretome studies.

The secretome studies were conducted with reciprocally labeled arginine and lysine, i.e. for example, among the three replicates of a screen, two of the replicates had heavy labeling of amino acids while the third replicate was labeled with the intermediate isotope. This accounted for selective incorporation of specific amino acids isotopes and to determine the reproducibility of the screen by assessing the correlation between the replicates. As shown in Figure 7B, the reproducibility of the screens was in the acceptable range of 70-85 %, with the highest correlation for the BA ± NE screen (85 %).

Thus, due to the expected classification of the secreted proteins and acceptable reproducibility of the screens, the protein hits obtained from the secretome studies were used considered for further functional studies.

Proteins common between WA (+NE) vs. BA (+NE) and BA ±NE screens were selected for further studies.

Among the significant candidates (p.adj-value <0.01) obtained from the three screens, the proteins common between the two screens involving NE-treated white vs. brown adipocyte and NE-treated and untreated BA were selected for further functional characterization. These proteins were selected on the hypothesis that the systemic beneficial effects of BAT are associated with its beta-adrenergic activation via the sympathetic nervous system in response to cold stimuli and therefore, potential 'batokines' would not only be differentially secreted between NE-stimulated iWA and BA but also between NE-stimulated and unstimulated BA.

A)

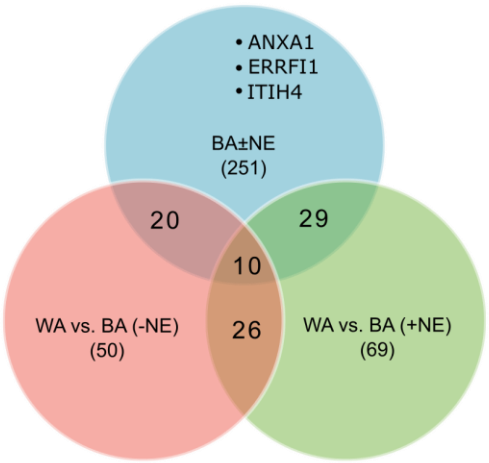

B)

Gene names	Protein names	Secretion evidence	log2 BA +NE/-NE	log2 +NE WA (+NE)/BA (+NE)
Hspa5 Grp78	78 kDa glucose-regulated protein	+		
Adipoq Acdc Acrp30 Apm1	Adiponectin	+		
Angptl4 Farp Fiaf Ng27	Angiopoietin-like protein 4	+		
Agt Serpina8	Angiotensinogen;Angiotensin-1;Angiotensin-2;Angiotensin-3	+		
Cat Cas-1 Cas1	Catalase			
Ctss Cats	Cathepsin S	+		
Col1a1 Cola1	Collagen alpha-1(I) chain	+		
Col3a1	Collagen alpha-1(III) chain	+		
Col1a2 Cola2	Collagen alpha-2(I) chain	+		
Col4a2	Collagen alpha-2(IV) chain;Canstatin	+		
Col5a2	Collagen alpha-2(V) chain	+		
Cfd Adn Df	Complement factor D	+		
Dpt	Dermatopontin	+		
Enpp2 Npps2 Pdnp2	Ectonucleotide pyrophosphatase/phosphodiesterase family member 2	+		
Fah	Fumarylacetoacetase			
Hspa8 Hsc70 Hsc73	Heat shock cognate 71 kDa protein			
Hmox1	Heme oxygenase 1			
Ltbp2	Latent-transforming growth factor beta-binding protein 2	+		
Lpl	Lipoprotein lipase	+		
Scp2 Scp-2	Non-specific lipid-transfer protein			
Spp1 Eta-1 Op Spp-1	Osteopontin	+		
Plin1 Peri Plin	Perilipin-1			
Pla1a Pspla1	Phospholipase A1 member A	+		
Plod1 Plod	Procollagen-lysine,2-oxoglutarate 5-dioxygenase 1	+		
Retn Fizz3	Resistin	+		
Sparcl1 Ecm2 Sc1	SPARC-like protein 1	+		
Taldo1 Tal Taldo	Transaldolase			
Tagln Sm22 Sm22a	Transgelin			
Tpi1 Tpi	Triosephosphate isomerase			

C)

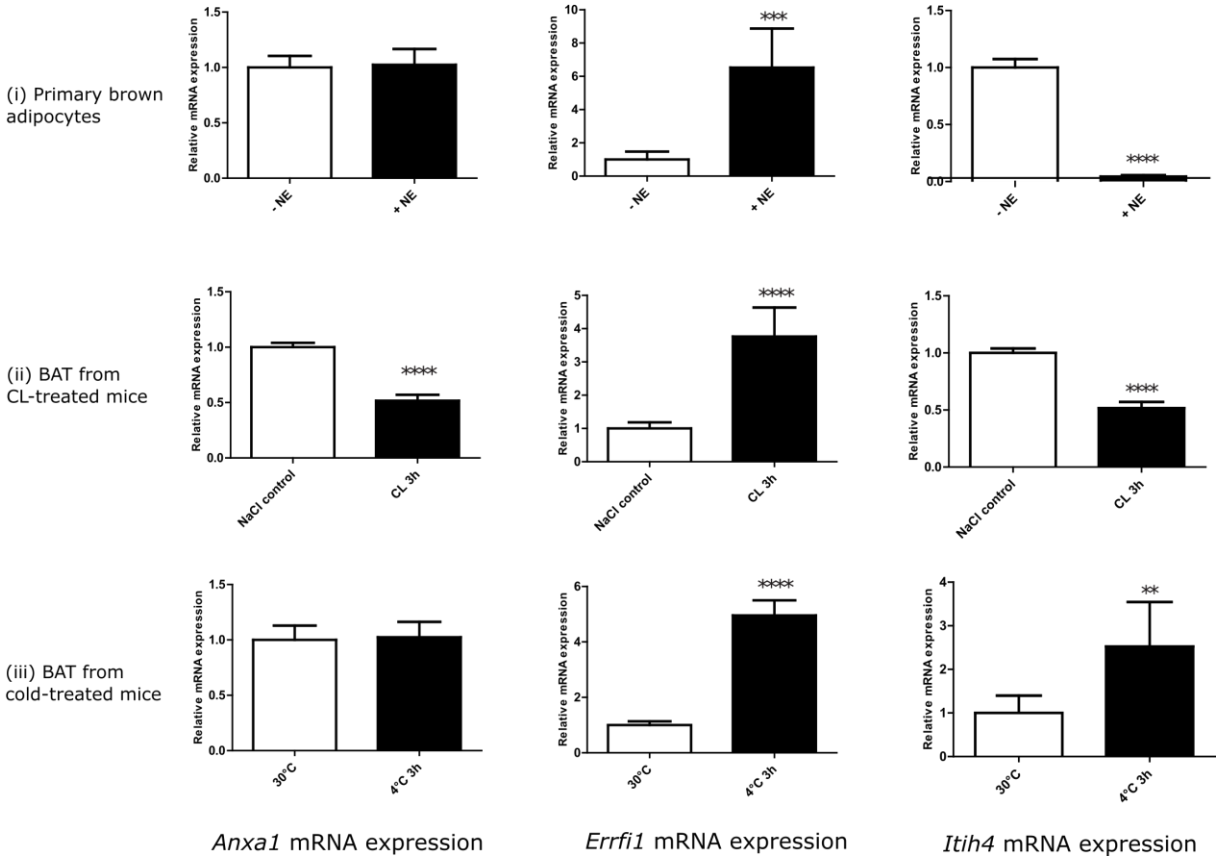

Figure 8: Significant candidates from the secretome screen and mRNA expression of some candidates. (A) Venn diagram depiction of the significant secretome candidates from the three secretome studies and the common significant candidates between the screens. (B) Heat map with the 29 secretome candidates common between two screens: WA (+NE) vs. BA (+NE) and BA ±NE. The list represents significant candidates with p.adj<0.01 and average log2 normalized ratio. (C) Validation of mRNA levels of three candidates: *Anxa1*, *Erffi1* and *Itih4* in three different experiments: (i) differentiated primary brown adipocytes from the SVF of C57BL/6J 8 weeks old male mice at day 08 with and without norepinephrine (NE) treatment, (ii) BAT from of C57BL/6J 12 weeks old females injected with NaCl for 14 days via an osmotic pump and CL-316,243 (CL), a thermogenic beta 3-agonist or NaCl (control) for 3 hours and lastly, (iii) BAT from cold-treated NMRI 8 weeks old females exposed to thermoneutrality as controls (30°C) for 2 weeks followed by 4°C for 3 hours. n=3, means ±SEM, * indicates significance compared to the appropriate controls.

Based on the above criteria, 29 proteins common between the two screens (Figure 8A) were selected as potential batokine candidates. Figure 8B shows the heat map of these 29 candidates along with their evidence of secretion. Among the candidates, 9 proteins were not known to be secreted. Majority of the common candidates also showed lower secretion from BA with NE- treatment. The mRNA expression of three candidates from the BA±NE screen was investigated in three different BAT activation experiments to determine their co-relation to the secretome studies and to activated BAT. The expression of candidates *Anxa1*, *Erffi1* and *Itih4* was measured using qPCR in i) NE-treated primary BA, ii) BAT from CL-treated mice (3h) and iii) BAT from cold-exposed (3h) mice. As observed from Figure 8C, *Anxa1* showed a reduced expression in BAT from CL-treated mice, while *Erffi1*

showed a consistent increase in mRNA expression in all three experiments which correlated with the secretion in the secretome screen. *Itih4* on the other hand showed a very strong reduction with NE and CL-treatment in primary BA and BAT respectively that matched its secretion levels in the screen and a moderate increase with cold-exposure.

Thus, the selected candidates showed mRNA expression in at least one experiment that corresponded to their protein secretion. In addition, expression data from microarray transcriptome analysis of BAT from the afore-mentioned cold-exposed mice correlated with the secretion of the secretome candidates (data not shown). These observations reinforced the notion that the 29 candidates could be promising batokine candidates for further unbiased functional studies.

Batokine study

The 29 candidates selected from the secretome screens were considered for a series of unbiased *in vitro* assays that highlight possible batokine functions. As depicted in Figure 9A, these studies would start with transfection of HEK 293A cells with cDNA expression vectors and collection of conditioned media (CM) from these cells. The CM, potentially containing the secreted proteins, would then be utilized in different functional assays. These *in vitro* assays include: glucose stimulated insulin secretion, lipolysis, hepatic gluconeogenesis, insulin sensitivity and browning (Figure 9A).

Optimization of glucose stimulated insulin secretion (GSIS) assay for secretome candidates

Krebs-Ringer bicarbonate HEPES buffer gives the highest fold increase in GSIS.

As mentioned above, the functional characterization of the candidates involves the use of CM. Different types of CM were analyzed for their effect on GSIS to determine how the CM alone would in turn affect the assay. RPMI and Krebs-Ringer bicarbonate HEPES (KRBH) buffer with the addition of glucose, bovine serum albumin (BSA), fetal bovine serum (FBS) or combinations of them were used in the assay (Table 3). The concentration of these additives was selected based on experiments to determine their effect on the growth of HEK 293A cells and ectopic EGFP expression (data not shown). RPMI and KRBH buffer were used because RPMI is the growth media of INS-1E cells and KRBH buffer is used in GSIS assays.

Table 3: The composition of the different types of CM used in the GSIS optimization assay.

Name	Media/Buffer	Glucose	FBS	BSA
RPMI - -	RPMI	-	-	-
RPMI+G	RPMI	0.5 g/L	-	-
RPMI+FBS	RPMI	-	5 %	-
RPMI+G+FBS	RPMI	0.5 g/L	5 %	
RPMI+G+BSA	RPMI	0.5 g/L	-	1 %
RPMI-fresh	RPMI	-	-	-
KRBH - -	KRBH	-	-	-
KRBH+G	KRBH	0.5 g/L	-	-
KRBH+FBS	KRBH	-	5 %	-
KRBH+G+FBS	KRBH	0.5 g/L	5 %	
KRBH+G+BSA	KRBH	0.5 g/L	-	1 %
KRBH-fresh	KRBH	-	-	-

A)

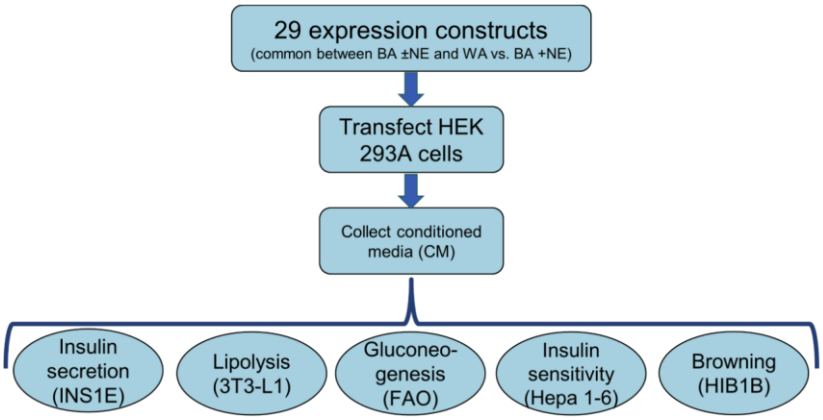
29 expression constructs
(common between BA ±NE and WA vs. BA +NE)
Transfect HEK 293A cells
Collect conditioned media (CM)
Insulin secretion (INS1E)
Lipolysis (3T3-L1)
Gluconeo-genesis (FAO)
Insulin sensitivity (Hepa 1-6)
Browning (HIB1B)

B)

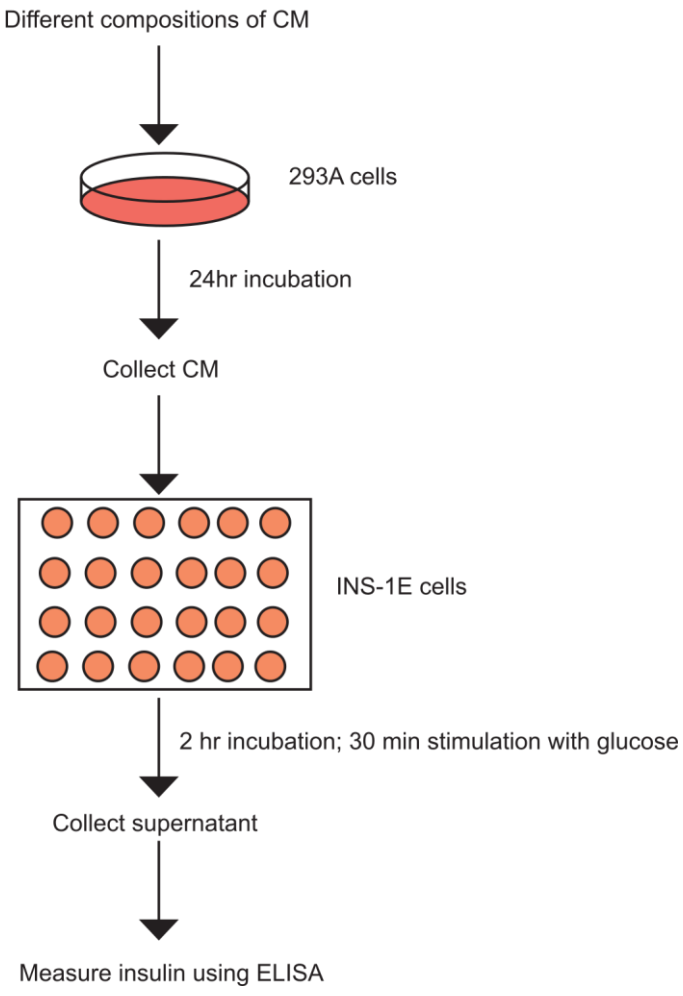
Different compositions of CM
293A cells
24hr incubation
Collect CM
INS-1E cells
2 hr incubation; 30 min stimulation with glucose
Collect supernatant
Measure insulin using ELISA

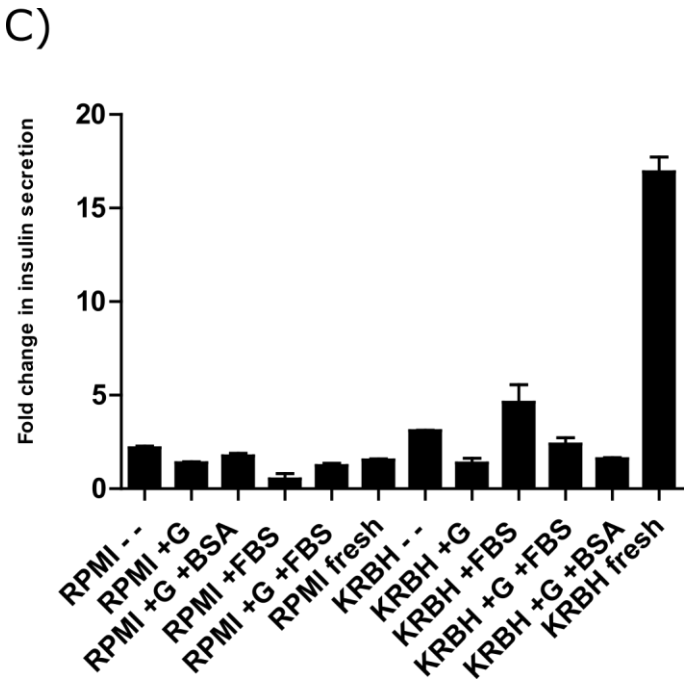

Figure 9: Batokine study and optimization of GSIS assay. (A) The setup to study the batokine candidates would include the 29 candidates from the secretome studies and transfection of their expression constructs in to HEK 293A cells. The conditioned media containing the over-expressed secreted candidate would then be used for different functional assays like insulin secretion (INS-1E cells), lipolysis (3T3-L1), gluconeogenesis (FAO cells), insulin sensitivity (Hepa 1-6) and browning (HIB1B). (B) The set up for optimizing the GSIS assay involves incubating HEK 293A cells with different compositions of condition media (CM) for 24 hours and then treating INS-1E cells with this CM followed by glucose stimulation for 30 minutes. The secreted insulin is measured from the supernatant using ELISA. (C) Using the setup mentioned above, different compositions of CM were used and the fold change in insulin secretion (glucose stimulated to unstimulated insulin secretion) was measured. Abbreviations: BSA, bovine serum albumin; FBS, fetal bovine serum; G, glucose; KRBH, Krebs-Ringer bicarbonate HEPES. n=2 (B), means ±SEM, * indicates significance.

The optimization experiment was carried out as shown in Figure 9B. Briefly, different CMs were incubated on HEK 293A cells for 24 hours. After the incubation, the CMs were used to treat INS-1E cells for 2 hours, followed by 2 hour glucose stimulation by the addition of 20 mM glucose. In addition to these CMs, fresh RPMI (‘RPMI fresh’) and KRBH (‘KRBH fresh’) - which were not in contact with HEK 293A cells, were also used in the assay. The supernatant was collected and the secreted insulin was measured using ELISA. As shown in Figure 9C, the highest fold change (ratio of glucose treated to untreated) in insulin secretion was observed for KRBH fresh although the absolute values of secreted insulin values were low (data not shown) compared to the other samples.

Thus, the highest fold change in GSIS and in turn the highest responsiveness to glucose was achieved when INS-1E cells were stimulated with glucose in fresh KRBH. Therefore, KRBH buffer was used for GSIS assays in the subsequent experiments.

Recombinant proteins lead to higher GSIS compared to conditioned media

Next, the INS-1E cells were treated with either adiponectin CM or recombinant protein to determine an optimum method to expose the INS-1E cells to the secretome candidates. Adiponectin was used as a positive control in this experiment because it increases GSIS in INS-1E cells (Patane, Caporarello et al. 2013) and was also one of the 29 secreted proteins. The two pilot assays involved the use of adiponectin CM or recombinant adiponectin protein.

A)

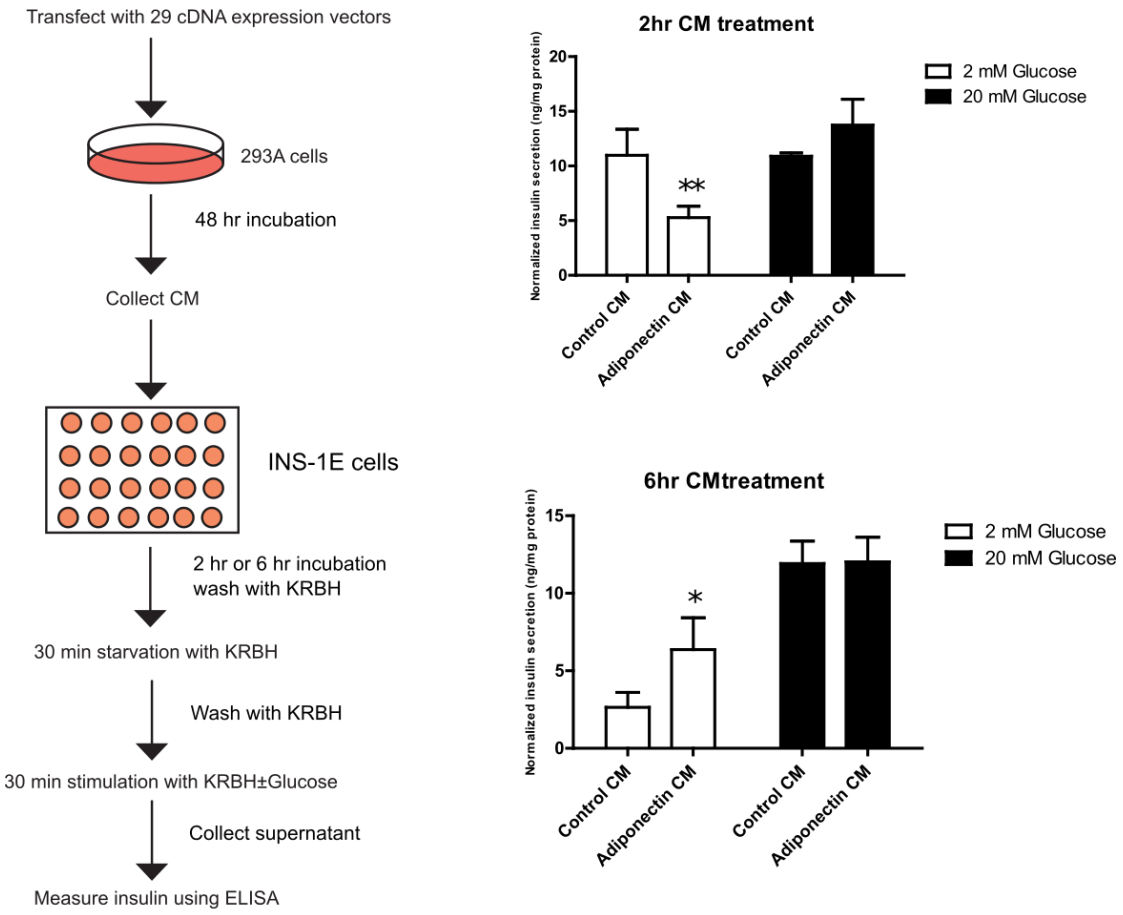

GSIS assay with conditioned media

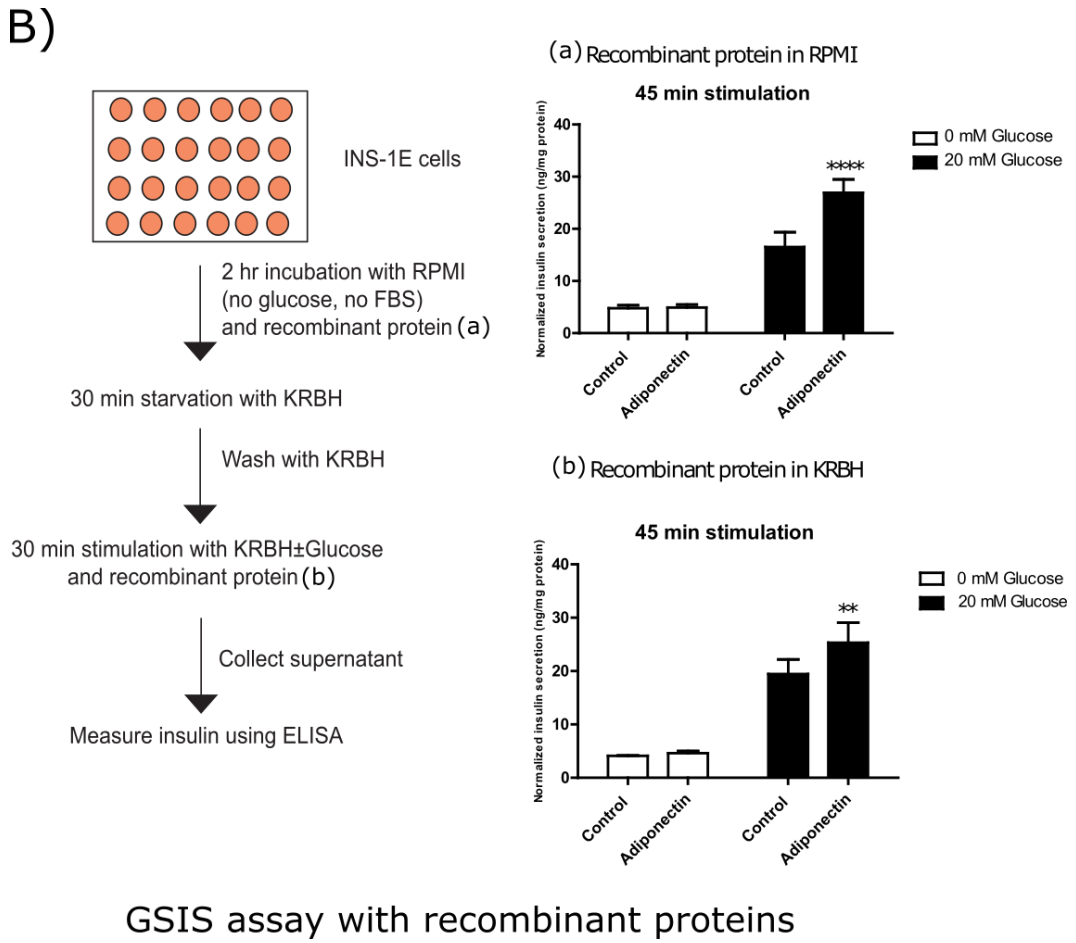

Figure 10: GSIS assay with conditioned media and recombinant proteins. (A) Conditioned media (CM) from HEK 293A cells transfected with adiponectin cDNA expression vector (Origene, MC208100) was collected after 48 hours and used to treat INS-1E cells. After 2 hours or 6 hours incubation with the CM, the INS-1E cells were washed with KRBH and starved in fresh KRBH for 30 minutes, washed again and stimulated with 20 mM glucose. The insulin secreted was measured using ELISA. The graphs depict the normalized insulin secretion for CM containing adiponectin (as a positive control) with subsequent glucose stimulation. (B) The INS-1E cells were directly treated with recombinant proteins either in RPMI for 2 hours (a) or with glucose in KRBH after 30 minutes of starvation (b). The supernatant was collected and insulin was measured using ELISA. The graphs show normalized insulin secretion using recombinant adiponectin (as positive control) with 20 mM glucose stimulation. n=4, means ±SEM, * indicates significance compared to respective control.

The setup of the assays is depicted in Figure 10. Briefly, the adiponectin CM was obtained from HEK 293A cells and used to treat INS-1E cells for 2 hours and 6 hours followed by GSIS in KRBH with glucose stimulation (Figure 10A). As shown in the graphs, GSIS was not significantly increased with treatment with adiponectin CM but a trend was visible with 2 hour treatment. On the other hand, the use of recombinant adiponectin involved either (a) addition of the protein in RPMI with 2 hours of incubation or (b) addition of the protein in KRBH along with 20 mM glucose stimulation (Figure 10B). As can be seen from the graphs, both protocols resulted in a significant increase in GSIS in the presence of

recombinant adiponectin. The increase was larger when INS-1E cells were treated with recombinant adiponectin in RPMI.

Thus, it can be concluded from the above data that, at least in the case of adiponectin, the use of recombinant protein was more effective than the use of CM to increase GSIS.

ITIH4 and its role in adipocyte biology

As stated above, the use of recombinant proteins seemed to be the most plausible option for use in the GSIS assay. However, obtaining the recombinant proteins for all the 29 candidates was not feasible in the limited project period and the focus of the project was shifted to a single secretome candidate: inter-alpha-trypsin inhibitor heavy chain H4 (ITIH4). ITIH4 is a 120-kDa acute phase protein that is cleaved by plasma kallikrein and is detectable in human and mouse serum. ITIH4 was one of the candidates from the initial secretome comparison between inguinal white and brown adipocytes. It was found to be about 4-fold highly secreted from brown adipocytes compared to white (Figure 11A) and its secretion was suppressed 4-fold by treatment with norepinephrine (NE) (data not shown).

ITIH4 is preferentially secreted from brown adipocytes but serum levels are not changed after cold-exposure

Owing to its secretion profile in the secretome screening, it was hypothesized that changes of ITIH4 levels in the serum would reflect the degree of BAT activity or its role as a possible batokine. To investigate this, ITIH4 levels were measured in the serum of cold-treated mice.

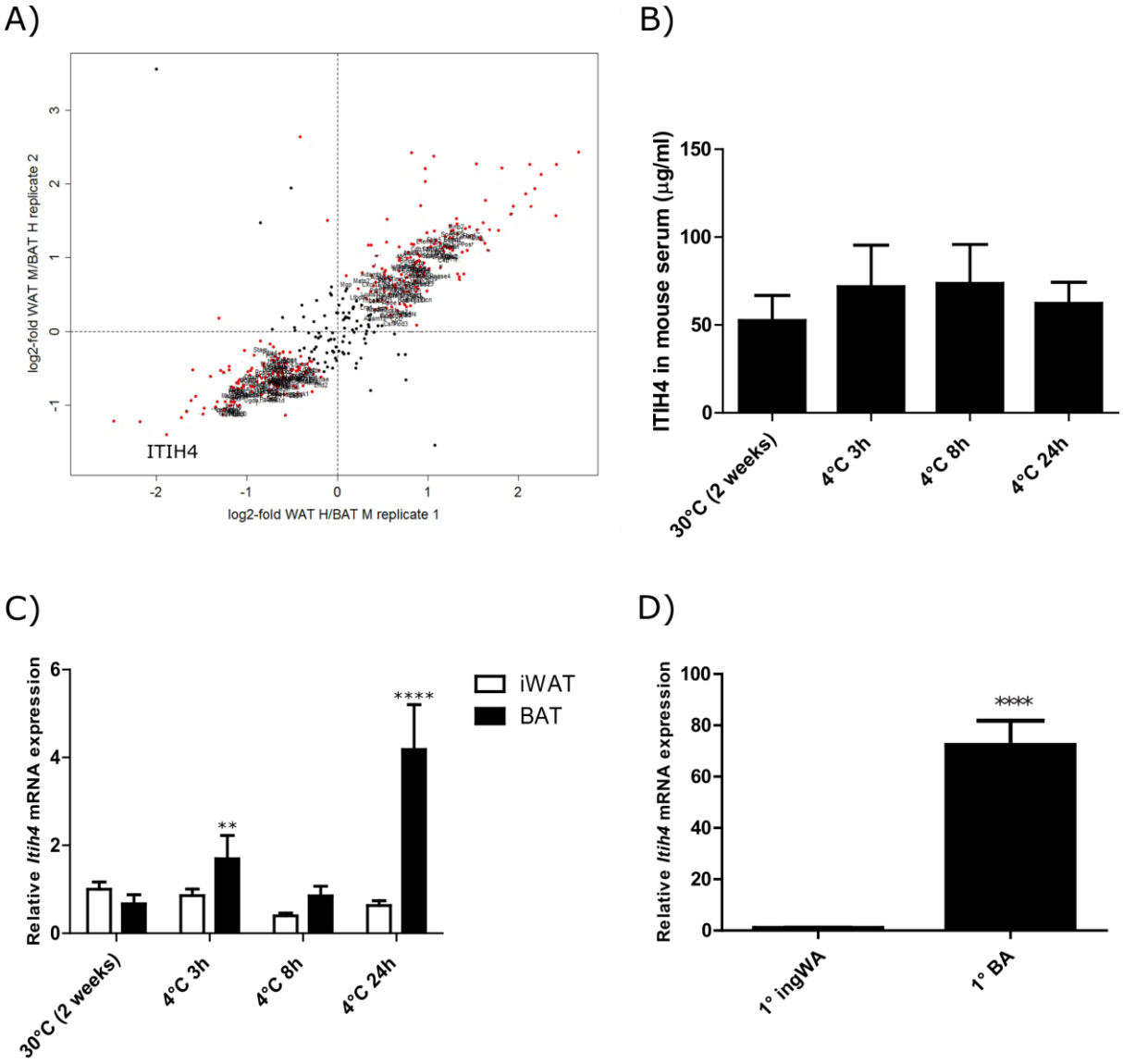

Figure 11: ITIH4 in the preliminary secretome screen, serum and mRNA levels. (A) ITIH4 was found to be preferentially secreted from primary brown adipocytes compared to white adipocytes in one of the secretome screens. ITIH4 was measured in the serum of cold-treated NMRI 8 weeks old females exposed to thermoneutrality as controls (30°C) for 2 weeks followed by 4°C for 3 hours, 8 hours and 24 hours (B). (C) *Itih4* mRNA expression was measured in the iWAT and BAT from the same animals from (B). (D) *Itih4* mRNA expression was measured in differentiated primary inguinal white and brown adipocytes at day 08 from the SVF of C57BL/6J 8 weeks old male mice. n=6 means ±SEM, * indicates significance.

As shown in Figure 11B, the levels of ITIH4 were detectable in the serum but were unchanged in cold-exposed mice. Interestingly, *Itih4* mRNA levels increased in the intrascapular BAT of these mice (Figure 11C) and a 70-fold higher mRNA expression in primary brown adipocytes compared to inguinal white adipocytes was also detected (Figure 11D). Therefore, it was concluded that ITIH4 might not correlate with BAT activity or be a potential batokine candidate under cold stimulation but could play a role in brown adipocytes biology or function.

Itih4 mRNA levels increase with adipogenesis and are higher in brown adipocytes

Having observed an increase with cold-exposure in mRNA expression and higher mRNA levels in primary brown adipocytes, *Itih4* mRNA levels were investigated *in vitro* in different adipocyte cell lines and in primary adipocytes (Figure 12).

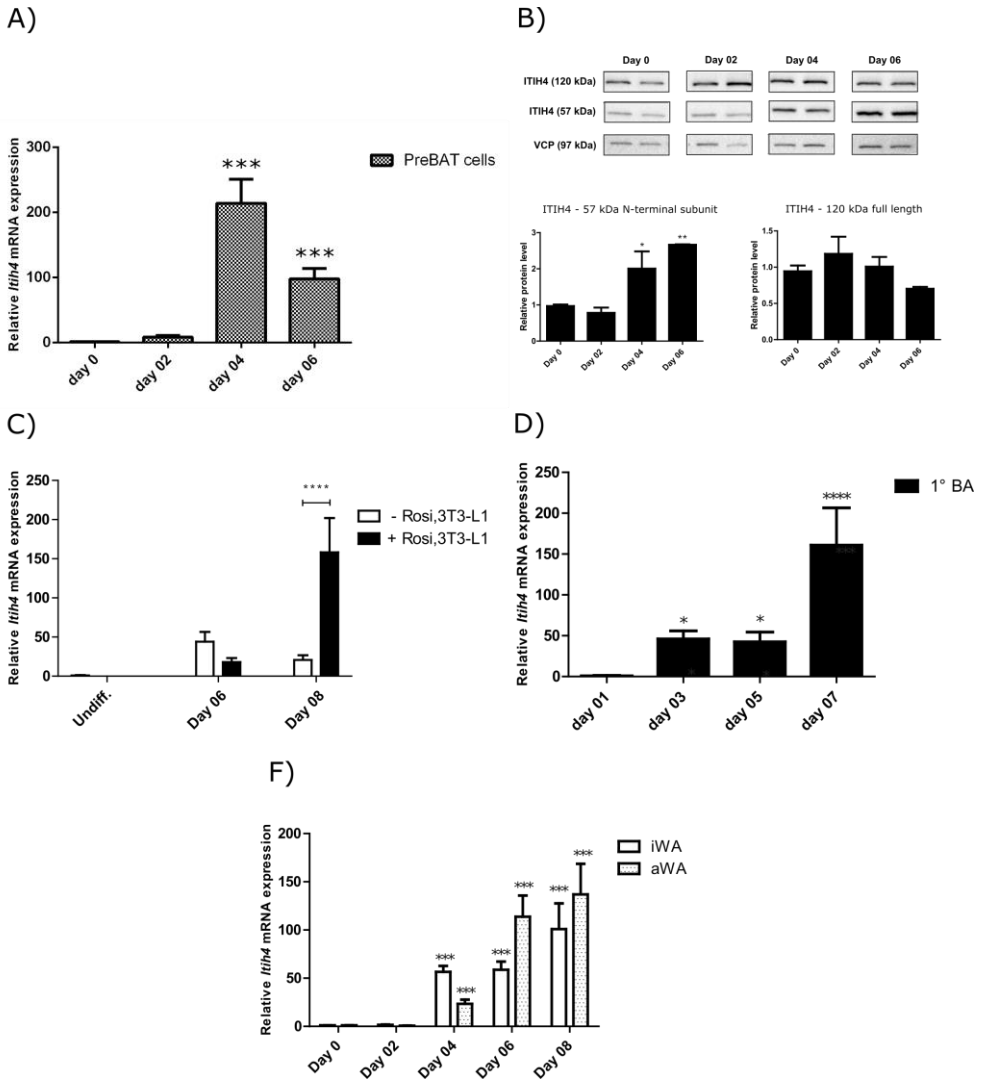

Figure 12: ITIH4 expression in cell lines and primary adipocytes during differentiation. PreBAT cells were differentiated and *Itih4* mRNA (A) and protein expression (B) (with quantification relative to VCP using Image Labs) was measured on day 0, 02, 04 and 06. (C) 3T3-L1 cells were differentiated with or without rosiglitazone and *Itih4* mRNA expression was measured at the end of differentiation (day 06 and day 08). *Itih4* mRNA expression was measured during the differentiation of primary brown adipocytes (D), inguinal and abdominal white adipocytes (F) from the SVF of C57BL/6J 8 weeks old male mice. n=6, means ±SEM, * indicates significance

ITIH4 expression was first measured in PreBAT cells. This cell line was generated by immortalizing pre-adipocytes from the intrascapular BAT of newborn mice using the SV40 Large T antigen (Hoppmann, Perwitz et al. 2010). These cells can be differentiated in to mature brown adipocytes by treatment with an induction media followed by differentiation media for 6 days. As shown in Figure 12A and B, *Itih4* mRNA and protein expression increased with differentiation (adipogenesis) of PreBAT cells. Interestingly, the protein expression of full length 120 kDa ITIH4 was not changed with differentiation apart from small increase at day 02. However, the amount of the 57 kDa N-terminal fragment was increased with differentiation of PreBAT cells. Similarly, *Itih4* mRNA expression also increased with differentiation of 3T3-L1 and the expression was higher in the presence of rosiglitazone - a potent *Pparg* agonist and browning agent (Figure 12C). Concerning primary adipocytes, *Itih4* mRNA levels were higher in differentiated primary brown adipocytes compared to primary inguinal white adipocytes (Figure 12 D-F) but in addition, *Itih4* mRNA expression increased with the differentiation of primary brown adipocytes, inguinal and white adipocytes.

Thus, ITIH4 expression increased with differentiation in both adipocyte cell lines and primary adipocytes with a higher expression associated with brown adipocytes and browning.

Rosiglitazone and isoproterenol significantly reduce *Itih4* mRNA expression in differentiated PreBAT cells while IL-6 has no effect.

As shown in the previous section, *Itih4* mRNA expression increases with adipogenesis. In addition, *Itih4* mRNA expression has also been shown to increase in hepatocytes and HepG2 cells with IL- 6 treatment (Pineiro, Alava et al. 1999, Bhanumathy, Tang et al. 2002). Therefore, *Itih4* expression levels in mature adipocytes were investigated after treatment with IL-6 and compounds that affect mature adipocyte functions. PreBAT cells at day 06 of differentiation were treated with etomoxir (fatty acid oxidation inhibitor), AICAR (AMPK activator), rosiglitazone (PPARg agonist), isoproterenol (beta adrenergic agonist), LPS (endotoxin that stimulates the innate immune response) and thapsigargin (ER stress inducer) for 6 hours and also with different amounts of IL-6 for 48 hours.

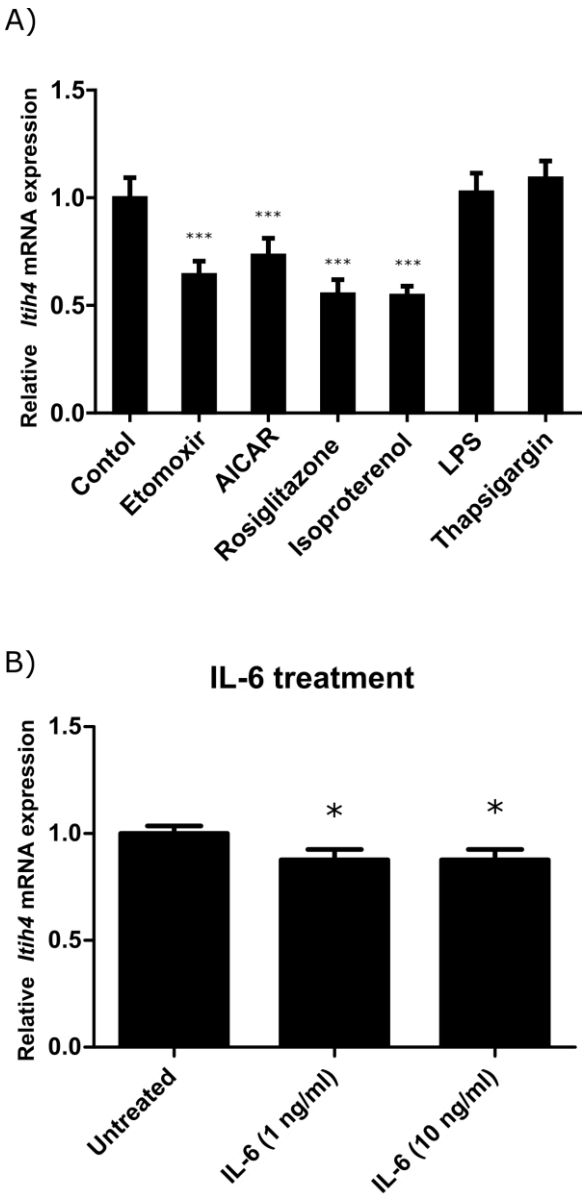

Figure 13: *Itih4* mRNA expression with different extracellular treatments. Differentiated PreBAT cells at day 06 were treated with etomoxir (100 µM), AICAR (1 mM), rosiglitazone (10 µM), isoproterenol (10 µM), LPS (10 ng/ml), thapsigargin (0.2 µM) for 6 hours (A) and with 1 ng/ml and 10 ng/ml IL-6 for 48 hours (B). Itih4 mRNA expression was measured using qPCR. n=6, means ±SEM, * indicates significance. Abbreviations: AICAR, 5-Aminoimidazole-4-carboxamide ribonucleotide; LPS, lipopolysaccharides.

As observed from Figure 13A, etomoxir, AICAR, rosiglitazone and isoproterenol reduced the expression of *Itih4* mRNA after 6 hours of treatment. Among these four compounds, treatment with rosiglitazone and isoproterenol resulted in almost 50 % reduction in *Itih4* expression. Interestingly, unlike in hepatocytes and HepG2 cells, IL-6 treatment failed to increase *Itih4* mRNA expression (Figure 13B).

Itih4 expression increases with Treg depletion in BAT and decreases with adipose tissues in *db/db* mice

ITIH4 is an acute-phase protein and is associated with inflammatory processes (Pineiro, Alava et al. 1999) and infections (Pineiro, Andres et al. 2004, Gangadharan, Antrobus et al. 2007) . In order to check the effect of a pro-inflammatory environment, *Itih4* mRNA expression was measured in two different mouse models. In the first model, *Iith4* mRNA expression was measured in the inguinal WAT and intrascapular BAT of regulatory T cell (Treg)-depleted mice. These are the same transgenic mice used by Medrikova, Sijmonsma et al. (2015) and express the diphtheria toxin (DT) receptor under the control of Foxp3 gene regulatory elements driving the expression of DTR in Tregs. Administering DT led to the whole body depletion of Treg cells and resulted in a significant increase in the invasion of pro-inflammatory macrophages in BAT. In the second model, *Itih4* levels were investigated in the adipose tissue of *ob/ob* obese mice (experiment conducted by Dr. Roldan de Guia) that are known to have a chronic state of adipose tissue inflammation (Xu, Barnes et al. 2003). This would also be an interesting comparison to ITIH5, another member of the inter-α-trypsin inhibitor (ITI) family that has been shown to increase with obesity in human adipose tissue (Anveden, Sjoholm et al. 2012).

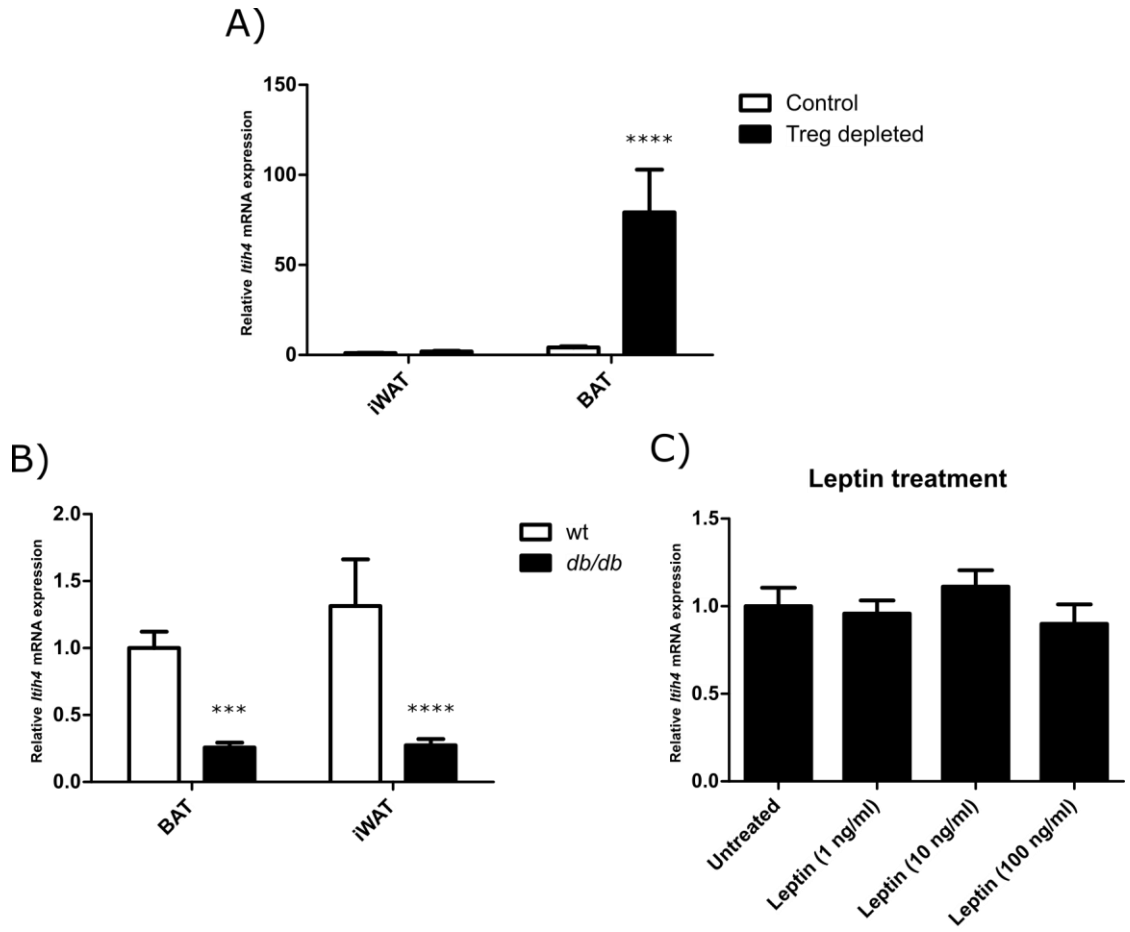

Figure 14: *Itih4* mRNA expression in iWAT and BAT from Treg depleted mice and *db/db* mice. *Itih4* mRNA expression was measured using qPCR in inguinal WAT and intrascapular BAT from 7 week old FoxP3DTR female mice that were either injected with 1xPBS (control) or diphtheria toxin (Treg depleted) (A) and from random-fed 12 week old BKS.Cg-m+/+ Lepr DB/J (*db/db*) or C57Bl6/J control mice (wt) (B). (C) Differentiated PreBAT cells at day 06 were treated with indicated amounts of leptin for 48 hours. n=9 (A), n= 4 (B), means ±SEM, * indicates significance. Abbreviations: iWAT, intrascapular white adipose tissue; BAT, brown adipose tissue; Treg, T regulatory cells.

As shown in Figure 14A, depletion of Tregs in BAT led to a 20-fold and 70-fold increase in *Itih4* mRNA expression compared to control BAT and iWAT respectively. However, the increase in *Itih4* mRNA expression after Treg depletion in iWAT was only 2-fold compared to control iWAT. Interestingly, a significant degree of reduction in *Itih4* mRNA expression was observed in iWAT and BAT from *db/db* mice (Figure 14B). This decrease was only observed in the adipose tissues while other metabolic organs like liver and the gastrocnemius muscle (GC) showed no change in *Itih4* mRNA levels (data not shown). To investigate if this decrease in *Itih4* mRNA levels was due to high amounts of leptin (hyperleptinemia) in *db/db* mice, differentiated PreBAT cells were treated with different amounts of leptin for 48 hours. Interestingly, leptin had no effect on *Itih4* expression (Figure 14C).

Thus, *Itih4* mRNA levels increased drastically with Treg depletion in BAT and decreased in iWAT and BAT of obese *db/db* mice.

ITIH4 knockdown *in vitro* was achieved using siRNA

ITIH4 was postulated to play an important role in adipocyte function because of its expression in adipogenesis (*in* vitro), inflammation and obesity (*in* vivo). Therefore, to further understand its role in adipocyte biology ITIH4 knockdown was attempted using siRNA in PreBAT cells. First, the transfection and siRNA knockdown was optimized in PreBAT cells using siPka (siRNA against *Prkaca* - Protein Kinase, CAMP-Dependent, Catalytic, Alpha) as a positive control siRNA and different transfection reagents.

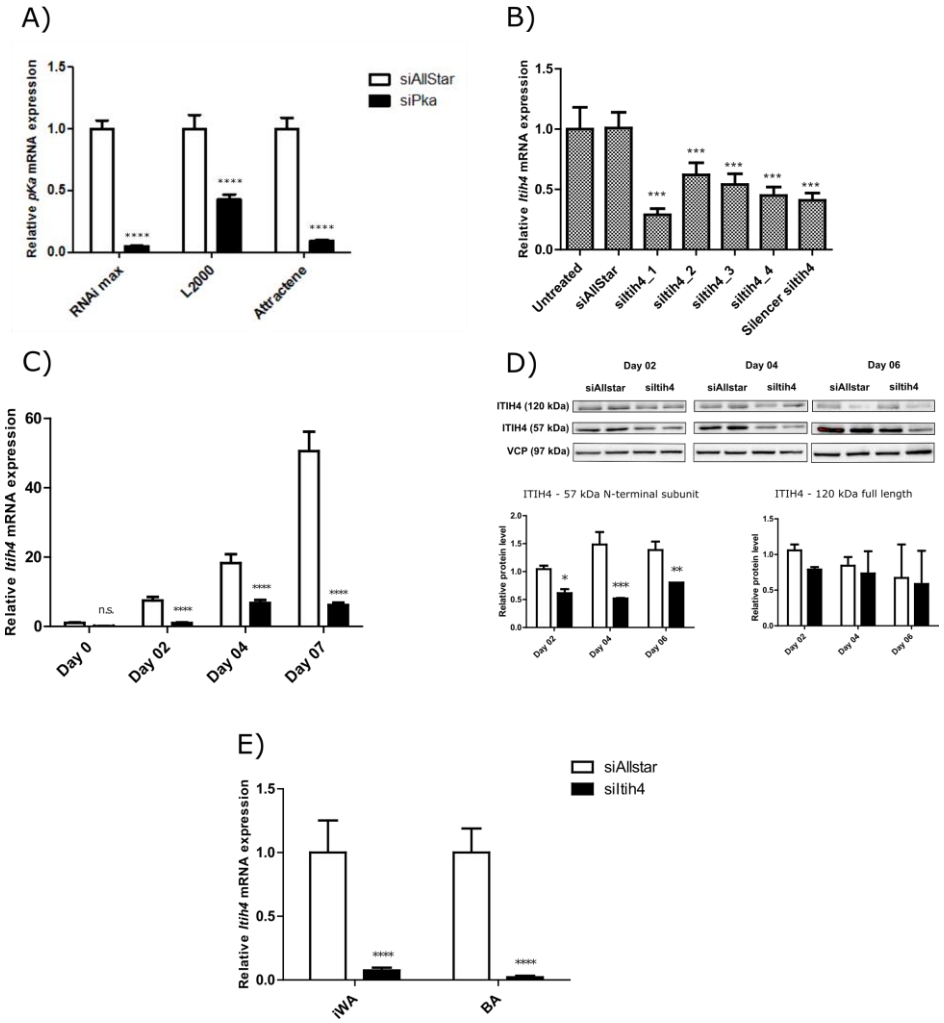

Figure 15: Knockdown of ITIH4 *in vitro* using siRNA. (A) PreBAT cells were transfected with 20 nM of siPka (positive control) and siAllstar (negative control) using different transfection reagents before the start of differentiation. *pKa* mRNA expression was measured on day 06 of differentiation. (B) Five different siRNAs for ITIH4 were used to transfect PreBAT cells using RNAiMAX before differentiation. *Itih4* mRNA expression was measured on day 06 of differentiation. siItih4_1 (20 nM) was used to transfect undifferentiated PreBAT cells and ITIH4 mRNA (C) and protein (D) expression (with quantification relative to VCP using Image Labs) was measured at different time points after differentiation using qPCR and immunoblotting. (E) Brown and inguinal white preadipocytes from the SVF of C57BL/6J 8 weeks old male mice were transfected with siItih4 (20 nM) and negative control (siAllstar) and mRNA expression was measured after 8 days of differentiation. n=6, means ±SEM, * indicates significance to siAllstar (negative control).

Lipofectamine® RNAiMAX transfection reagent gave the highest knockdown of *Pka* when compared to the negative control (siAllstar) (Figure 15A). Using RNAiMAX, five different siRNAs against *Itih4* were tested. The PreBAT cells were transfected with 20 nM of siRNAs 2 days before the start of differentiation and mRNA expression was measured after 6 days of differentiation. Among them, siItih4_1 gave a 70 % reduction in *Itih4* mRNA levels (Figure 15B). A time course experiment was also carried out to check the prevalence of ITIH4 knockdown during different time points of differentiation using siItih4_1 siRNA. As shown in Figure 15C, *Itih4* mRNA levels were consistently low throughout 7 days of differentiation. The 57 kDa N-terminal subunit of ITIH4, which was previously shown to increase with differentiation, was also reduced when the cells were transfected with siItih4_1 (Figure 15D). Using similar transfection conditions, a high degree of knockdown (> 80 %) was also observed in differentiated primary inguinal white and brown adipose tissues (Figure 15E).

Thus, an effective knockdown of ITIH4 was achieved using 20 nM of siItih4_1 and Lipofectamine® RNAiMAX transfection reagent in PreBAT cells and primary adipocytes. In further experiments siItih4_1 was used as the default siRNA for ITIH4 knockdown.

Effects of ITIH4 knockdown

ITIH4 knockdown in PreBAT cells leads to lower acidification of culture media and lower glucose utilization

Next, the effects of ITIH4 knockdown *in vitro* were investigated using the optimized siRNA knockdown conditions.

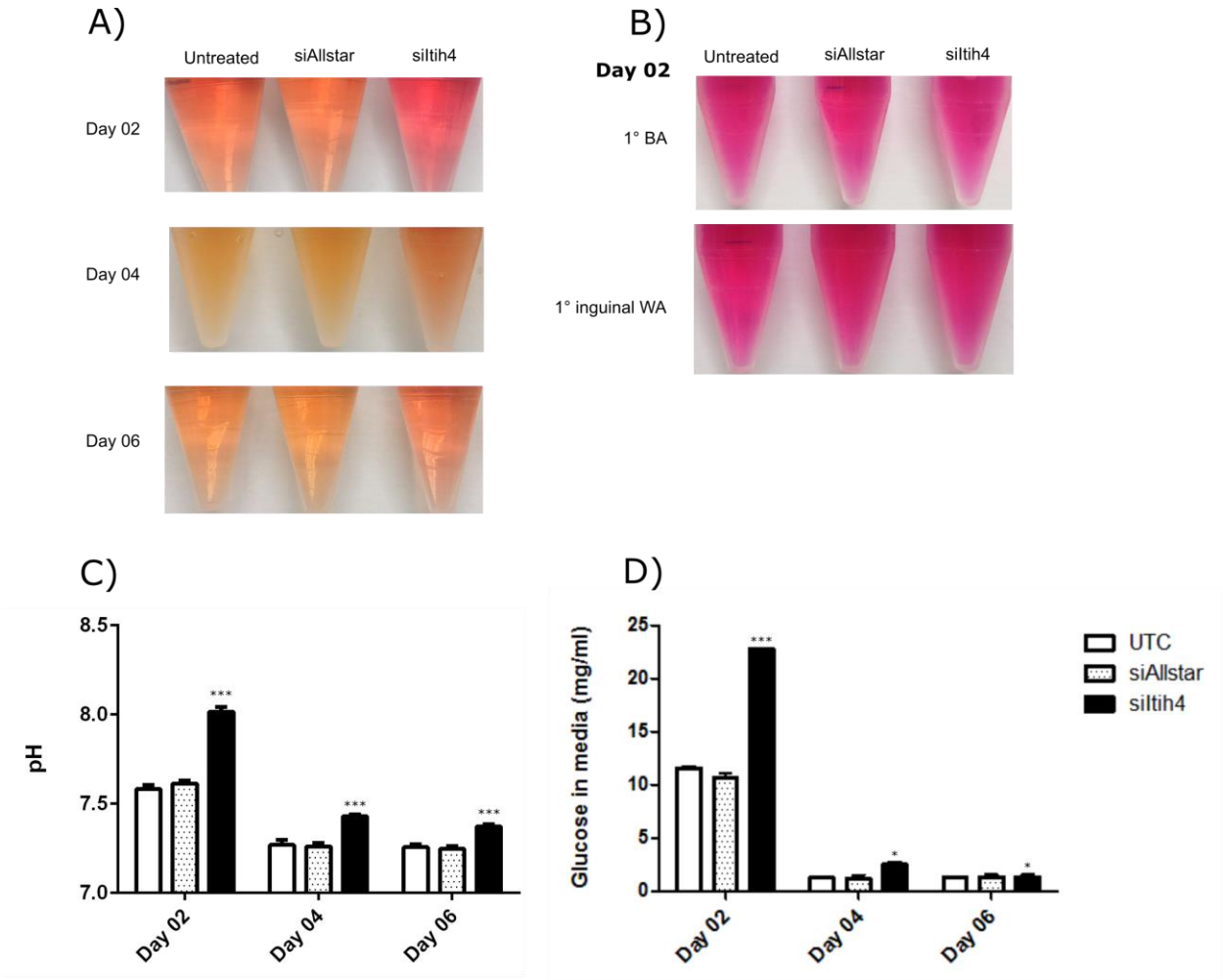

Figure 16: Changes in media color, pH and media glucose with ITIH4 knockdown. PreBAT cells were transfected with siItih4 (20 nM) or siAllstar (negative control, 20 nM) before differentiation and changes in media color (A), pH (C) and glucose in the media (D) were recorded at different time intervals of differentiation. (B) Primary brown and inguinal white preadipocytes from the SVF of C57BL/6J 8 weeks old male mice were also transfected with siItih4 and the change in media color was measured on day 02 of differentiation. n=3, means ±SEM, * indicates significance.

The most striking and noticeable change after ITIH4 knockdown was the reduction of acidification of the PreBAT culture media. This reduction in acidification, as visualized by red media color (Figure 16A) and quantified by a higher media pH (Figure 16C) for siItih4 transfected cells, was observable till day 06 of differentiation albeit the difference was stronger at the early stages of differentiation. These observations point to possible reduced metabolism which was indirectly confirmed by a higher residual glucose amount in the culture media for cells with ITIH4 knockdown (Figure 16D). However, similar changes were not observed with primary adipocytes (Figure 16B).

Thus, ITIH4 knockdown appeared to have an effect on PreBAT cells which could be due to reduced growth or lower overall differentiation.

ITIH4 knockdown leads to reduced lipid staining in both PreBAT cells and primary adipocytes

Next, lipid staining of PreBAT cells after ITIH4 knockdown was investigated to explain the afore-mentioned reduction in media acidification and glucose utilization.

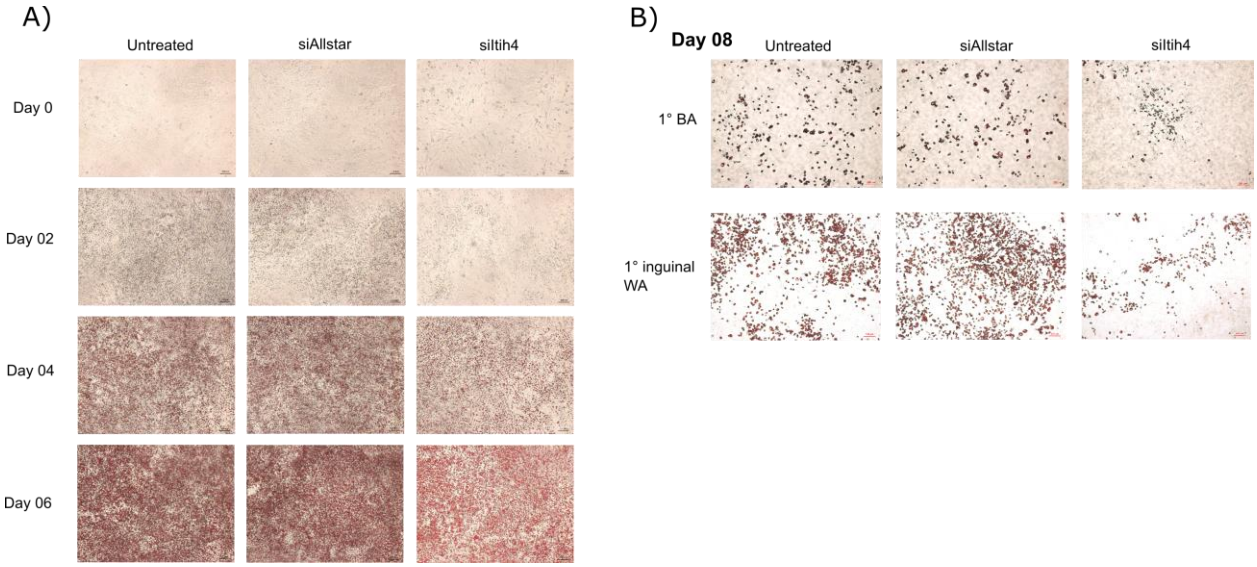

Figure 17: Oil red O staining of differentiated PreBAT and primary adipocytes with ITIH4 knockdown. ITIH4 was knocked down using siItih4 (20 nM) before the start of differentiation in PreBAT cells and primary brown and inguinal white preadipocytes from the SVF of C57BL/6J 8 weeks old male mice. Oil red O staining was carried out at different differentiation time points for PreBAT cells (A) and at day 08 of differentiation (B) for primary differentiated adipocytes after the start of differentiation.

As shown from the time course Oil Red O staining in Figure 17A, ITIH4 knockdown before differentiation in PreBAT cells resulted in a reduction in lipid staining when compared to untreated or negative (siAllstar) controls. This effect was even stronger in the case of primary intrascapular brown and inguinal white adipocytes (Figure 17B). Although the differentiation efficiency of the primary brown adipocytes was low in this experiment, subsequent knockdown experiments showed that the effect of ITIH4 knockdown was stronger in brown adipocytes than in inguinal white adipocytes (data not shown).

Thus, using Oil Red O staining it was shown that ITIH4 knockdown leads to decreased lipid staining and this effect is stronger in primary adipocytes compared to the PreBAT cell line.

ITIH4 knockdown does not lead to decrease in BAT and adipogenic markers

In order to fully characterize the effect of ITIH4 knockdown in adipocytes, the expression of some BAT and adipogenic markers was measured after ITIH4 knockdown.

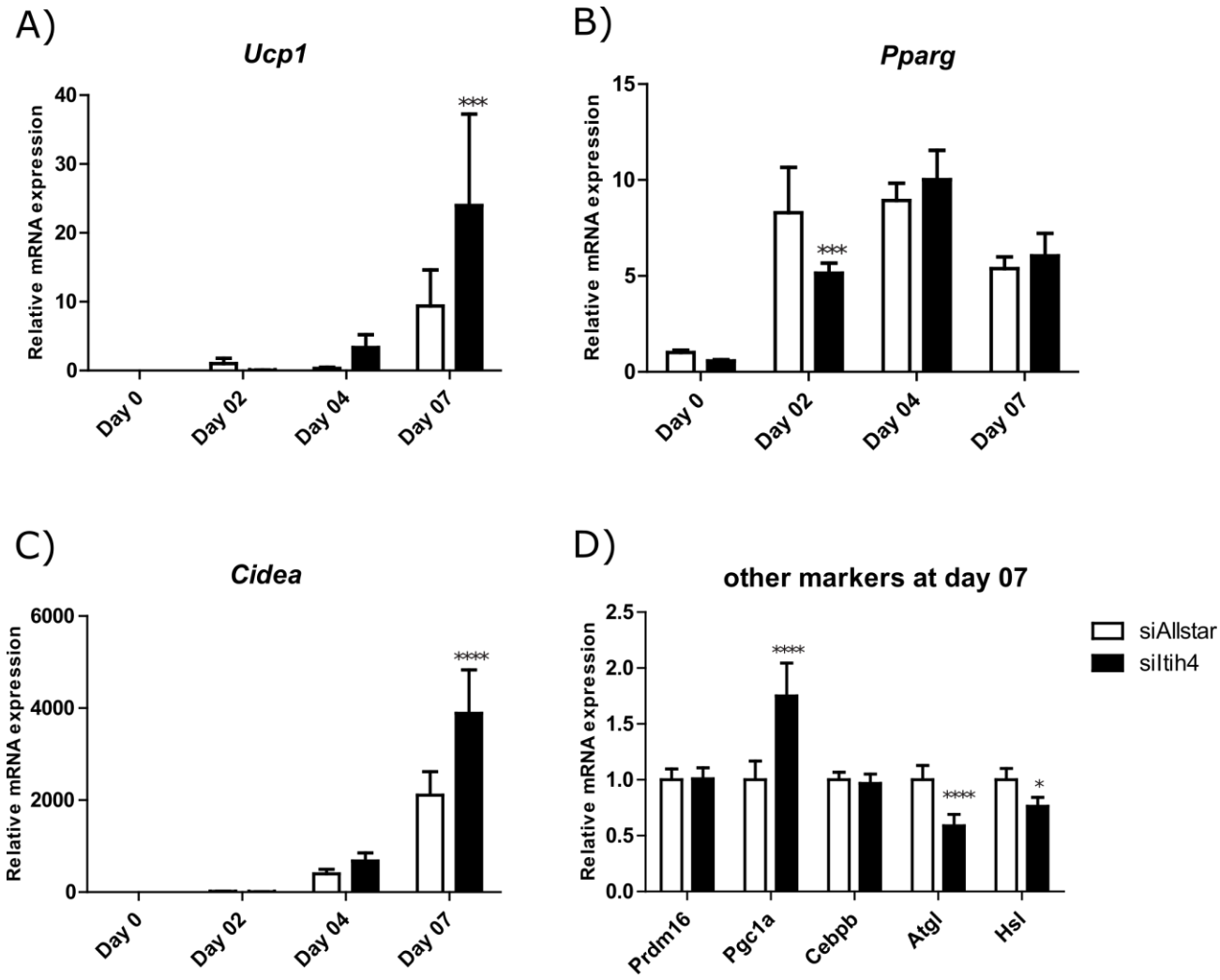

Figure 18: mRNA expression of BAT and mature adipocyte markers after ITIH4 knockdown. PreBAT cells were transfected with siItih4 (20 nM) or siAllstar (negative control, 20 nM) before differentiation and mRNA expression of various BAT markers like *Ucp1* (A), *Pparg* (B), *Cidea* (C), *Prdm16* (D), *Pgc1a* (D), *Cebpb* (D) and mature adipocyte markers like *Atgl* (D) and *Hsl* (D) were measured using qPCT at different time points of differentiation. n=3, means ±SEM, * indicates significance compared to siAllstar.

Contrary to what was expected BAT differentiation markers like *Ucp1, Cidea* and *Pgc-1a* were increased at the end of differentiation of ITIH4 knockdown PreBAT cells. Moreover, *Ucp1* and *Cidea* mRNA expression increased with differentiation of these cells. Other BAT markers like *Prdm16* and *Cebpb* and adipogenic marker *Pparg* were not changed (Figure 18 A - D). Interestingly, mature adipocyte markers like *Atgl* and *Hsl* were decreased with ITIH4

knockdown (Figure 18D). In the case of primary adipocytes, markers like *Cidea* and *Fabp4* were reduced with ITIH4 knockdown before differentiation (Supplementary figure 1).

Thus, at least in PreBAT cells the knockdown of ITIH4 did not lead to a decrease in the expression of BAT differentiation markers.

Intracellular triglyceride amounts and lipolysis were significantly reduced with ITIH4 knockdown

As mentioned above, the effect of ITIH4 on differentiation of PreBAT cells could not be confirmed using BAT and adipogenic markers. In order to validate this effect, both lipolysis and intracellular triglyceride (TG) accumulation were investigated in ITIH4 knockdown cells since lower overall lipolysis and TG amounts would be indicative of reduced differentiation and mature adipocytes. PreBAT cells were transfected with siItih4 and siAllstar (negative control) 2 days prior to the start of differentiation and lipolysis and TG amounts were analyzed on day 06 of differentiation. For the lipolysis assay, the cells were first starved and then stimulated with isoproterenol (10 µM). The non-esterified fatty acids (NEFA) were measured in the supernatant using a commercial NEFA kit. TG amounts were also measured at day 06 of differentiation. The cells were harvested, sonicated and centrifuged to obtain cell lysates containing TGs. The intracellular TG was measured using the Serum Triglyceride Determination Kit from Sigma.

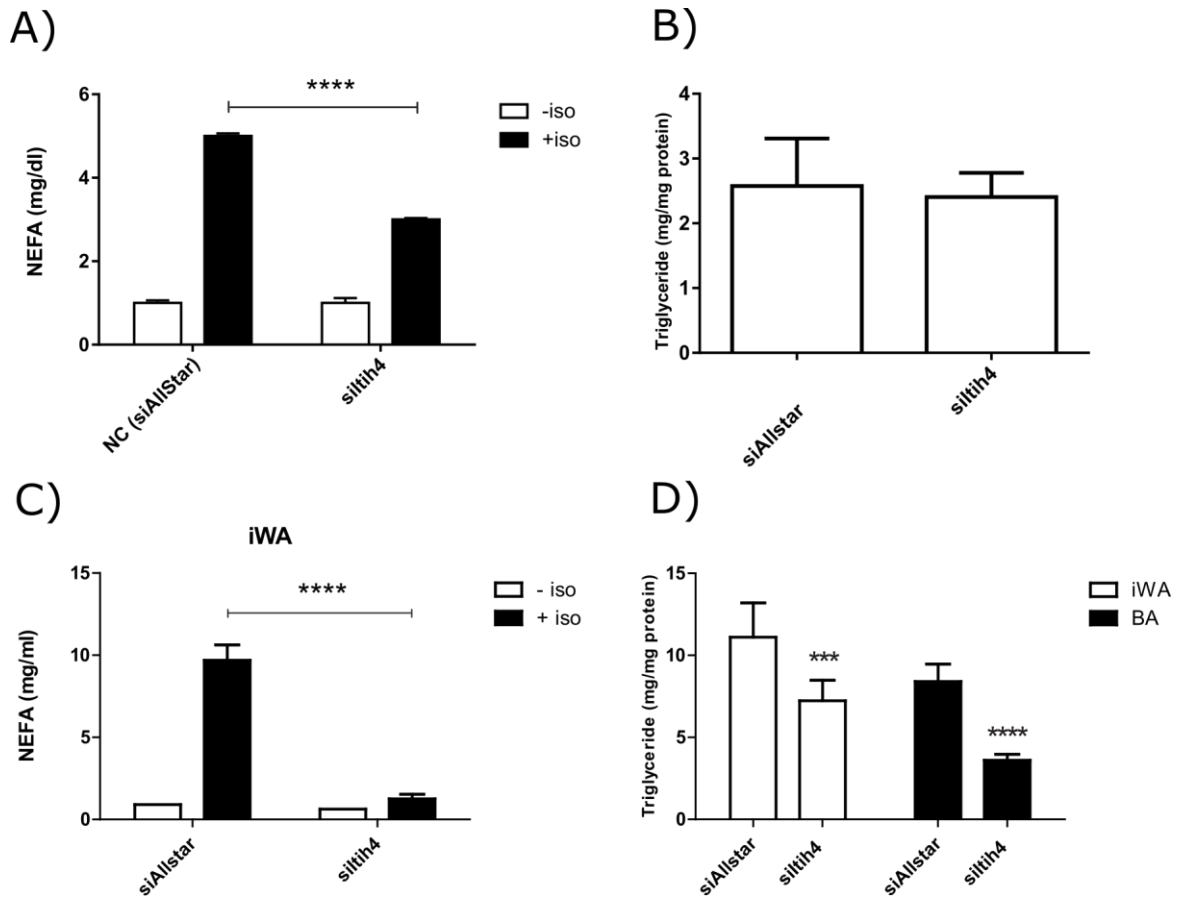

Figure 19: Lipolysis and triglyceride (TG) amounts after ITIH4 knockdown. ITIH4 was knocked down using siIth4 (20 nM) 2 days before differentiation in PreBAT cells. Lipolysis (depicted as non-esterified fatty acids, NEFA) after 3 hours of 10 µM isoproterenol treatment (A) and intracellular TG amounts (B) were measured at day 06 of differentiation. Primary brown and inguinal white preadipocytes were transfected with siItih4 (20 nM) or siAllstar (negative control, 20 nM) 2 days before the start of differentiation and lipolysis for inguinal white adipocytes (C) and TG amounts for both brown and inguinal white adipocytes were measured at day 08 of differentiation (D). n=3, means ±SEM, * indicates significance compared to siAllstar (negative control).

As observed from Figure 19A, ITIH4 knockdown resulted in a significant decrease in lipolysis when the differentiated PreBAT cells were treated with isoproterenol (β-adrenergic agonist) for 3 hours but no change in TG amounts was observed (Figure 19B). In primary cells however, ITIH4 knockdown led to significant reduction in lipolysis as well as TG amounts (Figure 19 C and D). Lipolysis in primary brown adipocytes could not be measured because ITIH4 knockdown led to very few differentiated brown adipocytes.

Thus, ITIH4 knockdown affected both lipolysis and TG amounts in primary adipocytes while only lipolysis was affected with PreBAT cells.

ITIH4 knockdown reduces glucose uptake and lipogenesis in PreBAT cells

In order to further validate the role of ITIH4 in differentiation, glucose uptake and lipogenesis- both crucial functions of differentiated adipocytes- were investigated in absence of ITIH4. As with previous experiments, ITIH4 was knocked down using siRNA before the start of differentiation. At day 02 of differentiation, the cells were incubated with D-[14C(U)]-Glucose and stimulated with insulin for 2 hours after which the cells were harvested and glucose uptake and lipogenesis were measured using a scintillation counter.

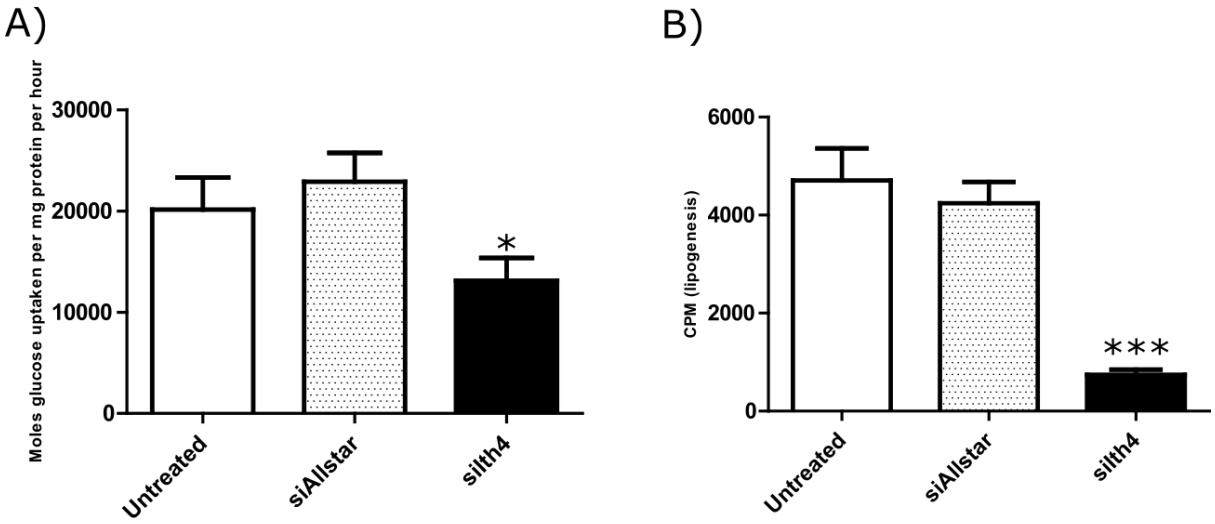

Figure 20: Glucose uptake and lipogenesis after ITIH4 knockdown in PreBAT cells. ITIH4 was knocked down in PreBAT cells using 20 nM siRNA before the start of differentiation. Glucose uptake (A) and lipogenesis (B) were measured at day 02 of differentiation after incubating the cells with D-[14C(U)]-Glucose (0.5 µCi/well) and insulin (10 nM) for 2 hours. n=3, means ±SEM, * indicates significance compared to untreated.

As shown in Figure 20A, ITIH4 knockdown led to a significant decrease in glucose uptake when compared to both untreated and negative controls (siAllstar). Similarly, lipogenesis was significantly reduced in the absence of ITIH4 (Figure 20B).

Thus, it can be concluded that ITIH4 knockdown in undifferentiated PreBAT cells alters mature adipocyte functions like lipolysis, TG accumulation, glucose uptake and lipogenesis possibly due to its effect on differentiation.

Transcriptome analysis of ITIH4 knockdown in PreBAT cells at different time points of differentiation

Next, global gene expression profiling was carried out on samples from different time points of differentiation following siRNA-mediated ITIH4 knockdown. This was done to fully characterize the gene expression changes occurring during differentiation with ITIH4 knockdown using Affymetrix chips. Similar to previous ITIH4 knockdown experiments, PreBAT cells were transfected with siAllstar (negative control) or siItih4 and differentiation was started after 2 days. Cells were harvested at day 02, day 04 and day 07 of differentiation and were subjected to microarray analysis. The microarray and subsequent analysis was carried out by Dr. Carsten Sticht from the Center of Medical Research, University of Heidelberg.

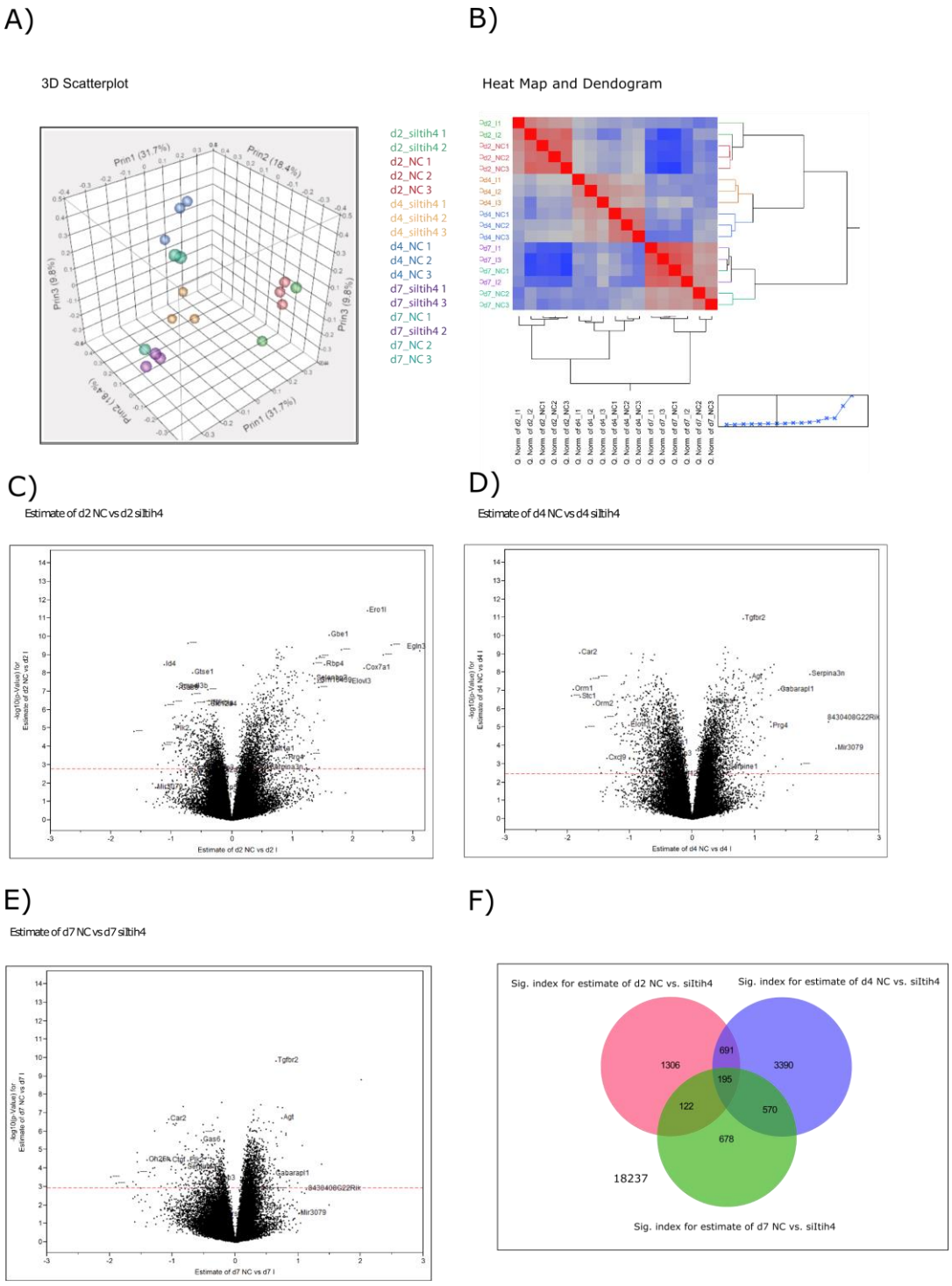

Figure 21: Gene expression profiling of PreBAT cells at different differentiation time points with ITIH4 knockdown. PreBAT cells were transfected with siItih4 (20 nM) and siAllstar (depicted here as NC, 20 nM) 2 days before induction of differentiation. Cells were harvested at day 02, 04 and 07 of differentiation and microarray analysis was carried out on GeneChip® Mouse Transcriptome Assay 1.0 chips. The 3D scatterplot (A), heat map (B), volcano plots for day 02 (C), day 04 (D), day 07 (E) and Venn diagram of significant hits (F) (from comparing negative control and siItih4 samples from the same time point) were generated from the transcriptome data. Abbreviations: d2, day 02; d4, day 04; d7, day 07; NC, negative control (siAllstar). n=3 for each group.

Figure 21 shows the data obtained from the microarray analysis. It can be observed from the 3D scatterplot (Figure 21A) and heat map (Figure 21B) that most of the biological replicates (with the exception of d7_NC1: day 07 negative control 1) cluster together. Thus, there was a high degree of reproducibility among the replicates. It can also be inferred from the heat map that the effect of time (day of differentiation) is stronger that the siRNA treatment since both the negative control (NC) and siItih4 samples for a time point cluster together. The volcano plots (Figure 21 C, D and E) show all the 25,190 genes obtained from the microarray analysis compared day-wise (in other words, negative control vs. siItih4 for day 02, for day 04 and for day 07) and all significantly altered genes (q-value < 0.05) are shown above the threshold (red dotted line). Figure 21F depicts the same day-wise comparison of significant genes (significant index = 1) including the genes common between the groups in the form of a Venn diagram.

Further analysis of ITIH4 knockdown transcriptome reveals regulation of important metabolic pathways and possible targets

The transcriptome data obtained from the microarray analysis of ITIH4 knockdown PreBAT cells during differentiation was further analyzed using Cytoscape and gene set enrichment analysis (GSEA) of KEGG pathways. Significant genes with a 2-fold or higher change in expression were selected and visualized using the 'Venn and Euler Diagrams' plugin for Cytoscape. Alternatively, for the GSEA of KEGG pathways, the list of genes were first annotated using entrez-IDs which resulted in reduction of the dataset to about 22,000 probe sets/genes. Using this dataset GSEA was performed using the KEGG pathway database. Dr. Carsten Sticht from the Center of Medical Research, University of Heidelberg, carried out this analysis.

A)

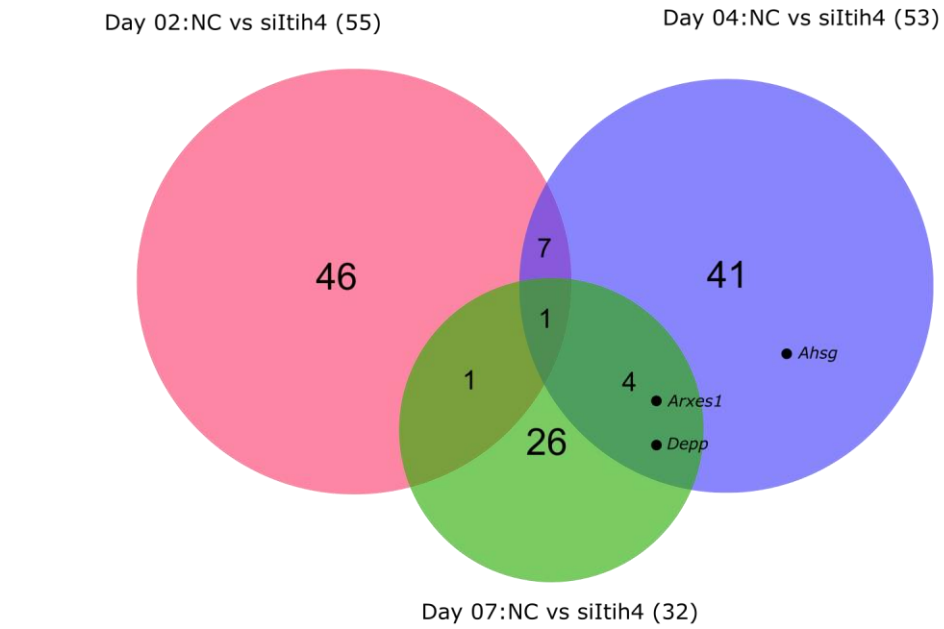
Day 02:NC vs siItih4 (55)
Day 04:NC vs siItih4 (53)
46
7
41
1
Ahsg
1
4
Arxes1
26
Depp
Day 07:NC vs siItih4 (32)

B)

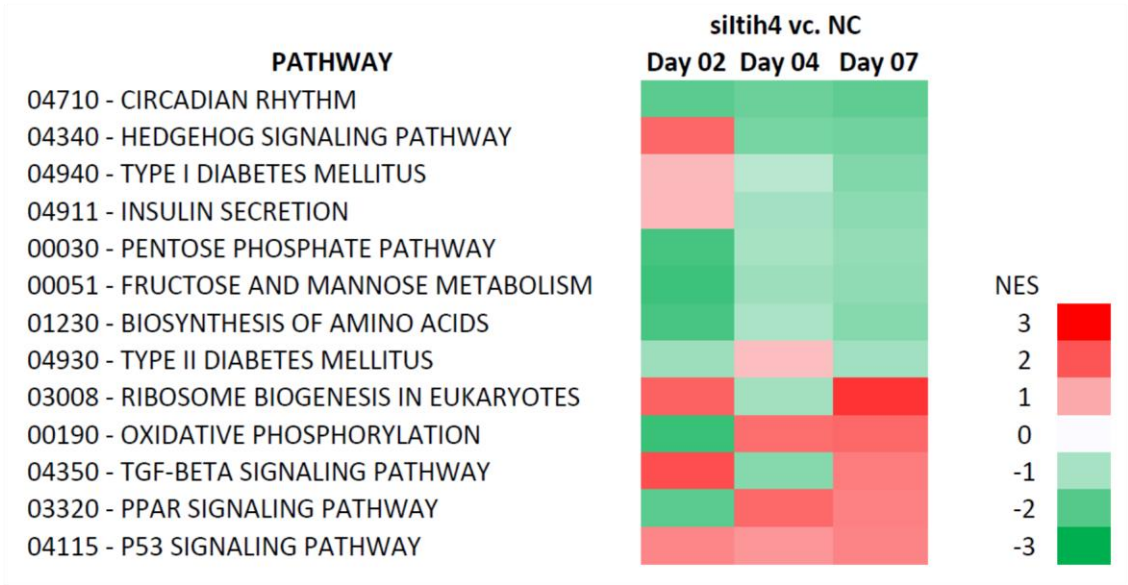
siItih4 vc. NC
PATHWAY
Day 02
Day 04
Day 07
04710 - CIRCADIAN RHYTHM
04340 - HEDGEHOG SIGNALING PATHWAY
04940 - TYPE I DIABETES MELLITUS
04911 - INSULIN SECRETION
00030 - PENTOSE PHOSPHATE PATHWAY
00051 - FRUCTOSE AND MANNOSE METABOLISM
01230 - BIOSYNTHESIS OF AMINO ACIDS
04930 - TYPE II DIABETES MELLITUS
03008 - RIBOSOME BIOGENESIS IN EUKARYOTES
00190 - OXIDATIVE PHOSPHORYLATION
04350 - TGF-BETA SIGNALING PATHWAY
03320 - PPAR SIGNALING PATHWAY
04115 - P53 SIGNALING PATHWAY
NES
3
2
1
0
-1
-2
-3

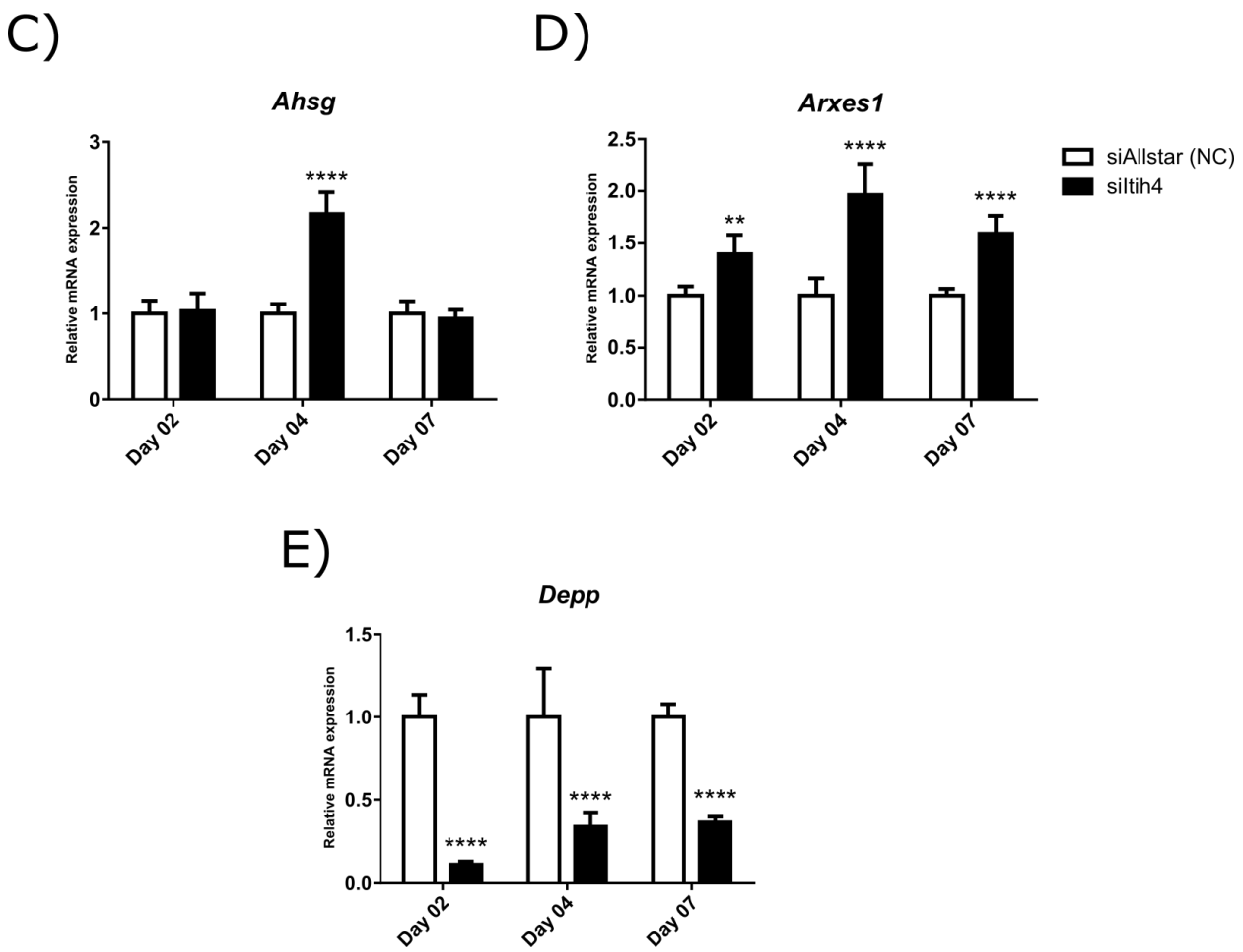

Figure 22: Further analysis of microarray data from ITIH4 knockdown cells. (A) A 2-fold cut off was selected for significant genes for the different groups and the Venn diagram was generated using Cytoscape. (B) Gene Set Enrichment Analysis (GSEA) was carried out on KEGG pathways and some of the pathways important in metabolism are depicted. Some of the promising targets from the microarray like *Ahsg* (C), *Arxes1* (D) and *Depp* (E) were validated using qPCR.. n=3, means ±SEM, * indicates significance compared to day 02 siAllstar (negative control). Abbreviations: NC, negative control (siAllstar); NES, normalized enrichment score.

Table 4: List of top 10 genes that were downregulated with ITIH4 knockdown according to the rank metric score from GSEA.

Day 02	Day 04	Day 07
Egln3 (Egl-9 Family Hypoxia-Inducible Factor 3)	*Depp* (Decidual Protein Induced By Progesterone)	*ITIH4* (Inter-Alpha-Trypsin Inhibitor Heavy Chain Family, Member 4)
C10orf99 (Chromosome 10 Open Reading Frame 99)	*Doc2b* (Double C2-Like Domains, Beta)	*Ppp1r15a* (Protein Phosphatase 1, Regulatory Subunit 15A)
Cox7a1 (Cytochrome C Oxidase Subunit VIIa Polypeptide 1)	*Cxcl13* (Chemokine (C-X-C Motif) Ligand 13)	*Depp* (Decidual Protein Induced By Progesterone)
Prelid2 (PRELI Domain Containing 2)	*Serpina3n* (Serpin Peptidase Inhibitor, Clade A Member 3N)	*Tbx5* (T-Box 5)
Tshr (Thyroid Stimulating Hormone Receptor)	*Prg4* (Proteoglycan 4)	*Gadd45a* (Growth Arrest And DNA-Damage-Inducible, Alpha)
Pdk1 (Pyruvate Dehydrogenase Kinase, Isozyme 1)	*Mmp11*(Matrix Metallopeptidase 11)	*Hoxc10* (Homeobox C10)
Elovl3 (ELOVL Fatty Acid Elongase 3)	*Fbxo31* (F-Box Protein 31)	*Tas2r126* (Taste Receptor, Type 2, Member 41)
Ppp1r3b (Protein Phosphatase 1, Regulatory Subunit 3B)	*Tat* (Tyrosine Aminotransferase)	*Gm867* (predicted gene 867)
Adrb2 (Adrenoceptor Beta 2, Surface)	*Ahsg* (Alpha-2-HS-Glycoprotein)	*Slc9b2* (Solute Carrier Family 9, Subfamily B Member 2)
Ero1l (ERO1-Like)	*Ctla2a* (Cytotoxic T Lymphocyte-Associated Protein 2 Alpha)	*Gm7168* (predicted gene 7168)

As can be observed from the Venn diagram in Figure 22A, very few targets with a fold change of two or greater were common between the different day-wise groups. Interestingly, the common target between all three different groups was miRNA-3079. In order to validate the microarray data three genes: *Ahsg*, *Arxes1* and *Depp* were selected from the different sample groups (Figure 22A) and their mRNA expression was analyzed using qPCR (Figure 22 C - E). The mRNA expression of the three candidates corresponded with the expression from the microarray analysis. Figure 22B shows the important metabolic pathways that were regulated with ITIH4 knockdown. Some of the pathways that were upregulated include the p53 signaling and TGF-β signaling pathway. Other pathways like circadian rhythm, hedgehog signaling pathway, type I diabetes mellitus, insulin secretion, pentose phosphate pathway, fructose and mannose metabolism and biosynthesis of amino acids were downregulated with ITIH4 knockdown. Other pathways that were significantly downregulated (NES>2) at day 02 were the oxidative phosphorylation pathway, PPAR

signaling, insulin signaling, carbon metabolism, glycolysis/gluconeogenesis and biosynthesis of unsaturated fatty acids (Supplementary figure 2). This initial time point (day 02) is important since effects of ITIH4 knockdown on differentiation would be strongest at the early stages of differentiation. Table 4 shows the top 10 genes that were downregulated with ITIH4 knockdown. These genes include *Egln3* (HIF-1 signaling), *Cox7a1* (oxidative phosphorylation), *Ppp1r3b* (insulin signaling), *Elovl3* (fatty acid elongation), *Tshr* (cAMP signaling pathway), *Gadd45a* (MAPK, FoxO and p53 signaling) and *Pdk1* (PPAR, FoxO and AMPK singaling). Thus, it can be concluded from this data that ITIH4 knockdown affects important metabolic pathways and genes.

ITIH4 knockdown in mature differentiated PreBAT cells

So far the effect of ITIH4 knockdown had been studied with its knockdown before the initiation of differentiation. To investigate its possible effects on mature adipocyte function, adenoviral vectors were used to knockdown ITIH4 near the end of differentiation. PreBAT cells were differentiated and transduced at day 06 of differentiation with Ad_shItih4 or Ad_NC (negative control virus) with an MOI of 100. *Itih4* mRNA expression and lipolysis was measured 2 days after transduction.

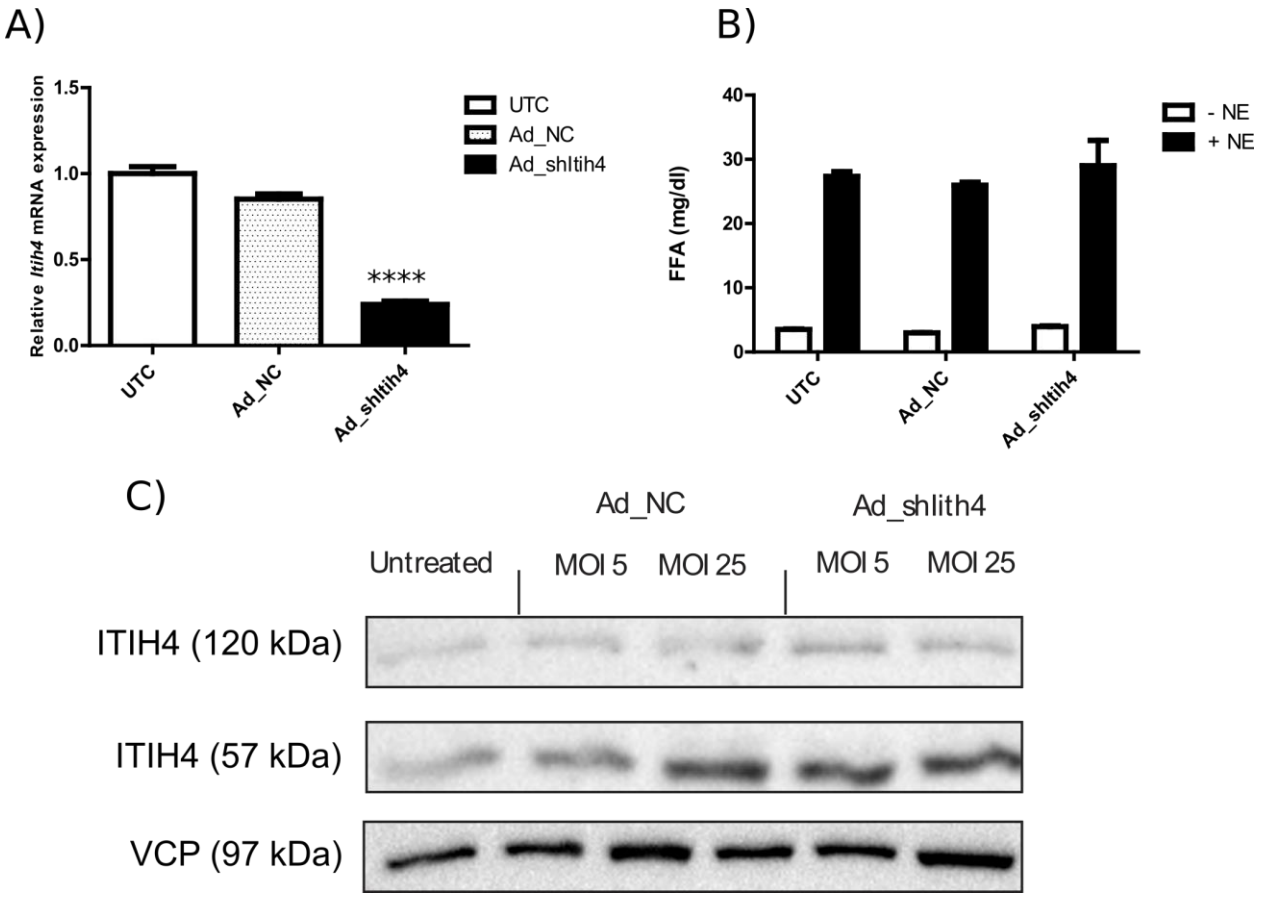

Figure 23: ITIH4 knockdown in mature adipocytes using adenoviral vectors. PreBAT cells were differentiated and were transduced with adenoviral vectors: Ad_NC (negative control) and Ad_shItih4 at an MOI of 100. *Itih4* mRNA expression (A) and lipolysis (B) was measured 2 days after transduction. (C) Immunoblotting of similarly transduced cells two days post-transduction. * indicates significance compared to untreated control. Abbreviations: NC, negative control (siAllstar); MOI, multiplicity of infection.

As shown in Figure 23A, transduction with Ad_shItih4 resulted in 75 % reduction of Itih4 mRNA levels compared to the untreated and negative controls. However, there was no change in lipolysis in these cells (Figure 23B). Immunoblotting of Ad_NC and Ad_shItih4 transduced mature PreBAT cells surprisingly did no show a reduction in protein expression of the 57 kDa N-terminal subunit (which was observed with siRNA knockdown) or the full length ITIH4 (Figure 23C).

Thus, using adenoviral vectors ITIH4 knockdown was possible at the mRNA level but not at the protein level in differentiated PreBAT cells. No change in lipolysis was observed with adenoviral ITIH4 knockdown. Therefore, ITIH4 knockdown at least at the mRNA levels did not result in changes in the lipolytic capacity of the mature adipocytes.

Discussion

Current technologies used in adipose tissue/adipocyte secretome studies

Due to their high sensitivity and speed soft ionization techniques like MALDI (matrix-assisted laser desorption) and electrospray along with mass analyzers like time of flight (TOF), ion trap or quadrupole analyzers have made mass spectroscopy the technique of choice for extensive proteomic studies. Therefore, it comes as no surprise that liquid chromatography-tandem mass spectrometry (LC-MS/MS) is used in most secretome studies and screens. The most challenging problem in secretome studies is the elimination of protein contaminants that usually mask the presence of relevant protein candidates. The common techniques to circumvent this problem include: 1) the treatment of cells with Brefeldin A (BFA) which blocks the classical secretory pathway and distinguishes the secreted proteins from leaked proteins, 2) growth of cells in the absence of serum and serum contaminating proteins and 3) the use of labeling techniques like radioactive labeling with 35S methionine to discriminate contaminating non-labeled serum proteins. In general these methods help identify proteins secreted by the classical secretory pathway and discriminate secreted proteins from serum contaminants. However, treatment with BFA and the absence of serum are stressful to the cells and affect the cell physiology while 35S labeling induces DNA damage and leads to cell cycle arrest and apoptosis (Hu, Heikka et al. 2001). Thus, these methods have profound effects on the cells and could alter the normal cellular secretome.

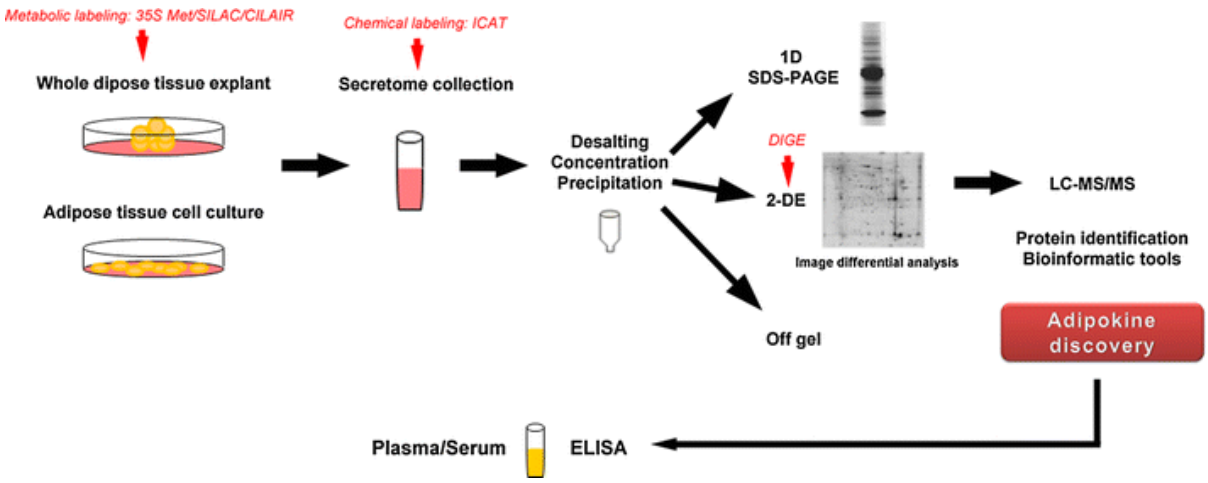

Figure 24: Common workflow involved in adipose tissue/adipocyte secretome screening. Quantitative applications are depicted in red. Abbreviations: SILAC, stable isotope labeling by amino-acid in cell culture; CILAIR, comparing isotope-labeled amino acid incorporation rates; ICAT, isotope-coded affinity tag; DIGE, Difference gel electrophoresis. Adapted from Pardo, Roca-Rivada et al. (2012).

Figure 24 shows a workflow of a typical adipose tissue secretome study. First, either adipose tissue explants or adipocytes are subjected to appropriate labelling techniques that allows labeling of newly synthesized proteins. These techniques include: SILAC (stable isotope labeling by amino-acid in cell culture) in which cells are treated with different amino acid isotopes in cell culture media, CILAIR (comparing isotope-labeled amino acid incorporation rates) which consists of comparing secreted proteins based on different incorporation rates of a labeled amino acid (like 13C-labeled lysine) and radioactive 35S methionine labeling. Next, the supernatant containing the secreted proteins are collected and enriched using a variety of methods which include desalting, precipitating and concentrating using appropriate columns. The next step usually involves techniques for electrophoretic protein separation like 1D SDS-PAGE or 2-dimenstional electrophoresis (2-DE) followed by LC-MS/MS and bioinformatics analysis of the identified proteins.

The secretome workflow used in this study uses the SILAC method to label the newly synthesized proteins. However, the novel aspect of this secretome study was the use of Click-iT® AHA labeling which replaces methionine with its analogue L-azidohomoalanine (AHA) in the newly synthesized proteins. Due to this incorporation the secreted proteins can be efficiently and selectively fished out by covalent capture on alkyne-activated resin using click chemistry (copper-catalyzed azide–alkyne cycloaddition). The advantage of this step allows for the efficient elimination of protein contaminants especially from media serum which is a major hurdle in secretome studies (as mentioned earlier). In addition, the incorporation of AHA does not seem to have adverse effects on cellular growth as was measured here with the degree of LDH release. Click-iT® AHA labeling also eliminates the need for extensive time-consuming peptide fractionation. Another advantage of the present secretome study is use of pulsed-SILAC (pSILAC). pSILAC, unlike full SILAC labeling, is capable of differentiating and quantifying newly synthesized proteins from pre-existing proteins. The

efficacy of this screening system had been validated by Eichelbaum, Winter et al. (2012) by comparing the secretomes of primary hepatocytes and cell lines – Hepa1-6 and Hepa1c1.

Thus, the combination of Click-iT® AHA and pSILAC labeling circumvents some of the fundamental drawbacks of common secretome screens and can be considered a powerful and reliable tool in the study of adipose tissue/adipocyte secretomes.

Comparative brown adipocyte secretome screen

The secretome screening carried out in this study is the first documented secretome analysis involving brown adipocytes. The secretome screens involved comparing the secretome from inguinal white adipocytes and brown adipocytes in the presence and absence of norepinephrine stimulation as well as factors from only brown adipocytes under the same stimulatory conditions. Among the 1013 unique proteins identified, 406 proteins had evidence of secretion (experimental and prediction by SignalP). This list does not include proteins that were secreted through alternative non-classical secretory pathways. Therefore, this number might underrepresent the actual number of truly secreted proteins. Moreover, this number is close to what was obtained in other adipocyte secretome studies. For example, the first whole human adipose tissue secretome by Alvarez-Llamas, Szalowska et al. (2007) identified 259 proteins, of which 108 contained a signal peptide. Similarly, Roca-Rivada, Alonso et al. (2011) detected about 50% secreted proteins from the secretome mapping of their secretome analysis of different rat adipose tissue depots. Another aspect of the current study is the number of detected secreted proteins that were represented as extracellular proteins and signaling molecules according to Panther protein classification. This is also in accordance to other adipocyte secretome studies (Alvarez-Llamas, Szalowska et al. 2007, Chiellini, Cochet et al. 2008) and further underlines the importance of extracellular remodeling and extracellular matrix proteins secreted by the adipose tissue (As reviewed by Mariman and Wang 2010).

Potential batokine candidates

As mentioned earlier, 29 candidates that were differentially secreted proteins between two screens were selected for further evaluation. Namely, these candidates were common between NE-stimulated white vs. NE-stimulated brown adipocytes and NE-stimulated vs. unstimulated brown adipocytes. This criterion was selected on the assumption that a potential batokine would have differential secretion when BAT is activated by the sympathetic nervous system (SNS) (for example, with cold stimulation). Of course these candidates also include proteins that show increased or decreased secretion with NE stimuli.

The following table shows the classification of these 29 candidates and what their secretion levels imply.

Table 5: Distribution of the 29 batokine candidates and their potential classification

BA +NE vs. BA –NE	WA +NE vs.BA +NE	Classification and description	Number of candidates
↑	↑	**General adipokine:** Proteins secreted in NE-stimulated BA and WA.	6
↑	↓	**Potential batokines:** Higher with NE in BA and higher than NE-stimulated WA.	4
↓	↑	**Novel adipokine from WA:** Down-regulated with NE stimulation in BA but higher in WA.	10
↓	↓	**NE-inhibited batokine:** Down-regulated with NE in BA but higher in BA compared to WA.	9

As evident from Table 5, the secretion of most batokine candidates was lowered with NE stimulation of BA. Therefore, the secretion of these candidates is inversely correlated with activated BA and a reduction in their secretion could perhaps bring about the beneficial systemic effects of activated BAT. It is also feasible that the list of batokine candidates contains a pair of counter-regulatory hormones whose secretion is regulated in opposite directions with BAT activation.

Known adipokines like adiponectin, resistin, ANGPTL4, LPL, adipsin (complement factor D) etc. were present in the list of selected 29 batokine candidates. In contrast, other prominent adipokines like leptin, IL-6 and TNF-α were absent in the selected list as well in the complete the secretome screen. This could be due to primary adipocyte culture and stimulation conditions, stability of the factors during the 24 hour incubation period or no secretion from one cell population of the comparative study.

Interestingly, 5 members of the collagen alpha chain proteins were among the 29 batokine candidates. As mentioned earlier, extracellular matrix proteins like the collagen alpha chains are important secreted factors for the maintenance of the adipose tissue extracellular matrix. An interesting secretome candidate is osteopontin (OPN) which so far has been known to be primarily secreted from immune cells including adipose tissue macrophages and contributes to obesity-induced macrophage infiltration, inflammation and insulin resistance (Nomiyama, Perez-Tilve et al. 2007). In addition, OPN also stimulates hepatic gluconeogenesis (Kiefer, Zeyda et al. 2010). It would be interesting to investigate the relationship between OPN function and BAT activation. Other interesting candidates are dermatopontin (DPT) which regulates ECM architecture (Kato, Okamoto et al. 2011) and nucleotide pyrophosphatase/phosphodiesterase 2 (ENPP2, autotaxin) that has been shown to influence BAT activity, energy expenditure and adipose tissue expansion (Nishimura, Nagasaki et al. 2014).

It is worth noting that other extracellular stimuli, apart from SNS response to cold, can also activate thermogenesis in BAT. These activators include irisin, natriuretic peptides, bile acids and FGF21 (As reviewed by Villarroya and Vidal-Puig 2013). Therefore, it is possible that batokines released by such alternative activation of BAT might not be included in this secretome study.

GSIS and other functional assays for batokines

The GSIS assay using INS-1E cells was the first functional assay to be optimized for investigating the effects of the batokine candidates on insulin secretion. It was concluded from these experiments that glucose stimulation in fresh KRBH buffer and the use of recombinant batokine adiponectin were the optimum conditions for this assay. It was surprising to note that fresh RPMI and KRBH - - CM resulted in a very low fold change in insulin secretion due to very high basal insulin secretion in the absence of glucose. This would suggest that an insulin secretagogue (or secretagogues) is present in the RPMI media and is also released by HEK 293A cells that stimulates insulin secretion on its own independent of glucose. Nonetheless, this complicates the direct use of CM for the GSIS assay and makes the use of fresh KRBH the optimum method for the stimulation and detection of GSIS.

At least in the case of adiponectin, the recombinant protein resulted in an increase in GSIS while adiponectin CM had no effect. Furthermore, preliminary experiments using two commercially available recombinant secretome candidates affected GSIS (data not shown) but additional experiments are needed to confirm this observation. However, not all 29 candidates were commercially available and it could be possible that the other candidate CMs are more effective than adiponectin in modulating GSIS. Therefore, it would be still be worthwhile to pursue the optimization of the assay using conditioned media.

ITIH4 as a batokine and BAT activity marker

Inter-alpha-trypsin inhibitor heavy chain H4 (ITIH4) is a 120 kDa acute-phase glycoprotein which is strongly expressed in liver where it has shown to be important in early liver development and regeneration (Bhanumathy, Tang et al. 2002). It is well documented as a biomarker for various diseases like prostrate cancer (Davalieva, Kiprijanovska et al. 2015), heart disease (Nayak, Kashyap et al. 2012), amyotrophic lateral sclerosis (Tanaka, Shimazawa et al. 2013). It is highly sensitive to cleavage by plasma kallikrein and is cleaved in to smaller fragments that are thought to be bioactive (Pu, Iwamoto et al. 1994, Nishimura, Kakizaki et al. 1995) .

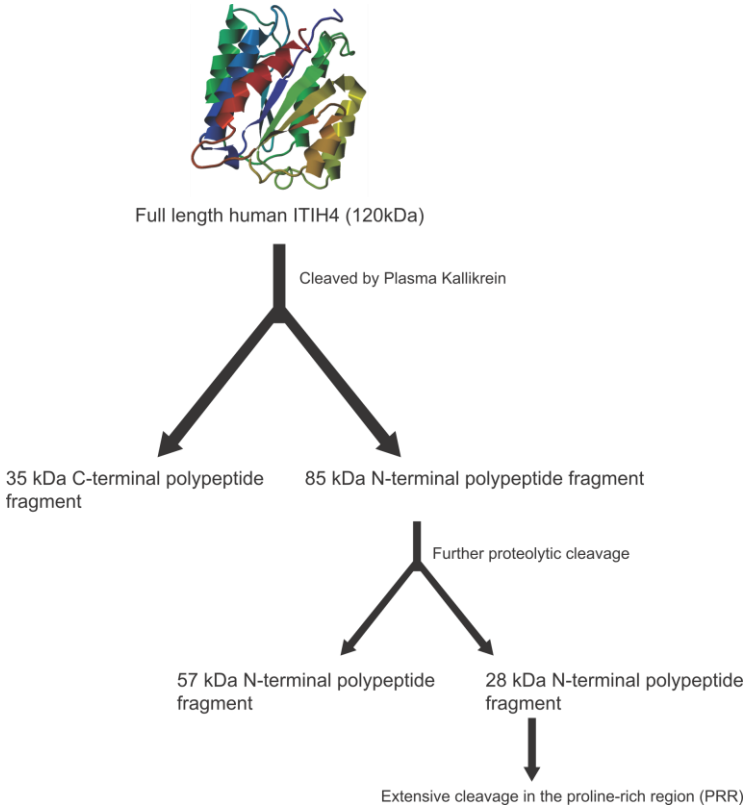

Figure 25: Proteolytic cleavage of ITIH4. Full length ITIH4 (120 kDa) is initially cleaved in to two polypeptides with molecular weights of 85kDa (N-terminal) and 35 kDa (C-terminal). The 85 kDa polypeptide is further cleaved culminating with extensive cleavage in the proline-rich region (PRR).

As shown in Figure 25, the full-length ITIH4 is first cleaved into the 35 kDa C-terminal and 85 kDa N-terminal polypeptides. The 85 kDa polypeptide is further cleaved into several fragments including the 57 kDa N-terminal polypeptide that was detected in PreBAT cells. The 35 kDa fragment is O-glycosylated and not cleaved further. Interestingly, Mohamed, Abdul-Rahman et al. (2008) showed that this fragment is increased in the serum of certain cancer patients like breast cancer, epithelial ovarian carcinoma and germ cell ovarian carcinoma but not in nasopharyngeal carcinoma and osteosarcoma. In addition, Song, Patel et al. (2006) characterized the cleavage products from the proline-rich region (PRR) of ITIH4 and showed that certain diseases like diabetes, colon cancer, breast cancer etc. have specific cleavage patterns in this region.

Thus, it is possible that BAT activation could lead to changes in certain ITIH4 bioactive fragments in the serum rather than the whole protein and this change in ITIH4 cleavage profile could bring about the systemic changes observed with BAT activation and reflect BAT activity. In conclusion, an ELISA would be insufficient to capture the complete ITIH4 profile in the serum and more sensitive and comprehensive methods like LC-MS/MS would be needed.

ITIH4 as a regulator of adipocyte differentiation

The role of ITIH4 in adipocyte biology was investigated after observing a 70-fold higher expression of *Iith4* mRNA expression in primary brown compared to inguinal white adipocytes. *Itih4* mRNA levels were shown to increase with differentiation of various adipocyte cell lines and primary adipocytes. *Itih4* expression was also higher with rosiglitazone treatment during the differentiation of 3T3-L1 cells which induces a brite-like phenotype in these cells. Moreover, only *Itih4* mRNA levels among the six members of the ITIH protein family were increased with differentiation of inguinal white precursor cells in the presence of $cPGI_2$ (a potent browning agent) (Supplementary figure 3). Therefore, *Itih4* expression was also upregulated with browning and differentiation *in vitro*.

Upon ITIH4 knockdown, impairment of differentiation was observed with a stronger phenotype displayed in primary adipocytes compared to PreBAT cells. This was concluded from reduction in lipolysis, TG accumulation, glucose uptake, lipogenesis and Oil Red O staining. However, the adipogenic markers were not changed with differentiation for PreBAT cells. The change in adipogenic markers is generally considered a gold standard in studying effects on adipogenesis. One reason for the lack of changes in adipogenic markers could be the PreBAT cell physiology. The presence of the Large T antigen could push these cells to a stronger differentiation phenotype thereby making them immune to the effects of ITIH4 knockdown to a certain extent. This could also be the reason for the stronger differentiation phenotype observed in the primary adipocytes compared to PreBAT cells. Only two adipogenic markers - *Cidea* and *Fabp4* - were measured in primary adipocytes. These markers were decreased after ITIH4 knockdown. Other markers also need to be measured in primary adipocytes to conclusively prove the effect of ITIH4 on differentiation. Alternatively, another plausible explanation for no changes in adipogenic markers could be that ITIH4 has a differentiation independent effect on adipocyte function. For example, the observed changes in lipolysis, lipogenesis and TG accumulation could be due to increased fatty acid oxidation after ITIH4 knockdown. To investigate this hypothesis, fatty acid oxidation assays using the Seahorse XF analyzers or radioactive tracers can to be carried out. Alternatively, the same metabolic assays like lipolysis, lipogenesis and TG accumulation can be carried out after ITIH4 knockdown in differentiated adipocytes to investigate the differentiation independent effects of ITIH4. This was attempted in differentiated PreBAT cells using adenoviral vectors. Adenoviral-mediated knockdown resulted in reduction of mRNA levels but not in protein levels. This could be due to fact that ITIH4 is heavily glycosylated (Chandler, Brnakova et al. 2014), which increases its stability.

The exact mechanism as to how ITIH4 affects differentiation could not be elucidated. However, the transcriptome analysis of ITIH4 knockdown cells was able to shed light on possible target genes and pathways affected. An interesting target is *Depp* (Decidual protein induced by progesterone) or *Fig* (Fasting-induced gene) which is highly expressed in

human WAT. Mouse *Depp* mRNA expression was shown to increase with fasting in lung, skeletal muscle and WAT and also with differentiation of 3T3-L1 cells (Kuroda, Kuriyama et al. 2010). Another target could be *Arxes1* (Adipocyte-related X-chromosome expressed sequence 1) which was shown to be required for adipogenesis (Prokesch, Bogner-Strauss et al. 2011). Various microRNAs have been shown to be important for adipogenesis (As reviewed by Peng, Yu et al. 2014). In this regard, miR-3079 is also a promising target since its expression was significantly altered at all time points after ITIH4 knockdown. Interestingly, at day 02 its expression was transiently increased and later decreased. So far miR-3079 has not been functionally characterized. However, it should be noted that ITIH4 is not a transcription factor and most likely affects the expression of these targets indirectly.

The pathways affected with ITIH4 knockdown also hint to the possible mechanism behind its effect on adipocyte differentiation. The oxidative phosphorylation pathway was initially downregulated with ITIH4 knockdown. The top component decreased in this pathway was *Cox7a1* which was shown to be highly expressed at the protein level with cold exposure (4°C) in mice BAT (Forner, Kumar et al. 2009) as well as hypothesized to be the more active isoform of COX7a which might increase the thermogenic capacity of BAT (Maurer, Fromme et al. 2012). Similar to the oxidative phosphorylation pathway, PPAR signaling was also decreased initially with ITIH4 knockdown. The expression of CD36 - which promotes adipocyte differentiation and adipogenesis (Christiaens, Van Hul et al. 2012) - was significantly decreased in this signaling pathway. Other important pathways were also downregulated at the initial time point like insulin signaling, carbon metabolism etc. Interestingly, these pathways and the afore-mentioned genes were back to normal levels at later time points of differentiation. This would imply that the PreBAT cells adapt and compensate for the downregulation of these pathways. In contrast, one of the pathways that were upregulated was the TGF-β signaling pathway. TGF-β signaling pathway plays an important role in browning (As reviewed by Yadav and Rane 2012) and inhibition of this pathways leads to browning in WAT (Yadav, Quijano et al. 2011). Therefore, it could be possible that ITIH4 interacts with a component of the TGF-β signaling pathway and influences differentiation.

It is interesting to note the control of ITIH4 expression in mature adipocytes. A reduction in *Itih4* mRNA expression was observed in differentiated PreBAT cells with isoproterenol and rosiglitazone treatment. Both these stimuli are adipogenic and a significant reduction in ITIH4 expression could again point to a differentiation independent function of ITIH4 in mature adipocytes. In addition, *Iith4* mRNA expression did not increase with IL-6 treatment as was observed in hepatocytes and HepG2 cells. Taken together, this would indicate that in adipocytes transcription of *Itih4* is not under the control of IL-6 signaling but is influenced by AMPK, β-adrenergic and PPARγ signaling.

Surprisingly, *Itih4* mRNA levels were decreased in the adipose tissues of *db/db* mice while they were increased with Treg depletion. Both these models exhibit a pro-

inflammatory state in their adipose tissue depots but a possible explanation for this difference could be that the adipose tissues in *db/db* mice exhibit a more chronic grade inflammation while Treg depletion leads to an acute type of inflammation. As mentioned earlier, ITIH4 is an acute phase protein and therefore, its expression increases with Treg depletion. The high amounts of leptin in *db/db* mice could not be the reason for the decrease in *Itih4* levels as *in vitro* treatment of differentiated PreBAT cells with recombinant leptin did not lead to changes in *Itih4* mRNA levels. Other differences between the Treg depleted and *db/db* models like the presence of crown-like structures (CLS) and hypertrophic adipocytes in the adipose tissues of *db/db* mice could somehow affect *Itih4* expression and result in this discrepancy in *Itih4* mRNA expression between the two models (Murano, Barbatelli et al. 2008). The decrease in *Itih4* levels in *db/db* mice also hint to a possible role of ITIH4 in stabilizing the extracellular matrix (like the other members of the ITI family) since chronic models of inflammation and obesity involve extensive remodeling of the extracellular matrix and expansion of adipose tissues (Bost, Diarra-Mehrpour et al. 1998).

ITIH4 is a special member of the Inter-α-trypsin inhibitors (ITI) family of plasma protease inhibitors in terms of its structural properties. It possesses some unique features in its C-terminal region like a plasma kallikrein cleavage site, an ATP-dependent-protease like domain and a proline rich region (PRR). In addition, unlike the other members it cannot bind to hyaluronic acid and bikunin (light chain member of the ITI family) and is only 30-38 % identical to the other members of the ITI family both in humans and mice. By virtue of its difference structural properties, it is possible that ITIH4 has distinct functions compared to the other ITI family members and is therefore, an interesting serine protease inhibitor worth investigating.

Summary and outlook

The combination of Click-iT® AHA labeling and pulsed-SILAC is a powerful tool for studying secretomes. In addition, the brown adipocyte secretome has not been investigated in detail. Thus, using these techniques to characterize the brown adipocyte secretome is a promising strategy to discover novel adipokines secreted from brown adipocytes (‘batokines’) that help BAT communicate with different organs and influence whole-body metabolism. Indeed the data obtained from the three screens was in accordance to previously reported adipose tissue/adipocyte secretome studies in terms of number and functional classification of the secreted proteins. In addition, a number of unique and interesting secretome candidates were detected in the screen like dermatopontin, osteopontin and ectonucleotide pyrophosphatase/phosphodiesterase 2. To identify the metabolically relevant candidates a series of unbiased functional assays were planned. In this regard, the glucose stimulated

insulin secretion (GSIS) assay was optimized with regard to buffer/CM conditions for glucose stimulation and the use of CM or recombinant proteins. The use of CM would be further optimized and the assay will be tested in other insulin secreting cell lines like the mouse MIN6 cell line. This is a mouse insulinoma cell line and would be more compatible with the secretome candidates which are over-expressed mouse proteins. In addition, the high throughput lipolysis assay will be a promising assay to test whether the candidate batokines induce lipolysis in white adipocytes. An additional approach to study the batokine candidates would be to investigate the expression of corresponding receptors in different organs in order to narrow down possible function. For example, higher receptor expression of a batokine candidate in iWAT would point to its possible role in browning, lipolysis or glucose uptake in white adipocytes.

The data presented in this dissertation work elucidates the function of ITIH4 in adipocyte biology. Knockdown of ITIH4 in primary preadipocytes and preadipocyte cell lines showed that ITIH4 is required for adipogenesis and affects key adipocyte functions. The only other known reported function of ITIH4 is its role in liver growth and regeneration (Bhanumathy, Tang et al. 2002). The findings presented here underlie the biological significance of ITIH4 apart from its extensive documentation as a biomarker for various diseases. In this regard, it would also be important to reaffirm the role of ITIH4 in adipogenesis through over-expression and rescue experiments as well as measuring adipogenic markers in primary adipocytes after ITIH4 knockdown. For ITIH4 over-expression and rescue studies, the electroporation of PreBAT cells using EGFP expression construct (pEGFP-N1) was optimized for use with ITIH4 expression constructs (Supplementary figure 4). However, the mechanism through which ITIH4 influences adipocyte differentiation still needs investigation. MiR-3079 is a promising target and experimental modulation of its expression in PreBAT cells could yield valuable insights to the function of ITIH4. Also a co-immunoprecipitation screen for ITIH4 interacting proteins would provide useful information in this direction. A recombinant ITIH4 myc-flag tag protein was successfully co-immunoprecipitated using the flag tags (Supplementary figure 5). Another potential experiment would be to carry out a proteome analysis with ITIH4 knockdown and combine it with the transcriptome analysis. In addition to its mechanism, the role of ITIH4 *in vivo* also needs to be investigated. For this purpose, an adeno-associated virus (AAV) was generated which expresses *Itih4* microRNA only in UCP1 expressing cells. Furthermore, it will be interesting to investigate the function of ITIH4 in other models of genetic and experimental obesity such as *ob/ob* or HFD fed mice respectively.

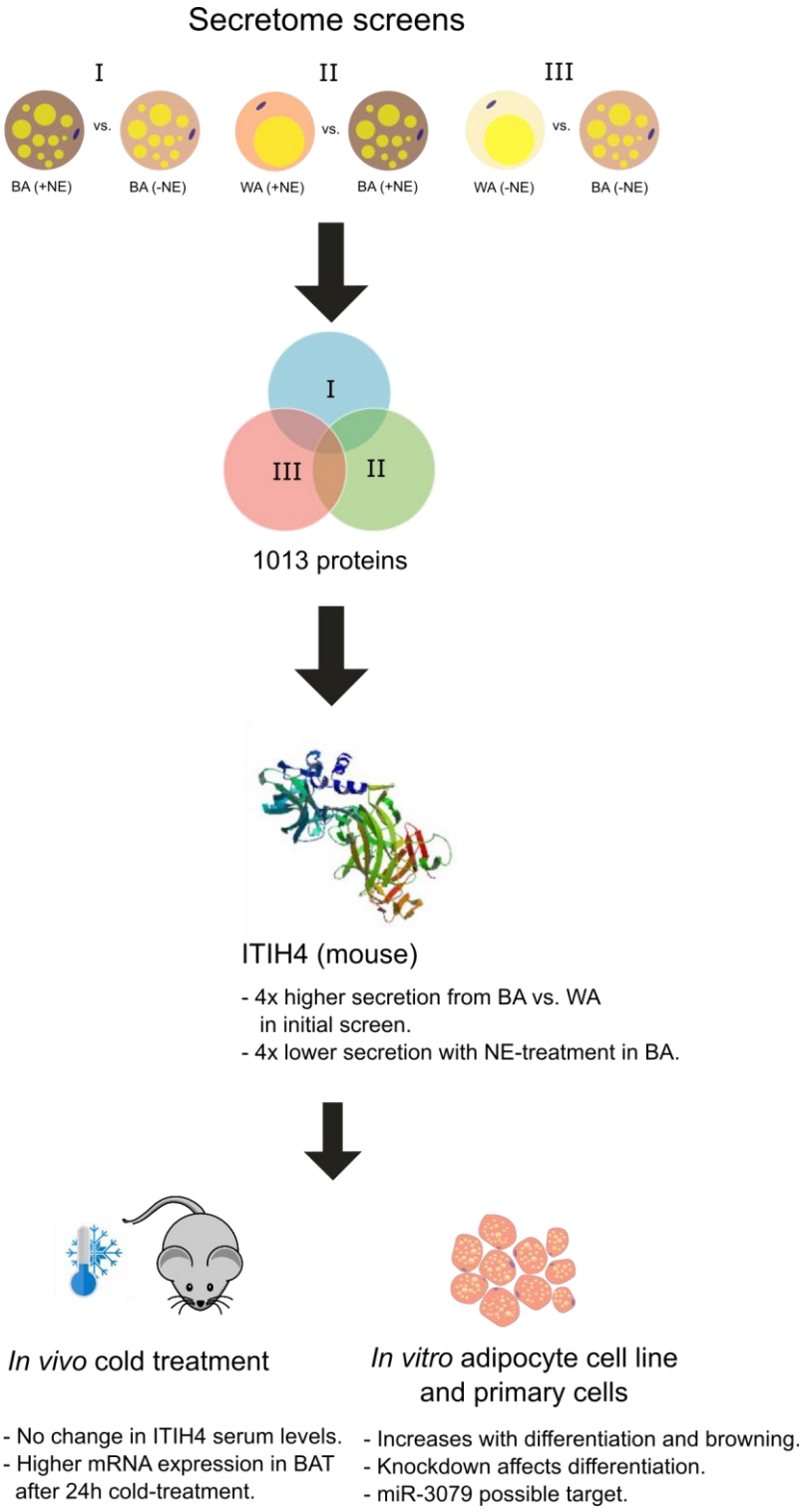

Figure 26: Overview of the project. The dissertation work started with three different secretome screens involving BA and WA with or without NE stimulation to identify batokine candidates. ITIH4 was among the 1013 distinct proteins identified and was differentially secreted in the screens. Serum levels of ITIH4 did not change with cold treatment but *Itih4* mRNA was increased in BAT. *In vitro* experiments in adipocyte cell lines and primary adipocytes pointed to a function of ITIH4 in adipogenesis. Abbreviations: BA, brown adipocytes; WA, white adipocytes; NE, norepinephrine.

Methods

Molecular biology

Genomic DNA Isolation from differentiated primary adipocytes

The cells were first lysed using 500 µl of Lysis Buffer (10 mM Tris pH 8.0, 100mM NaCl, 15 mM EDTA, 0,5% SDS, 0,5 mg/mL Proteinase K) and incubated overnight at 37°C. The lysis solution was then transferred to 2ml tubes and 250 µl of 6M NaCl was added. The tubes were gently mixed by inverting them and shaken at 800 rpm at room temperature for 5 minutes. The tubes were then centrifuged for 10 minutes at 13000 rpm (4°C) and the supernatant was transferred to pre-chilled peqGOLD PhaseTrap A 2ml tubes (peqlab, 30-0020A-01). Next, 700 µl of phenol/chloroform was added and mixed by inverting the tubes. The tubes were again centrifuged for 10 minutes at 13000 rpm (4°C) and the supernatant separated by the PhaseTrap™ was transferred to fresh pre-chilled peqGOLD PhaseTrap A 2ml tubes. Next, 700 µl of chloroform was added and the same procedure of mixing and centrifugation was carried out as above. The supernatants were transferred to new 1.5 ml tubes and 1 µl of Pellet Paint® Co-Precipitant (Millipore, 69049) was added to each sample along with 550 µl isopropanol. The samples were mixed by inverting, shaken for 2 minutes (800 rpm) and centrifuged at 8000 rpm for 10 minutes (4°C). The supernatants were decanted and the pellets (visible due to the Pellet Paint® Co-Precipitant) were washed with 1 ml 75% ethanol then centrifuged at 13,000 rpm for 5 minutes at 4°C. The pellets were air-dried for 5 minutes and then re-solubilized in 150 µl Tris-EDTA buffer (pH 8.0) at 60°C for 2 hours or overnight at 4°C.

Plasmid DNA isolation

Plasmid DNA from *E.coli* cultures was isolated using Qiagen kits. For small cultures of 2 ml – 5 ml, QIAprep Plasmid Miniprep Kit was used while QIAGEN Plasmid Mega Kit was used for larger cultures of 200 ml or more. The manufacturer's protocol provided along with the kit was followed for the plasmid isolations.

RNA isolation using Trizol

Animal tissues (10-30 mg) were transferred into a 2 mL nuclease-free reaction tube containing 1 mL of Qiazol™ Lysis reagent and a stainless steel bead. The samples were lysed using the TissueLyser™ for 90 sec/30 Hz. In the case of adherent cells, 700 µl (for 12-well plates or 500 µl for 24-well plates) of Qiazol™ Lysis reagent was added per well after removing the growth media. Lysates were incubated at room temperature for 5 minutes and then transferred to fresh 1.5 mL nuclease-free safe-lock tube containing 150 µl of chloroform ($1/4^{th}$ the volume of Qiazol™ Lysis reagent). The tubes were mixed well and incubated at room temperature for 5 minutes. The tubes were then centrifuged at 13,000 rpm for 15 minutes at 4°C. The upper aqueous phase was carefully transferred into a fresh reaction tube containing 350 µl of isopropanol (half the volume of Qiazol™ Lysis reagent used). The tube was inverted several times then incubated at room temperature for 10 minutes followed by a 10-minute centrifugation step at 12,000 rpm, 4°C. The supernatant was aspirated completely and the pellet was washed once with 1 mL of 70% ethanol. The tube was spun at 8000 g for 5 minutes at 4°C. The solvent was discarded and the pellet was briefly air-dried and re-suspended in 30 µl of pre-heated water, 65°C.

Quantification of nucleic acids

DNA/RNA concentration along with the degree of contamination was determined by using the NanoDrop ND-1000 spectrophotometer (NanoDrop Technologies, Inc., Delaware, USA). 2 µl of DNA or RNA samples were used for each measurement. TE buffer or water was used as the reagent blank depending in which solvent the DNA/RNA was eluted. The concentration was determined based on the absorbance of the sample at 260 nm. The purity was in turn assessed based on the ratios of the absorbances: 260/280 = ~1,8 (“pure” DNA), = ~2,0 (“pure” RNA); 260/230 = ~2,0 – 2,2 (“pure” nucleic acid), < 1,8 or 2,0 (with residual contaminants – phenol, guanidine, glycogen).

cDNA synthesis from mRNA templates

The First Strand cDNA Synthesis Kit (Fermentas GmbH, Sankt Leon-Rot, Germany) was used to generate full length cDNA from mRNA templates. Briefly, 1 µg of purified RNA in a total volume of 10 µl nuclease-free water was used for the cDNA synthesis. After adding 1 µl of oligo(dT)18 primers, the samples were denatured at 70°C for 5 minutes. After the denaturation, 9 µl of reaction mixture (4 µL 5x Reaction buffer, 2 µL 10 mM dNTP mix, 1 µL Ribolock™ Ribonuclease Inhibitor and 2 µL Moloney Murine Leukemia Virus (M-MuLV) Reverse Transcriptase) was added to the tubes. A ‘-RT’ control, without M-MuLV, was also

included to check for possible genomic DNA contamination in the RNA samples and reagents. The samples were then incubated for 60 minutes at 37°C followed by heat inactivation at 70°C for 10 minutes. The samples were then diluted 10 folds with the addition of 180 µl of water. The samples were stored at -20°C.

Primer Sequence:

Oligo(dT)$_{18}$ primer Thermo Fisher Scientific Cat. No. S0132

5'- d(TTTTTTTTTTTTTTTTT) -3'

100 µM (0,5 µg/µL)

Quantitative real-time PCR

The following reaction mixture was set up in 1.5 ml tubes based on the number of samples:

Components	Volume, µL	
	Gene of Interest	Endogenous Control Gene (i.e. TBP)
2X TaqMan® Gene Expression Master Mix	10	10
qPCR Probe (5 mM)/TaqMan® Small RNA Assay (20X)	0.5	0.5
Forward primer, 10 mM	-	1
Reverse primer, 10 mM	-	1
Nuclease-free water	4.5	2.5
	15	15

The reaction mixture of 15 µl was pipeted into each well of a MicroAmp™ Fast Optical 96-well reaction plate along with technical duplicates of the cDNA samples (5 µL) for a final reaction volume of 20 µL. Water was used as a negative no template control (NTC) and '-RT' as a control for genomic DNA contamination. The plate was covered with a MicroAmp™ Optical Adhesive Film and then centrifuged to spin down contents. The plate was run on the StepOnePlus™ Real-Time PCR System (Life Technologies GmbH, Darmstadt, Germany) using the standard running mode with the following thermal cycling conditions:

Steps	Enzyme Activation	PCR	
	HOLD	40 Cycles:	
		Denaturation	Annealing/Extension
Temperature, °C	95	95	60
Time	10 minutes	15 seconds	60 seconds

For data analysis, the amplification plots were visualized and the baseline & threshold values were set to determine the threshold cycles (C_T) for the amplification curves. All quantifications were normalized to the endogenous control (TBP) to account for variability in the initial concentration and quality of the total RNA. Relative-comparative C_T ($\Delta\Delta C_T$) method was used for quantitation.

Polymerase chain reaction (PCR)

Phusion high-fidelity DNA polymerase (Thermo Scientific) was used for PCR reactions. The manufacturer's protocol (shown below) was followed for setting up the reactions.

Components	Volume, µL	
	50 µl reaction	Final conc.
Nuclease-free water	Add to 50 µl	1x
5x Phusion HF Buffer	10 µl	200 µM each
10 mM dNTPs	1 µl	0.5 µM
Primer A	X µl	0.5 µM
Primer B	X µl	-
Template DNA (100 ng)	X µl	-
Phusion DNA polymerase	0.5 µl	0.02 U/µl
	50	

The PCR was performed in a T300 Thermocycler (Biometra) using the following cycling conditions:

	2-step protocol		3-step protocol		Cycles
	Temperature	Time	Temperature	Time	
Initial Denaturation	98°C	30 s	98°C	30 s	1
Denaturation Annealing Extension	98°C - 72°C	5-10 s - 15-30 s/kb	98°C X °C 72°C	5-10 s 10-30 s 15-30 s/kb	25-35
Final extension	72°C 4°C	5-10 min hold 1 µl	72°C 4°C	5-10 min hold	1

The 2-step protocol was utilized for large PCR products (> 1.5kb) and when the primer Tm values are at least 72°C. The annealing temperature was Tm +3°C of the lower Tm primer for primers larger than 20 nucleotides. For cDNA templates, the extension time was increased to 40s/1kb.

Gel electrophoresis & extraction of DNA from agarose gel

DNA Agarose Gel Electrophoresis. Agarose gel electrophoresis (AGE) was used to analyze DNA samples like PCR products and digested plasmids for contamination and fidelity. The agarose gel (1-3 %) was prepared with 1X TBE/TAE. The appropriate amount of agarose was melted in a microwave oven until the solution became clear. After cooling, 0.5 µg/mL ethidium bromide was added. The melted agarose was poured into appropriate casting tray with the well-comb and allowed to solidify. The gel was placed in the electrophoresis chamber and TBE/TAE buffer was poured until there was about 2-3 mm of the buffer over the gel. Appropriate amount of the DNA Sample Loading Buffer was added to the PCR product or digested plasmid (~0.5 µg). Gels were run at 120 V with constant current. The power was allowed to run until the blue dye approaches the end of the gel. The gel was

then visualized & documented with Intas Gel Imager and Intas GDS v3.32 program (Intas Scientific Imager Instruments GmbH, Göttingen, Germany) at λ=312 with varying intensity.

RNA Agarose Gel Electrophoresis. Agarose electrophoresis was also used for assessing quality of total RNA isolated. The gel tray and electrophoresis chamber were washed thoroughly and cleaned with RNaseZap® RNase Decontamination Solution (ThermoFisher Scientific). A 2% agarose gel was used for 0.5 – 1 µg RNA with 10 µL of the RNA Sample Buffer. The mixture was heated at 60°C for 10 minutes then allowed to cool on ice for 2 minutes prior to gel loading. A clear, smear-free 2:1 ratio of band intensity for the 28S (~3 kb) and 18S (~1.5 kb) ribosomal RNA was used as an indication of good RNA quality.

Extraction of DNA from Agarose Gel. DNA fragments (70 bp to 10 kb up to ~10 µg) were excised from agarose gels under a UV lamp (λ=312, low instensity) using a scalpel and purified using the QIAquick Gel Extraction Kit according to the manufacturer's instructions. The column was eluted with 30 µL of TE buffer.

Restriction digestion of DNA

PCR-amplified products or plasmid vectors (minimum of 500 ng) were incubated with 5 units of restriction enzyme/s (New England Biolabs or Fermentas) per µg of the DNA and 1X Reaction buffer for 2 hours. Bovine serum albumin (BSA) was also added depending on the enzyme/s. Final volume of the reaction varied from 20-50 µL using water as diluent. For majority of the enzymes, digestion was done at 37°C on a heat block. Inhibition of the enzymes was done according to the manufacturer's recommendation. The digested products were then analyzed via Agarose Gel Electrophoresis.

Molecular Cloning

Insert generation

Insert DNA was generated by either annealing artificial oligonucleotides (denatured at 95 °C followed by slow cooling on a thermocycler), by restriction digest from existing constructs as described above or by Polymerase Chain Reaction (PCR). The insert DNA after the restriction digestion or PCR reactions were purified using the QIAquick PCR Purification Kit (Qiagen).

Ligation

Restriction digested plasmids (100 ng) were ligated with either double stranded insert DNA generated by PCR, restriction digestion (at a vector to insert molar ratio of 1:4) or with 10 - 100 picomoles of annealed artificial oligonucleotide, using T4 Ligase (New England Biolabs) and corresponding buffers for 2 hours at room temperature.

Transformation

One Shot TOP10 Chemically Competent *E.coli* (Life Technologies) (25 µl) were supplemented with 2.5 µl of ligation reaction, incubated for 30 minutes at 4 °C, heat shocked for 30 sec at 42 °C, supplemented with 250 µl S.O.C. medium (Life Technologies), incubated for 60 minutes at 37 °C at 600 rpm and plated on LB agar plates (Roth) containing either 50 mg/L Ampicillin (Sigma) or 50 mg/ml Kanamycin (Sigma). After overnight incubation at 37°C, single colonies were picked and cultured in LB medium containing appropriate antibiotic for another round of overnight incubation at 37°C at 180 rpm.

Plasmid purification and analysis of clones

Plasmid DNA was isolated using the QIAprep Plasmid Miniprep Kit (Qaigen) and 500 ng of plasmid DNA was digested with respective restriction digestion enzymes and analyzed by AGE to test for positive clones.

Sequencing of plasmid DNA

After confirmation using restriction digestion, the plasmid DNA was sequenced using sample sequencing services provided by LGC Genomics GmBH. For ‘Ready2 Run’ samples, 10 µl of plasmid DNA (minimum concentration 100 ng/ml) and 4 µl of primer (5 µM) were submitted in a 1.5 ml tube with the appropriate bar code sticker.

Cloning of recombinant plasmids

The following are the DNA constructs/ recombinant plasmids that were used in the present study:

pdsAAV-Ucp1p-GFPmut-mir122site-miR-Itih4: Double stranded AAV vector expressing *Itih4* miRNA under the control of *Ucp1* mini-promoter and a miR-122 binding site.

pCMV6-Entry-mmItih4-Myc-DDK-tag: Double stranded expression plasmid expressing a mouse ITIH4 myc-flag protein.

Cloning of pdsAAV-Ucp1p-GFPmut-mir122site-miR-Itih4

Briefly, pdsAAV-Ucp1p-GFPmut-mir122site-miR-Itih4 was cloned by cutting out the 170 bp miR-Itih4 insert from pcDNA™6.2-GW/EmGFP-miR-mmItih4 using SalI/XbaI and cloning it into the pdsAAV-Ucp1p-GFPmut-mir122site-miR-Tbl1 backbone.

Cloning of pCMV6-Entry-mmItih4-Myc-DDK-tag

The mouse ITIH4 C-terminal Myc-DDK tag expression construct was generated by first cloning out the 3kb insert from pCMV6-Kan/Neo-mmItih4-untag (MC206371, OriGene Technologies) using the primers: mItih4_AsiSI_Fwd (TC GCGATCGCATGAAGAGCCCTGCCCC) and mItih4_MluI_Rev (TAACGCGTTATCTCCACTGTCCAGCA) along with the phusion polymerase 2-step protocol; digesting it with AsiSI/MluI and inserting it into the pCMV6-Entry-mmTigit-Myc-DDK-tag (MR213712, OriGene Technologies) backbone.

Cell biology

All cell culture experiments were performed in Class II laminar flow hoods under aseptic conditions. Cells were incubated in a controlled atmosphere (humidified 95% air/5% CO_2) at 37°C. Culture media, antibiotics, fetal calf or bovine serum and buffers like Krebs-Ringer Buffer (KRB) were warmed at 37°C before use. Unless otherwise stated, cell lines were cultivated in high glucose (4.5 mg/L) DMEM medium supplemented with 10% FBS, 100U/mL Penicillin, and 100 U/mL Streptomycin. The medium was changed every 3 or 4 days. Passages were performed at the beginning and end of the week.

Thawing, subculturing, and cryopreservation of Cells

Cryopreserved cells were resuscitated by taking the vial out of the liquid nitrogen and immediately (<60 seconds) thawing in a water bath maintained at 37°C. Two-milliliters of warm complete medium were combined with the cells. The cell suspension was transferred to properly labeled 15-cm culture plate containing appropriate amount of the medium.

Passaging was done by removing the medium with a Pasteur pipet and washing the adhering cellular monolayer once with 1X D-PBS (without Ca^{2+} & Mg^{2+}). The cell monolayer was trypsinized with 2 mL trypsin/EDTA solution. After incubation at 37°C for 5 minutes, the plates were gently tapped to detach the cellular monolayer. The plates were incubated again for 2-3 minutes if the monolayer did not detach. The cells were then suspended thoroughly by adding appropriate amount of the complete culture medium. The suspension was transferred into a 15-mL Falcon tube, centrifuged (2000 rpm, 2-3 minutes), and the pellet resuspended with appropriate amount of complete medium for further passaging.

For cryopreservation, cells were harvested in the log-phase of growth, resuspended in 1 mL of the freezing medium i.e. complete medium:DMSO (9:1) and transferred to 2-mL cryovials. The vial were then placed in the freezing container containing isopropanol and stored at -80°C for up to one week prior to eventual long term storage in a liquid nitrogen tank.

Determination of cell number, viability and seeding of cells

For manual cell counting, 10 µL of uniformly suspended cells were mixed with equal volume of 0.4% tryphan blue. The mixture was allowed to stand for 5-10 minutes and 10 µl was loaded on to the Neubauer hemocytometer. Cell number was counted in the four corner squares using an inverted cell culture microscope. The concentration of the cells was calculated using the following formula:

Concentration (cells/mL) = (Number of cells counted x 10,000 x dilution factor)/(Number of squares).

For automated cell counting and viability determination, Invitrogen™ Countess™ Automated Cell Counter was used. Similar to the hemocytometer, 10 µl of cell suspension was mixed with 10 µl of tryphan blue in a 1.5 ml tube and 10 µl of this cell solution was

pipetted on to one of the chamber of a disposable countess® chamber slide. Next, the focus on the Countess™ is adjusted and the cells were counted.

After counting, the cells were seeded on required culture dishes containing the recommended medium volume: 15-cm dish (25 ml), 10-cm dish (10 ml), 6-well plate (2 ml/well), 12-well plate (1 ml/well), 24-well plate (500 µl/well) or 96-well plate (100 µl/well).

Isolation of mouse preadipocytes from stroma vascular fraction (SVF) of intrascapular brown adipose tissue and inguinal white adipose tissue

On the day before the isolation, 20 mg of Collagenase II was weighed in 2 ml tubes and the amount of constituents needed for the collagenase solutions was calculated. Before the beginning the isolation, the work space was covered with SCIENCEWARE® LABMAT™ Bench Liner (Bel-Art), the surgical instruments placed in 80% ethanol and petri dishes containing 1X D-PBS (without Ca^{2+} & Mg^{2+}) were placed on ice. After sacrificing the mice, the inguinal white adipose tissues (iWAT) and intrascapular brown adipose tissue (BAT) were excised and placed in ice-cold 1X D-PBS. Next, the organs were cleaned: lymph nodes were removed from the inguinal white adipose tissue and residual white adipose tissue was removed from the intrascapular brown adipose tissue. The collagenase solutions were prepared for iWAT and BAT as follows:

Components	10 ml Volume		
	iWAT	BAT	Final conc.
Collagenase (2 mg/ml)	0.75 ml	0.75 ml	1.5 mg/ml
Bovine Serum Albumin (BSA)	0.5 ml	0.5 ml	0.5 %
HEPES (1 M)	-	0.15 ml	15 mM
$CaCl_2$ (1 M)	-	0.032 ml	3.2 mM
Fetal Calf or Bovine Serum (FCS, FBS)	-	1 ml	10 %
DMEM (4.5 g/l glucose)	8.75 ml	7.54 ml	-

The collagenase solutions were sterile filtered using 0.45 µm syringe filters and the minced tissue was added to the sterile solutions in 15 ml falcon tubes. For iWAT, 5ml of collagenase solution for 4 fat pads and 3ml for 2 BAT pads was used for digestion. The collagenase solutions were incubated for 10 minutes at 37°C in a water bath and then transferred to a 37°C incubator at 180 rpm for 1 hour. The tissue samples were checked for the completion of digestion by observing the presence of tissue clumps and the incubation time was decreased or increased accordingly. After the incubation, growth medium (DMEM, 10% FBS, 1% Pen/Strep) was added to the collagenase solutions to a volume of 14 ml and the solutions were allowed to stand for 10 minutes to separate the floating lipid and adipocyte fraction from the heavier SVF fraction at the bottom of the tubes. The lighter upper fraction was removed and the tubes were centrifuged for 10 minutes at room temperature at 1000 rpm. The supernatant was aspirated and the SVF pellets were collected in 1 ml growth media. Growth media was added to the cell suspension to a final volume of 10 ml and passed through a 70 µM cell strainer (BD biosciences). Additional growth media was added to the SVF cell suspension and the suspension was plated in appropriate cell culture plates or dishes.

Differentiation of mouse brown and white preadipocytes from the stroma vascular fraction (SVF)

The preadipocytes were washed twice with 1x D-PBS and fresh media was added for the first three days after isolation. Fresh media was added every second day till the cells reached confluency and differentiation was started (day 0).

Primary pre-adipocyte differentiation media:

475 ml DMEM high glucose (4.5 g/l glucose)

25 ml FBS (5%)

5 ml Pen/Strep (1%)

In addition to:

1:1000 dilution of 1 mg/ml Insulin (1 µg/ml final)

1:1000 dilution of 250 µM Dexamethasone (0.25 µM final)

1:100 dilution of 50 mM 3-isobutyl-1-methylxanthine (IBMX) (0.5 mM final)

1:1000 dilution of Ascorbate Biotin Pantothenate (ABP)

1:30000 dilution of 30 µM Triiodothyronine (T_3) (1 nM final) - only for brown preadipocytes

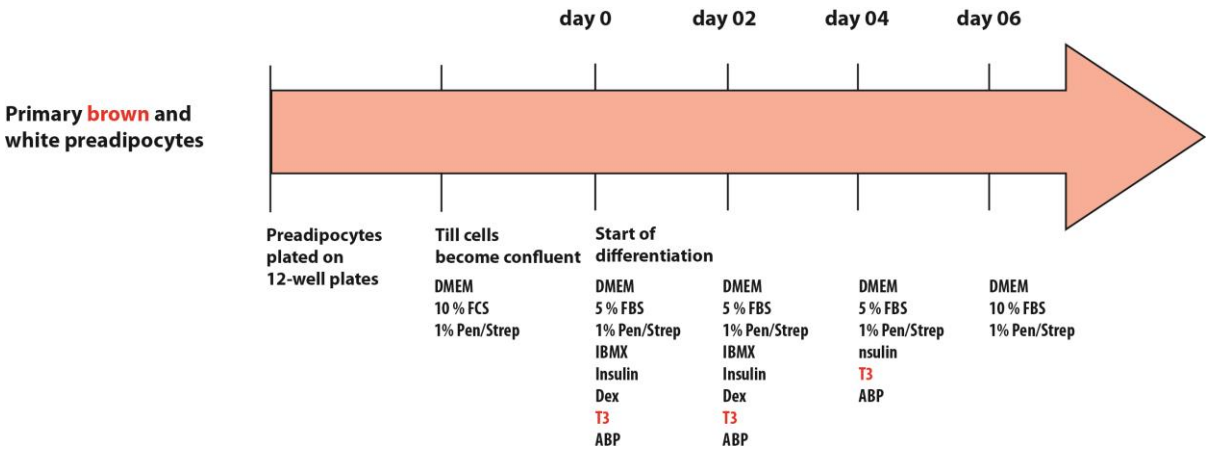

Transient transfection methods

Plasmid constructs and siRNAs were transfected into cells (70-80% confluency) using one of the following methods:

Calcium phosphate

Plasmid DNA (100 – 1000 ng/well) was mixed with 0.25 M $CaCl_2$ (80 µL for 6-well) and the same volume of 2X BBS. After incubation for 15-20 min at RT, the mixture was added to the cells in fresh medium. Medium was changed 6-12 h after transfection.

Cationic polymer or polyethyleneimine (PEI)

Cells were plated at the desired concentration of 70-80 % the day before the experiment on a 6-well plate. The amount of polyethyleneimine (PEI) was calculated according to the amount of DNA to be transfected, i.e. for a 6-well plate 3.5 µl of PEI (7.5 mM) per 1 µg of plasmid DNA was used. The PEI and DNA tubes per well were prepared as follows:

Components	50 µl Volume	
	PEI	DNA
PEI (7.5 mM)	3.5 µl	-
Plasmid DNA (100 ng/ml)	-	10 µl
Nuclease-free water	21.5 µl	15 µl
NaCl (300 mM)	25 µl	25 µl

The PEI and DNA tubes were mixed and incubated at room temperature for 15 minutes and DNA:PEI mixture was added to the cells dropwise. Medium was replaced after 18 hours and cell extracts were prepared 48 hours post-transfection.

Lipofectamine® 2000 transfection reagent

The manufacturer's protocol was followed for transfection of cells using the Lipofectamine® 2000 transfection reagent. Briefly, for 100 ng of DNA per well in a 96-well plate, 1.5 µl of Lipofectamine® 2000 in 25 µl of Opti-MEM® medium was mixed with 500 ng of plasmid DNA in 25 µl of Opti-MEM® medium. The mixture was incubated at room temperature for 5 minutes and 10 µl of it was added dropwise to each well. The growth media was replaced after 18 hours or earlier if cellular toxicity was observed. For a 6-well plate (1 µg of plasmid DNA per well), 9 µl of Lipofectamine® 2000 in 150 µl Opti-MEM® medium was mixed with 1.3 µg of plasmid DNA in 150 µl Opti-MEM® medium and added to the cells after 5 minutes of incubation.

Lipofectamine® RNAiMAX transfection reagent

For transfection of siRNAs, Lipofectamine® RNAiMAX Transfection Reagent was used. Briefly per well for a 12-well plate, 20 nM of siRNA was dissolved in 32 µl of Opti-MEM® medium and mixed with 4 µl of Lipofectamine® RNAiMAX Transfection Reagent in 32 µl of Opti-MEM® medium. The mixture was incubated for 10 minutes at room temperature and then growth media (DMEM, 10% FBS) was added to a volume of 1ml. The media was aspirated from the cells and the siRNA/ Lipofectamine® RNAiMAX solution was added dropwise. The growth media was replaced after 18 hours.

Neon® transfection system

The Neon® transfection system was used with large plasmids and/or for cells that were difficult to transfect like differentiated PreBAT cells. Briefly, an appropriate number of cells ($3x10^5$ differentiated PreBAT cells/well for 12-well plate; $7x10^4$ undifferentiated PreBAT cells/chamber for 8-well chamber slide) were resuspended in appropriate amount of Buffer R (10 µl/well for 10 µl Neon® tips) along with 1 µg of plasmid DNA. The Neon® tube was filled with 3ml of Buffer E2 and the corresponding plate/chamber slide for plating was filled with growth media (DMEM, 10% FBS) and placed in the incubator at 37°C. The cell suspension was then electroporated using the 10 µl tip at specific voltage, time pulse and number of pulses. Care should be taken that there should be not any bubbles in the Neon® tip as this will cause arcing. This can be prevented by carefully aspirating the cell suspension in to the tip. After electroporation, the cells were added to the plate/chamber slide containing the growth media. The growth media was exchanged and the cells were observed after 18 hours. For expression of the transgene, the cells were incubated for at least 48 hours.

Biochemistry

Total protein isolates from cells

Cells were harvested in RIPA buffer which consists of 50 mM Tris-HCl (pH 7.6), 150 mM NaCl, 1% NP-40, 0.25% Na-deoxycholate, 1 mM EDTA (pH 8.0) and 1x protease inhibitor cocktail (PIC) (Sigma), 1x phosphatase inhibitor cocktail (Sigma). The growth media was first aspirated and cells were washed with 1X D-PBS and ice-cold RIPA buffer was added (5-10% volume of growth media). The cells were transferred into 1.5 ml tubes using flat-bottomed pipette tips. The tubes were placed on a rotary wheel at 4°C for 30 minutes and the centrifuged at top speed for 5 minutes. The supernatant was transferred to a fresh ice-cold 1.5 ml tube. The samples were then stored at -80°C, used to measure protein concentration or to run an immunoblot.

Quantification of proteins by BCA assay

Protein concentration was determined using the Pierce® BCA Protein Assay Kit following the manufacturer's instructions. Protein lysates were diluted 1:10 so as not to exceed the linear range of the BSA standard curve (0.1 - 2 mg/ml) and were measured in 10µl duplicates along with BSA standards (10µl) with the addition of 200 µl of assay reagent.

SDS-Polyacrylamide gel electrophoresis and immnuoblotting (western blotting)

For SDS-polyacrylamide gel electrophoresis, 30 µg of protein samples containing SDS loading dye (1x) were denatured at 98°C for 5 minutes. The samples along with PageRuler™ prestained protein ladder were loaded on to a 10% or 12% SDS-polyacrylamide gel and separated at 120 V. The samples where then transferred to a nitrocellulose membrane using a wet blot transfer system at 4°C at 90 V for 60 minutes or 30 V for 18 hours. After the transfer, the immunoblots were stained with Ponceau S to determine the quality and efficiency of transfer. The immunoblots were then blocked in 5% skimmed milk in TBS-T for 1 hour and incubated at 4°C overnight with the primary antibody in 5% skimmed milk TBS-T or 5% BSA as per supplier's instructions. The immunoblots were then washed thrice with TBS-T for 10 minutes each and incubated with secondary antibody conjugated to horse radish peroxidase (HRP) at a dilution of 1:5,000 in 5% BSA or 5% skimmed milk for 1 hour. The immunoblots were washed again and the ECL™ Western Blotting Detection Reagent was applied on them to visualize the chemiluminescence using the ChemiDocTM XRS+ System.

Immunoprecipitation for Flag-tag and Myc-tag proteins

For co-immunoprecipitation of a desired protein, the cells were first harvested by aspirating the media and washing twice with ice-cold 1x D-PBS. Next, the cells were harvested in 300 µl per well (for 6-well plate) of lysis buffer (BLB-CHAPS with 1x protease and phosphatase inhibitors) and transferred to pre-chilled 1.5 ml tubes. The tubes were centrifuged at 13000 rpm for 5 minutes (4°C) and the supernatant was transferred fresh pre-chilled tubes. The protein concentration was measured using the BCA assay. The protein amount was normalized for each sample (250-500 µg) and the volume was adjusted to 400 µl with BLB-CHAPS. At this stage 10µl of the sample was stored separately as 'input'. Next, ANTI-FLAG® M2 affinity gel (25 µl) (A2220, Sigma-Alderich) was added to every sample and incubated in the cold room for 2 hours or overnight on the rotary wheel. After the incubation, the samples were washed thrice with BLB-CHAPS and 50 µl of 2X SDS sample buffer was added. The samples were heated at 98°C for 5 minutes. Similar procedure was followed for Myc-tag co-immunoprecipitation: 1µl of anti-Myc antibody (05-724, Upstate) was added to the 400 µl protein samples. After the incubation at 4°C, 20 µl of Protein A/G PLUS-Agarose (sc-2003, Santa Cruz) was added to each sample and the samples were incubated in the cold room for

additional hour on the rotary wheel. The samples were then analyzed using immunoblotting.

ELISA

MILLIPLEX® MAP mouse metabolic hormone panel

The MILLIPLEX® MAP Mouse Metabolic Hormone panel (Cat. # MMHMAG-44K) was used with the Luminex xMAP® platform (MAGPIX®) to detect leptin and resistin in tissue culture supernatant from primary adipocytes. The immunoassay procedure was carried out according to the manufacturer's instructions. The supernatant samples were centrifuged at 3000 rpm for 5 minutes at 4°C to remove cellular debris and assayed immediately or aliquoted and stored at -80°C. More than 2 freeze/thaw cycles were avoided. Briefly, 200 µl of Assay Buffer was added per well and the plates were shaken for 10 minutes at room temperature. Next, 10 µl of the matrix solution (growth medium- DMEM, 10% FBS, 1% Pen/Strep in this case) was added to the background, standard and control wells followed by the addition of 10 µl Assay Buffer to the background and sample wells. Standards, controls and samples (10 µl) were added to appropriate wells followed by 25 µl of the mixed anti-body immobilized beads. The plate was wrapped in foil and incubated overnight on a plate shaker at 4°C. After the incubation, the plate was allowed to reach room temperature and then washed thrice using a hand-held magnet and Wash Buffer. Detection antibodies (50 µl) were added to each well and the plate was sealed, covered with foil and stirred on a plate shaker for 30 minutes at room temperature. Without aspiration 50 µl of Streptavidin-Phycoerythrin was added to each well. The plate was again sealed, covered with foil and stirred on a plate shaker for 30 minutes at room temperature. The plate was then washed like previously and 100 µl of Drive Fluid was added to all wells. Lastly, the plate was analyzed on the MAGPIX® with the xPONENT software. The Median Fluorescent Intensity (MFI) data was analyzed using a 5-parameter logistic method for calculating the concentrations of leptin and resistin in the samples.

Mouse ITIH4 ELISA

The mouse ITIH4 ELISA for mouse serum was carried out using the ELISA kit from Uscn Life Science Inc. (E97776Mu) following the manufacturer's protocol. The sera samples were diluted 10 and 1000 folds in 1 xD-PBS. Briefly, 100 µl of standards, blank (or control serum) and samples were added to the wells and incubated at 37°C for 2 hours. The wells were decanted and 100 µl of Detection Reagent A was added to each well followed by 1 hour

incubation at 37°C. The wells were decanted again and washed thrice with 350 µl of 1x Wash Solution. After washing 100 µl of Detection Reagent B was added and incubated at 37°C for 30 minutes. The wells were washed 5 times and 90 µl of Substrate Solution was added each well. The wells were incubated with the Substrate Solution for 10 minutes at 37°C (protected from light) and 50 µl of Stop Solution was added to each well. The wells were then measured at 450 nm on a microplate reader (Mithras LB 940). The concentration of ITIH4 was determined using the standard curve.

Rat Insulin ELISA

Insulin in cell culture supernatant from INS-1E cells was measured using the Rat High Range Insulin ELISA from ALPCO™ (80-INSRTH-E01). The ELISA protocol was followed according to the manufacturer's manual. Briefly, 5 µl of the standards, control and samples were added to the respective wells. Next, 75 µl of the Working Strength Conjugate was added to each well and incubated for 2 hours at room temperature while shaking at 700 rpm on a microplate shaker. The wells were decanted and washed 6 times with 350 µl of Wash Buffer. After the final wash, 100 µl of TMB Substrate was added to each well, covered with a plate sealer and incubated at room temperature for 15 minutes (at 700 rpm). Next, 100 µl of Stop Solution was added to each well and gently shaken before measuring the absorbance at 450 nm on a microplate reader (Mithras LB 940). A 5 parameter logistic (pl) fit was used to calculate the insulin concentration from the standard curve.

Cell lines

PreBAT mouse brown preadipocyte cell line

The PreBAT cell line was created and provided by Hoppmann, Perwitz et al. (2010) by immortalizing pre-adipocytes from the intrascapular BAT of newborn mice using the SV40 Large T antigen.

Media compositions:

Growth media:

400 ml DMEM (4.5 g/l glucose)

100 FBS (20 %)

5 ml Pen/Strep (1%)

Differentiation media:

400 ml DMEM (4.5 g/l glucose)

100 FBS (20 %)

10 µl of 1 mM Insulin (20 nM final, 1:50,000 dilution)

16.7 µl of 30 µM Triiodothyronine (T_3) (1 nM final, 1:30,000 dilution)

Induction media (prepared fresh):

Appropriate volume of differentiation media

1:1000 dilution of 0.125 M Indomethacin (0.125 mM final)

1:1000 dilution of 2 mg/ml Dexamethasone (2 µg/ml final)

1:100 dilution of 50 mM 3-isobutyl-1-methylxanthine (IBMX) (0.5 mM final)

Passaging cells:

Cells were passaged when 60-70% confluency was reached and care should be taken that the cells never be allowed to become completely confluent as this will hamper their differentiation capacity. Cells were generally split at the ratio 1:80 in the beginning and end of the week. For a 15 cm dish, the cells were first washed with 1x D-PBS and 3 ml of trypsin-EDTA was added followed by 5 minute incubation at 37°C. The cells were collected in growth media and plated on to fresh plates or dishes. The cells were discarded after passage 25.

For transfections on 12-well-plates, $3x10^4$ cells per well were plated one day before transfection to reach the desired confluency.

Differentiation protocol:

Induction media was added to the cells when they reached complete confluency (day 0). On the following day the media was changed to differentiation media and fresh differentiation media was added every day till day 06.

Freezing and thawing protocol:

The cells were frozen in growth media supplemented with 10% DMSO. Generally, 2ml of cell suspension from a single 15 cm plate was split in to two cryotubes. Upon thawing, the cells were 50-60% confluent in a 15cm dish on the following day.

Note:

Mycoplasma contamination will result in growth retardation, differentiation becoming 'patchy' and a 'pale' appearance under the microscope.

Thorough washing with 1x D-PBS and starvation of cells in serum free DMEM (4.5 g/l glucose) for 4-48 hours is advisable for experiments involving growth factors like insulin (for example, glucose uptake assays).

INS-1E rat insulinoma cells

The INS-1E cells were obtained from AG Lammert (DDZ Düsseldorf).

INS-1E growth media:

50 ml heat inactivated FBS

5 ml glutamine 200mM

5 ml Penicillin/Streptomycin

5.6 ml HEPES 1M

5 ml sodium pyruvate 100mM

1.75 ml 2-Mercaptoethanol 50mM

500 ml RPMI 1640(1x) + GlutaMAX

Passaging cells:

INS-1E cells were passaged at a ratio of 1:4 every 3 days using trypsin-EDTA and INS-1E growth media.

Freezing and thawing cells:

A 10 cm dish was harvested and the cells were resuspended in 4ml freezing media (50% INS-1E growth media, 40% FBS, 10% DMSO). The cell suspension (1ml) was transferred to cryotubes and placed in the freezing container containing isopropanol, stored at -80°C for one week and transferred to long term storage in a liquid nitrogen tank. While thawing, one vial was plated on to a 10 cm dish and fresh growth media was added the next day.

HEK 293A Human Embryonic Kidney cells

The HEK 293A cells from the lab stock were used for transfection experiments and production of adenoviral vectors. The following culturing conditions were used:

HEK 293A growth media:

450 ml DMEM (4.5 g/l glucose)

50 ml FBS (10%)

5 ml Pen/Strep (1%)

Passaging cells:

The cells were split every 3 to 4 days by resuspending the cellular monolayer in 10 ml growth media (15 cm dish) and passaging them at a ratio of 1:10.

For PEI transfections on 6-well plates, $2x10^5$ cells per well were plated one day before transfection to reach the desired confluency of 70-75%. For chamber slides, $1x10^4$ cells per chamber were plated for the same confluency.

Freezing and thawing protocol:

For cryopreservation, cells were harvested in the log-phase of growth, resuspended in 1 ml of the freezing medium (growth media, 10% DMSO) and transferred to 2-ml cryotubes. The tubes were stored at –80°C as described previously. One tube was thawed and plated on to one 15 cm dish.

3T3-L1 mouse embryonic white preadipocyte cell line

The 3T3-L1 cells were used from the lab stock. The following conditions were followed for culturing them:

3T3-L1 growth media:

450 ml DMEM low glucose (1 g/l glucose)

50 ml FBS (10%)

5 ml Pen/Strep (1%)

3T3-L1 differentiation media:

450 ml DMEM high glucose (4.5 g/l glucose)

50 ml FBS (10%)

5 ml Pen/Strep (1%)

In addition to:

1:1000 dilution of 1 mg/ml Insulin (1 µg/ml final)

1:1000 dilution of 250 µM Dexamethasone (0.25 µM final)

1:100 dilution of 50 mM 3-isobutyl-1-methylxanthine (IBMX) (0.5 mM final)

1:1000 dilution of Ascorbate Biotin Pantothenate (ABP)

Note:

ABP stock solution:

50 mg/ml L-Ascorbate (1 g Sodium Ascorbate in 10 ml water)

1 mM D-Biotin (4.89 mg Biotin in 0.5 ml 1M NaOH)

17 mM D-Pantothenic acid hemicalcium salt solution (81 mg D-Pantothenic acid hemicalcium salt in 9.5 ml water)

Passaging cells:

The cells were first washed with 1x D-PBS and trypsinized (2ml) for 5 minutes at 37°C. The cells were then collected in 8ml growth media, centrifuged at 2000 rpm for 3 minutes and plated at a density of $3x10^4$ cells per 15 cm dish or at a ratio of 1:10. Cells were never allowed to become more than 80% confluent.

Differentiation protocol:

For differentiation of 3T3-L1 cells, $2x\ 10^4$ (6-well plate) and $4x\ 10^5$ (15 cm dish) were seeded and differentiation was started after 3 days when the cells were completely confluent (day 0). At day 0 and day 02, the differentiation media mentioned above was added to the cells while at day 04 differentiation media with only Insulin and ABP solution was used. At the end (day 06), normal 3T3-L1 growth media was added.

Freezing and thawing protocol:

The same protocol for HEK 293A cells was used for freezing and thawing 3T3-L1 cells.

In vitro metabolic assays

Adipocyte staining with Oil Red O

Adipocytes were stained with Oil Red O (a lipophilic dye) for the visualization of neutral triglycerides and lipids. This gives a rough visual estimate of the degree of differentiation.

Briefly, differentiated adipocytes were first washed with 1x PBS and then with 10% formalin (in PBS) for 5 min. The cells were then fixed by the addition of 10% formalin (in PBS) and incubated for 1 hour at room temperature. After washing with 60% isopropanol the wells were dried and subsequently stained with Oil Red O working solution for 10 min. The wells were washed 5 times with water to remove any unbound dye and pictures of the stained cells were taken under the microscope. The plates were preserved with water in the wells at 4°C. Alternatively, the dye was eluted out with 100% isopropanol and the O.D. measured at 550 nm (including an empty well stained by the dye to account for unspecific binding of the dye to the plastic).

Measurement of glucose in cell culture supernatant

The Glucose (HK) Assay Kit from Sigma (GAHK-20) was used to measure the glucose amount in cell culture supernatant. Briefly, the standards (0, 2.5, 5, 7.5 and 10 µl of 1 mg/ml Glucose Standard Solution) were pipetted first on to the plate to a final sample volume of 10 µl with water. The samples were pipetted next with a dilution of 1:2 or 1:4 with a final volume of 10 µl. The Glucose Assay Reagent (100 µl) was added and the measurements were taken at 355 nm. The glucose concentrations were calculated from the standard curve.

Lipolysis assay for adipocytes

The differentiated adipocytes were first washed once with Krebs-Ringer Buffer (KRB) (pH 7.4, 37°C) and then incubated in the same buffer for 2 hours at 37°C. The adipocytes were then stimulated for 3 hours with KRB supplemented with 3% BSA (fatty acid free). After the dissolution of the BSA, 25 mM HEPES and 5 mM glucose was added along with (or without) 0.5 µM norepinephrine or 10 µM isoproterenol to stimulate lipolysis in the cells. The cells were stimulated for 3 hours, the supernatant was collected and the non-esterified fatty acids (NEFAs) released by the cells were measured by the NEFA HR (2) Kit (WAKO). Briefly, two different volumes (5 µl and 50 µl) of samples and standard in duplicates were measured on 96-well microplates by first adding 100 µl of R1 buffer and incubating at 37°C for 10 minutes followed by adding 50 µl R2 buffer and followed by a similar incubation. The measurement was carried out at 550 nm and the NEFA amounts were calculated using the following formula:

NEFA (mg/dl) = (Esx28.2)/Estd

Es- Absorbance of the sample (= Raw absorbance of sample – absorbance of reagent blank i.e. water)

Estd- Absorbance of standard (= Raw absorbance of standard – absorbance of reagent blank i.e. water)

Intracellular triglyceride measurement from mature adipocytes

For isolation and measurement of triglyceride amount (TG) from adipocytes, the cells were washed once with 1x D-PBS and 100 µl of Tx buffer (with 1x protease inhibitors) was added to each well (for a 12-well plate) and the plate was frozen at -80°C for at least 24 hours. After thawing the cells, the monolayer was scraped off and transferred to 1.5 ml tubes. The tubes were then sonicated in a Bioruptor (Diagenode) with three cycles of sonication for 30 seconds (30 seconds on and 30 seconds off) at 4°C. The tubes were then centrifuged at 13000 rpm for 15 minutes at 4°C. The middle aqueous phase (6 µl of it), avoiding the lipids floating on top, was transferred to fresh pre-chilled tubes containing 54 µl of water for protein measurement using the BCA assay. The remaining supernatant was used for TG measurement using the Serum Triglyceride Determination Kit from Sigma (TR0100). Briefly, the samples and standard were measured in 15 µl duplicates with 100 µl of Triglyceride Working Reagent ('Assay Solution') and another set of duplicates with 100 µl of Triglyceride Reagent Blank ('Blank Solution'). The samples were incubated at 37°C for 5 minutes and the absorbance was measured at 550 nm. The NEFA amounts were calculated using the following formula and expressed per mg protein.

TG in samples (mg/ml) = (Es x 2.5 mg/ml)/Estd

Es- Absorbance of the sample (= absorbance of sample with Assay Solution - absorbance of sample with Blank Solution)

Estd- Absorbance of standard (= absorbance of standard with Assay Solution - absorbance of standard with Blank Solution)

Measurement of cytotoxicity using the cytotoxicity detection kit (LDH)

The cytotoxic effect of AHA supplemented media on primary adipocytes was measured using the Cytotoxicity Detection Kit (LDH) from Roche (Product No. 11644793001). Briefly, the amount of Reaction mixture was first calculated and prepared in the ratio of 1:45 for Catalyst to Dye solution. Next, 10 µl of the sample, blank (growth media) and positive control (primary white adipocytes treated with 1% Triton x100, diluted 1:10) and 40 µl of water were measured for LDH amount by adding 50 µl of Reaction mixture and incubating at room temperature for 30 minutes in the dark. The absorbance was measured at 490 nm. The LDH release (% cell death) was depicted as % LDH compared to the positive control (100 % cell death).

Glucose metabolism and lipogenesis assay for mature adipocytes

Cells were either grown and differentiated in 10 cm dishes and transferred to 12-well plates or directly differentiated on to 12-well plates. For insulin stimulation, the cells were first washed twice with KRB and then incubated with KRB (pH 7.4) supplemented with 25 mM HEPES, 0.5% BSA, 5 mM glucose and 5 µl/well of D-[14C(U)]-Glucose (0.5 µCi/well) with 10 nM insulin for 2 hours at 37°C. The left-over hot buffer was stored for the 'input' measurement later. The plates were harvested on ice by aspirating the buffer, washing twice with ice-cold KRB and lysing the cells in 200 µl 0.5 M NaOH/well with 5 minutes incubation on ice. Next, 400 µl PBS/well was added and the lysates (whole cell extract, WCE) were transferred to ice-cold 1.5 ml tubes. For measuring glucose metabolism 200 µl of the WCE was used and 300 µl of the WCE was used for lipid extraction (and measurement of lipogenesis). The rest of the WCE was frozen for protein measurement (BCA kit). For lipid extraction, 400 µl of chloroform:methanol (3:1) was added to 300 µl of WCE. The samples were mixed well, incubated for 2 minutes at room temperature and centrifuged for 2 minutes at 13,000 rpm. The lower phase (200 µl) was transferred to a scintillation tube and the lipids were dried overnight under the fume hood. For the scintillation measurements, 4ml of scintillation fluid (Rotiszimt Eco Plus, Roth) was added to the glucose and lipid samples, background sample (no radioactive material) and to 10 µl and 100 µl of input. Extreme caution should be taken not to contaminate the outside of the scintillation tubes. The samples were mixed properly and incubated for 1 day and the disintegrations per minute (DPM) were measured in a scintillation counter with 10 minute measurement per sample and automated background subtraction. The measurements were repeated after 2 days.

Glucose stimulated insulin secretion (GSIS) assay for INS-1E cells

For the INS-1E GSIS assay, the plates were first coated with 0.01% poly-ornithin solution (10 µg/ml) and incubated overnight at 37°C. On the next day the poly-ornithin solution was removed and the plates were washed twice with water and once with INS-1E growth media. The cells were plated on a 24-well plate ($1.5x10^5$ cells/well in 500 µl) and the assay was started after 5 days. For the assay, the cells were first incubated for 2 hours in RPMI 1640 media (without glucose, 1% FBS) and then washed twice with KRB (0.1% BSA) and incubated in the same buffer for 30 minutes. The cells were washed again with the same buffer and

then treated with 5 mM or 20 mM glucose in KRB (0.5% BSA) to stimulate insulin secretion. Insulin amounts were measured in the supernatant using the rat insulin ELISA. The cells were harvested in lysis buffer to measure protein amounts (BCA assay) or intracellular insulin using the same ELISA kit.

SILAC and AHA incorporation of primary adipocytes

Primary adipocytes were treated with SILAC and AHA supplemented medium in order to carry out the secretome analysis. Briefly, the mature primary adipocytes were washed once with 1x D-PBS. Next, to remove methionine, lysine and arginine the cells were incubated with SILAC-Met media for 30 minutes. The SILAC media was prepared with 0.2 µl of AHA (500 mM) and 1 µl labeled amino acids per 1 ml media (arginine 84 mg/ml, lysine 146 mg/ml). The depletion media was aspirated and the cells were incubated for 24 hours with appropriate replicate combinations of heavy and intermediate SILAC medium (as shown in the figure). After the incubation, the media was collected in 15 ml tubes and centrifuged at 1000 rpm for 10 minutes. The supernatant was collected, 1x protease inhibitor was added and the samples were frozen at -80°C. The cells were washed thrice with 1x D-PBS and harvested for DNA isolation. The samples were then analyzed in the Krijgsveld lab (at EMBL, Heidelberg) after normalization using the total DNA amounts.

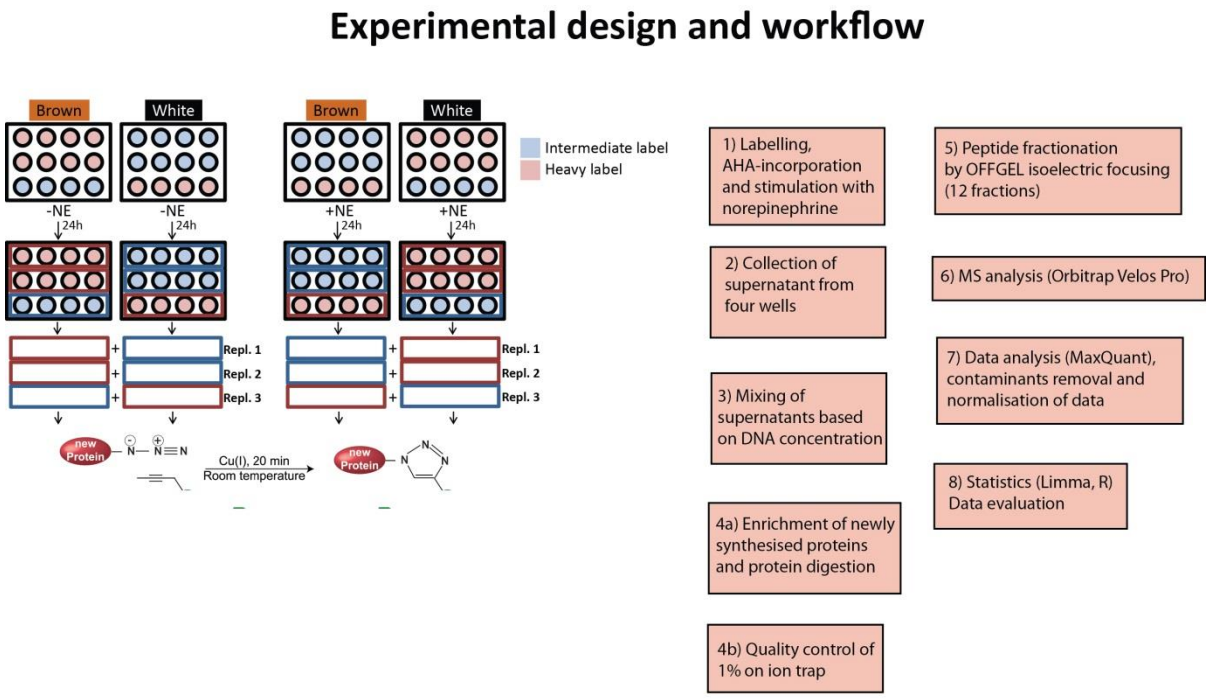

Adenoviral vector production

The adenoviral vectors were produced using the BLOCK-iT™ U6 RNAi Entry Vector Kit and the BLOCK-iT™ Adenoviral RNAi Expression System from Invitrogen. Briefly, the adenoviral vectors were generated as follows:

1. Designing the single-stranded DNA oligos: The Invitrogen's BLOCK-iT™ RNAi Designer tool was used to design the appropriate shRNA against a target gene. The ORF and the 3' UTR regions were selected as target regions and 'pENTR™/U6' was selected as the vector. The top four oligos were selected and the forward and reverse strands were ordered.

2. Generating the Double-Stranded Oligo (ds oligo): The annealing reaction was set up according to the manufacturer's protocol. However, after annealing at 95°C for 4 minutes, the temperature was decreased by 5°C every 1 minute till 20°C. The efficiency of oligomerization was visualized by agarose gel electrophoresis.

3. Ligation of oligos and pENTR™/U6 vector to generate entry clones: The ligation reaction between linearized pENTR™/U6 and diluted ds oligos was performed according to the manual and subsequently used for transforming TOP10 cells.

4. Determination of shRNA knockdown efficiency of the entry clones: Next, the knockdown efficiency of the shRNAs was determined by PEI-mediated transfection of 293A cells by co-transfecting 1 µg each of the pENTR™/U6-ds oligos with over-expression plasmid constructs and observing the protein levels of the target by immunoblotting.

5. LR recombination reaction: Two entry clones with the highest knockdown efficiency were selected for LR recombination reaction in to the pAd/BLOCK-iT™-DEST vector to generate expression clones. The recombination protocol was carried out as described in the manual. The expression clones were sequenced to confirm the recombination.

6. Adenovirus production:

    a. PacI digestion: The expression clones were digested with PacI to expose the left and right viral ITRs according to the manual. The digestion was confirmed by the presence of a 2000 bp fragment with agarose gel electrophoresis.

    b. Adenovirus production in 283A cells: The PacI-digested pAd/BLOCK-iT™-DEST expression plasmids were used to transfect (PEI) 293A cells on 6-well plates according to the protocol described in the manual. The cells were harvested from the 10 cm dishes after the cytopathic effect was observed in 80% of the cells and the cell suspension was used to make the crude viral lysate.

c. Generating the crude viral lysate by freeze-thawing: The harvested cell suspension was frozen at -80°C for 30 minutes and thawed in a 37°C water for 15 minutes. This process was repeated two more times. The cell debris was pellet by centrifugation at 3000 rpm for 15 minutes at room temperature.

d. Amplifying the adenovirus: Ten 15 cm dishes of 293 cells were infected with 100 µl of the crude viral lysate and the same procedure of cell harvest and freeze-thawing was carried out as described above.

e. Cesium Chloride Gradient Purification and dialysis. The gradient purification of the viral lysates was carried out by following the protocol developed in the lab. Briefly, the amplified crude virus lysates were thawed on ice and the viral solution diluted with PBS-TOSH buffer to a final volume of 20 ml. Before the gradient was poured, the pH of all solutions used was adjusted to pH 7.2. Forty-mL centrifuge tubes (Beckmann Polyallomer 25mm x 89 mm) were filled with 9 ml 4M CsCl and carefully covered by a second layer of 2.2M CsCl. Finally, the virus-containing solution was added slowly to generate a third layer. The tubes were weighed and balanced by adding the appropriate solution. The virus was purified by ultracentrifugation (Beckmann ultracentrifuge XL-70) for 2 hours with a swing bucket rotor (SW28 rotor) at 24000 rpm and 4°C. The virus band (between the 4M and 2.2M CsCl layers) was removed by carefully puncturing the tube with 5-mL syringe and diluted with the same volume of a saturated CsCl solution and transferred into a 15-mL centrifuge tube (Beckmann Polyallomer 14mm x 89 mm). The solution was gently over layed with 4M CsCl (1.5-2.5 mL). Subsequently, 2 to 3 mL 2.2M CsCl were added dropwise to form the third distinct layer and the step gradient was centrifuged for 3 hours at 35000 rpm and 4°C in a swing bucket rotor (SW41 Ti rotor). After the second purification step, a bluish-fluorescent virus band between the 4M and 2.2M layers was extracted using 5 ml syringe. The extracted virus band was sealed in a dialysis tube (Roth) and overnight dialysis was carried out in dialysis buffer (1 x PBS, 10% glycerol, pH 7.2) before adding 10% glycerol and storing the virus at -80 °C.

7. Virus titer determination: The Adenoviral titer was determined using the Tissue Culture Infectious Dose 50 (TCID50) method used in the lab. Briefly, HEK293A cells were seeded at a density of 10^4 cells/well on a 96-well plate. Two hours after seeding, 100 µl of virus solution with decreasing concentrations (from 10^{-7} to 10^{-14}) was added, infecting 10 wells per dilution. After 10 days of incubation at 37 °C, plaques were counted using the following formula:

Titer: $T_a = 10^{1+(s-0.5)}$ for 100 µl; $T = T_a x10$ for 1 ml (ifu/ml)

Where s is the sum of positive wells starting from the 10^{-1} dilution divided by 10 i.e., 10 positive wells per dilution is equal to 1.

Materials

Antibodies

Mus Musculus Target Protein	Source
Inter alpha-trypsin inhibitor, heavy chain 4 (ITIH4)	ab118283 Abcam
Valosin containing protein (VCP)	ab11433 Abcam
Glyceraldehyde-3-phosphate dehydrogenase (GAPDH)	sc-166545
Anti-mouse IgG-HRP (goat)	170-6516, Biorad
Anti-rabbit IgG-HRP (goat)	172-1019, Biorad
Anti-goat IgG (H+L)-HRP (rabbit)	R21459

Buffers

Buffer/Solution	Components
TX Lysis Buffer	150 mM NaCl, 0.05% Triton™ X-100, 10 mM Tris/HCl (pH 8.0), 1x Protease Inhibitor Cocktail
Tris/HCl (10 mM, pH 8.0)	1.21 g Trizma® Base, 1 l Millipore H2O (autoclaved)
Depletion/'SILAC-Met' media	500 ml DMEM, high glucose, no glutamine, no methionine, no cysteine, no arginine, no lysine (21013-024), 50 ml dialysed FBS (GIBCO 26400, heat-inactivted), 1 ml Primocin, 10 ml 200 mM L-glutamine, 31.5 mg L-cystine (100 mg/ml in 1M HCL)
SDS Loading Dye (5x)	250 mM Tris/HCl (pH 6.8), 0.5 M DTT (AppliChem), 10% SDS, 1 mg/ml

	Bromophenol Blue, 50% Glycerol
LB-Agar	40 g LB-Agar (Luria/Miller; 10 g/l tryptone, 5 g/l yeast extract, 10 g/l NaCl, 15 g/l agar-agar), 1 l Millipore H2O (autoclaved and supplemented with antibiotic poured on petri dishes)
LB-Medium	25 g LB-Medium (Luria/Miller; 10 g/l tryptone, 5 g/l yeast extract, 10 g/l NaCl), 1 l Millipore H2O (autoclaved)
SDS Running Buffer (1x)	200 mM Glycine, 25mM Trizma® Base, 0.1% SDS
SDS Transfer Buffer (1x)	25 mM Trizma® Base, 192mM Glycine, 20% Methanol, 0.01% SDS
PBS-TOSH (adenovirus production)	30.8 mM NaCl, 120.7 mM KCl, 8.1 mM Na2HPO4, 1.46 mM KH2PO4, 10 mM MgCl2, pH 7.2
Dialysis Buffer (adenovirus production)	1 x PBS, 10% glycerol, pH to 7.2
PEI Stock Solution	161.5 mg PEI in 500 mL dH2O; Stir for 1h; autoclave; freeze-thaw thrice
Blenis Lysis Buffer (BLB) with CHAPS (immunoprecipitation)	10 mM KPO_4 (PH 7.2), 1 mM EDTA, 5 mM EGTA, 10 mM $MgCl_2$, 0.3 % CHAPS
Krebs-Ringer Buffer (KRB) for lipolysis assay	115 mM NaCl, 5.9 mM KCl, 1,2 mM NaH_2PO_4, 1.2 mM $MgCl_2$, 1.2 mM Na_2SO_4, 2.5 mM $CaCl_2$, 25 mM $NaHCO_3$, pH 7.4
Krebs-Ringer Buffer (KRB) for GSIS assay	135 mM NaCl, 3.6 mM KCl, 5 mM $NaHCO_3$, 0.5 mM NaH_2PO_4, 0.5 mM $MgCl_2$, 1.5 mM $CaCl_2$, 10 mM HEPES, pH 7.4
Lysis Buffer for DNA extraction	10 mM Tris pH 8.0, 100mM NaCl, 15 mM EDTA, 0,5% SDS, 0,5 mg/mL Proteinase K

Tris-EDTA buffer (TE buffer)	1 mM EDTA, 10 mM Tris, bring to pH 8.0 with HCl
Tris-Borate-EDTA Buffer (TBE)	10 mM Tris, 0.1 mM EDTA, 9 mM boric acid, pH 8
1X RNA Sample Loading Buffer (for AGE)	0.5 µL Ethidium bromide (1:10) + 0.5 µL 10X MOPS + 5 µL Formamide + 1.75 µL Formaldehyde + 1.7 µL 6x Loading dye + 0.55 µL RNase-free water
RIPA buffer	50 mM Tris-HCl (pH 7.6), 150 mM NaCl, 1% NP-40, 0.25% Na-deoxycholate, 1 mM EDTA (pH 8.0)

Chemicals

Chemical	Supplier	Catalogue number
(+)-sodium L-ascorbate	Sigma	A4034
14C glucose D-[14C(U)]	Perkin Elmer	NEC042X250UC
14C-Mannitol, D-[1-14C]	Perkin Elmer	NEC314050UC
2-Deoxy-D-glucose	Sigma	D8375
3,3',5-Triiodo-L-thyronine sodium salt (T_3)	Sigma	T6397
3,3'-Diaminobenzidine (DAB)	Sigma	32741
30% Acrylamide/Bisacrylamide 37.5:1 (Rotiphorese Gel 30)	Carl Roth	3029.1
3H-Deoxy-D-glucose, 2-[1,2-3H (N)]	Perkin Elmer	NET328001MC
Acetic acid	Sigma	45731
Agarose	Applichem	A8963
Ammonium persulfate (APS)	Roth	9592.3
Ampicillin	Sigma	A9518
Attractene Transfection Reagent	Qiagen	301005
Barium hydroxide solution 0.3 N (Ba(OH)2)	Sigma	B4059
Biotin	Sigma	B4639
Boric acid	Sigma	31146
BSA FA free (for ChIP and lipid assays)	Sigma	A8806
BSA fraction V (for WB)	Biomol	1400
BSA in solution (for cell culture)	Sigma	A9576
Calcium chloride (CaCl2)	Carl Roth	CN93.1
Carbaprostacyclin ($cPGI_2$)	Biozol (Cayman)	69552-46-1
Cesium chloride	Carl Roth	7878.2
Chloroform	VWR	22.711.290
Cytochalasin B	Sigma	C6762
D-(+)-Glucose anhydrous	Applichem	A0883
Dexamethasone (Dex)	Sigma	D-8893
Dexamethasone water soluable (Dex)	Sigma	D2915

Dimethyl sulfoxide (DMSO)	Sigma	D2650
Disuccinimidyl glutarate (DSG crosslinker)	Proteochem	c1104
Dithiothreitol (DTT)	Carl Roth	6908.2
D-Mannitol	Sigma	M4125-100G
DMEM, high glucose, pyruvate	Life Technologies (Gibco)	11965-092
DMEM, low glucose, pyruvate	Life Technologies (Gibco)	31885-023
DMEM, high glucose, pyruvate	Life Technologies (Gibco)	11965-092
DMEM, low glucose, pyruvate	Life Technologies (Gibco)	31885-023
DMEM, no glucose	Life Technologies (Gibco)	11966-025
DMEM, no glucose,/pyruvate/L-glutamine,/phenol red/sodium bicarbonate, powder	Sigma	D5030
DNase / RNase free water	Life Technologies (Gibco)	10977023
dNTPs (10 mM)	Life Technologies	R0191
D-pantothenic acid hemicalcium salt	Sigma	P5710
Dulbecco's phosphate buffered saline (D-PBS)	Life Technologies (Gibco)	14190094
Eosin G	Carl Roth	7089.1
Ethanol 99%	DKFZ	
Ethanol absolute (for analysis)	Sigma	32205
Ethidium bromide (EtBr)	Carl Roth	2218.2
Ethylenediaminetetraacetic acid (EDTA)	Sigma	E5134
(+)-Etomoxir sodium salt hydrate (Etomoxir)	Sigma	E1905
Fetal calf serum (FCS)	Life Technologies (Invitrogen)	10091-148
Formaldehyde solution 37%	J. T. Baker	7040
Forskolin	Sigma	F3917
Gene Ruler 1kb DNA Ladder	Thermo Scientific	SM0314
Glycerol 2-phosphate disodium salt hydrate (G2P)	Sigma	G6251
Glycerol, 99%	Sigma	15523
Glycine	Sigma	33226
HEPES 1M	Life Technologies (Invitrogen)	15630-056
Histofix 4% Formaldehyde Solution for Histology	Carl Roth	P087.5
Hydrochloric acid 37% (12.1 M)	Sigma	30721
IBMX (3-Isobutyl-1-methylxanthin	Sigma	I5879-1G
Indomethacine	Sigma	I7378
Insulin human	Sigma	I2643
Isopropanol	Sigma	190764
Isoproterenol hydrochloride	Merck (Calbiochem)	420355
L-(-)-norepinephrine bitartrate (NE)	Sigma	A9512
Laminin	Santa Cruz	sc-29012
LB agar	Carl Roth	X969.1
LB Medium	Carl Roth	X968.1
L-Carnitine	Sigma	C0158
L-glutamine	Life Technoligies (Invitrogen)	25030-081
Lipofectamine 2000 Transfection Reagent	Life Technologies (Thermo)	11668027
Lipofectamine RNAiMAX Transfection Reagent	Life Technologies (Thermo)	13778075
Lithium Chloride (LiCl)	Carl Roth	3739.1
Magnesium chloride hexahydrate (MgCl2 *6H2O)	Sigma	M927
MEM Non-Essential Amino Acids Solution (NAA)	Life Technologies	11140

Methanol	Sigma	32213
N,N,N',N'-tetramethylethane-1,2-diamine (TEMED)	Carl Roth	2367.3
NP-40 (IGEPAL)	Sigma	56741
Oligo(dT)18 Primer	Thermo Scientific	SO132
One Shot TOP10 Chemically Competent E. coli	Life Technologies (Invitrogen)	C4040
Orange G	Sigma	O3756
PageRuler Prestained Protein Ladder	Thermo Scientific	26616
Penicillin-Streptomycin (10,000 U/mL)	Life Technologies	15140-122
Phenol/Chloroform/Isoamyl alcohol (25:24:1)	Carl Roth	A156.2
Phosphatase Inhibitor Cocktail 2	Sigma	P5726
Polyethylenimin (PEI)	Sigma	764647
Poly-L-lysine	Sigma	P9155
Potassium chloride (KCl)	Carl Roth	6781.1
Potassium dihydrogen phosphate (KH2PO4)	Carl Roth	3904.1
Protease Inhibitor Cocktail	Sigma	P8849
QIAzol lysis reagent	Qiagen	79306
Recombinant Mouse FGF basic (bFGF)	R&D Systems	3139-FB-025
Recombinant Ribonuclease Inhibitor (RNaseOUT)	Life Technologies (Invitrogen)	10777-019
Rosiglitazone	Cayman Chemicals	71740
Restore PLUS Western Blot Stripping Buffer-500 mL	Thermo Scientific	46430
Rotiszint scintillation liquid	Carl Roth	0016.3
S.O.C. medium	Life Technologies (Invitrogen)	15544-034
Skim milk powder extra grade	Gerbu	1602
Sodium acetate (NaAc)	Applichem	A1522
Sodium chloride (NaCl)	Sigma	31434
Sodium deoxycholate (NaDOC)	Sigma	D6750
Sodium dihydrogen phosphate (NaH2PO4)	Applichem	A3559
Sodium dodecyl sulfate (SDS)	Sigma	62862
Sodium fluoride	Sigma	S1504
Sodium hydrogen carbonate (NaHCO3)	AppliChem	A0384
Sodium hydrogen phosphate (Na2HPO4)	Neolab	4066
Sodium hydroxide standard solution 8 mol/l	Sigma	35255
Sodium orthovanadate (Na3VO4)	Sigma	S6508
Sodium palmitate	Sigma	P9767
Sodium pyruvate	Life Technologies	11360070
sodium sulfate (Na2SO4)	Applichem	A3487
Streptavidin MicroBeads	Miltenyi Biotec	130-048-102
Streptozotocin	Axxora	LKT-S7870
Sucrose	Sigma	S1888
Sulforhodamine B sodium salt	Sigma	S9012
TaqMan Gene Expression Master Mix	Life Technologies	4369016
Triolein [9,10-3H(N)]	Hartmann	ART 0199
Tris base	Sigma	T1503
tri-Sodium citrate dihydrate	Sigma	71405
Triton-X100	AppliChem	A1388
Trypsin-EDTA solution	Life Technologies (Invitrogen)	25200072

Tween 20	Sigma	P9416
Tyloxapol	Sigma	T0307
Xylene	Merck	1.08681.2500
Zinc sulfate solution 0.3 N Zn(SO)4	Sigma	Z2876

Instruments

Instrument	Supplier
0.5-10µl single-channel pipette (ErgoOne)	Starlab
100-1000µl single-channel pipette (ErgoOne)	Starlab
20-200µl single-channel pipette (ErgoOne)	Starlab
2-20µl single-channel pipette (ErgoOne)	Starlab
Analytical scales (M-Power)	Sartorius
Automated cell counter (Countess)	Life Technologies (Invitrogen)
Automatic glucose monitor (Accu-Chek Performa)	Roche
Bacterial incubator (Function Line)	Thermo Scientific (Heraeus)
Bacterial shaker	Infors AG
Bacterial shaker / incubator (Multitron Standard)	Infors HT
Benchtop centrifuge (Microfuge Heraeus Pico)	Thermo Scientific (Heraeus)
Benchtop centrifuge, cooling (Microfuge Heraeus Fresco)	Thermo Scientific (Heraeus)
Blot imager (ChemiDoc XRS)	Biorad
Bunsen Burner	Campingaz
Calorimeter (IKA C7000)	IKA
Centrifuge (Biofuge Prime) (cell culture)	Thermo Scientific (Heraeus)
Centrifuge (Labofuge 400R)	Thermo Scientific (Heraeus)
Centrifuge (Mikro 22R) (cell culture)	Hettich
Centrifuge (Multifuge X3R)	Thermo Scientific (Heraeus)
Centrifuge (Super T21)	Thermo Scientific (Heraeus)
CO2 incubator	Sanyo
Electrophoresis chamber	Steinbrenner
Electrophoresis power supply (PowerPac™ Basic)	Biorad
Electrophoresis power supply (PowerPac™ HC)	Biorad
Extracellular flow bioanalyser (Seahorse XF96)	Seahorse Bioscience
FPLC system (ÄKTA purifier)	GE Healthcare Life Sciences
Freeze dryer (Alpha 1-2)	Martin Christ
Freezer -20 °C (comfort / med line)	Liebherr
Freezer -80 °C (Herafreeze)	Thermo Scientific (Heraeus)
Fridge 4 °C (comfort / med line)	Liebherr
Fumehood (Airflow RXC 90.1)	WALDNER Laboreinrichtungen
Gel imager (IX)	Intas
Handheld Reader System for Wireless temperature detection (model DAS-7006/7s)	BioMedic Data Systems
Hotplate stirrer (Model 375)	VWR
Labcoat	Bierbaum Proenen
Liquid nitrogen cryogenic tank	Thermo Electron
Liquid scintillation counter (Tri-Carb® 2100TR or 2900TR)	Perkin Elmer
Manual pipetting system (Liquidator 96)	Mettler Toledo
Micro dismembrator S	Sartorius
Microplate reader (Mithras LB 940)	Berthold
Microplatereader SPECTROstar Omega	BMG Labtech

Microscope (Axio Imager.M2) (histology)	Zeiss
Microscope (Axiovert 40 CFL) (cell culture)	Zeiss
Microwave	Bosch
Mini Trans-Blot® cell (buffer tank, lid, cassettes, electrodes)	Biorad
Mini-PROTEAN Tetra cell (buffer tank, lid, running module)	Biorad
Mini-PROTEAN® Tetra handcast systems (casting module, plates, combs)	Biorad
Multichannel pipette reference 8- and 12-channel variable	Eppendorf
Multistep pipette (Multipette Plus)	Eppendorf
pH meter (GMH350)	GHM electronics, Greisinger
PhenoMaster cages	TSE Systems
Photometer (NanoDrop ND-1000)	Peqlab Biotechnology
Pipette controller (accu-jet® pro)	Brandtech Scientific
Real-Time PCR system (StepOnePlus)	Life Technologies (Applied Biosystems)
Rocking platform (Duomax 1030)	Heidolph
Rotating wheel	Neolab
Rotating wheel (model 2-1184)	Neolab
Scales (EG 2200-2NM)	Kern & Sohn Gmbh
Sonicator (Bioruptor)	Diagenode
Sterile biosafety cabinet (e3 Class II Type A/B)	SterilGARD
Tabletop centrifuge (Mini Spin Plus)	Eppendorf
Thermomixer comfort Heatblock	Eppendorf
Timer (TR 118)	Oregon Scientific
TissueLyser II	Qiagen
Ultracentrifuge (XL 70)	Beckman
Vacuum pump	Neolab

Kits

Kit	Supplier and catalogue number
BCA Protein Assay Kit	Thermo Scientific (Pierce), 23225
BLOCK-iT™ Adenoviral RNAi Expression System	Life Technologies, K4941-00
BLOCK-iT™ U6 RNAi Entry Vector Kit	Life Technologies, K4945-00
Cytotoxicity Detection Kit (LDH)	Roche, 11644793001
ECL Western Blotting Substrate	Thermo Scientific (Pierce) , 321061
First Strand cDNA Synthesis Kit	Fermentas, K1612
Glycerol Standard Solution	Sigma, G7793
HiSpeed Plasmid Maxi Kit 25	QIAGEN, 12663
MILLIPLEX® MAP Mouse Metabolic Hormone panel	Millipore, MMHMAG-44K
Mouse ITIH4 ELISA	Uscn Life Science Inc., E97776Mu
Minute™ Adipose Tissue Fractionation Kit	Invent Biotechnologies, Inc , AF-023
QIAprep Spin Miniprep	QIAGEN, 27106
QIAquick Gel Extraction Kit	QIAGEN, 28704
QIAquick PCR Purification Kit	QIAGEN, 28104
RNeasy Micro kit	QIAGEN, 74004
RNeasy Mini kit	QIAGEN, 74104
Rat High Range Insulin ELISA	ALPCO™, 80-INSRTH-E01
Glucose (HK) Assay Kit	Sigma, GAHK-20
NEFA Standard Solution	Wako, 276-76491

NEFA-HR Reagent 1	Wako, 434-91795
NEFA-HR Reagent 2	Wako, 436-91995
Serum Triglyceride Determination Kit	Sigma, TR0100

Plasmids

Name	Description	Source
pdsAAV-Ucp1p-GFPmut-miR122site-miR-NC	Double stranded AAV vector expressing control miRNA under the control of UCP1 promoter and miR-122 binding site.	Cloned with help from Karin Moessenboeck.
pdsAAV-Ucp1p-GFPmut-mir122site-miR-Tbl1	Double stranded AAV vector expressing Tbl1 miRNA under the control of mini-UCP1 promoter and miR-122 binding site.	Kindly provided by the Herzig lab (generated by Karin Moessenboeck).
pdsAAV-Ucp1p-GFPmut-mir122site-miR-Itih4	Double stranded AAV vector expressing Itih4 miRNA under the control of mini-UCP1 promoter and miR-122 binding site.	Generated by Asrar Ali Khan
pcDNA™6.2-GW/EmGFP-miR-mmItih4	pcDNA™6.2-GW/EmGFP-miR vector (from BLOCK-iT™ Pol II miR RNAi Expression Vector Kits) containing Itih4 miRNA	Generated by Asrar Ali Khan
pCMV6-Kan/Neo-mmItih4-untag	pCMV6-Kan/Neo expressing Mouse inter alpha-trypsin inhibitor, heavy chain 4 (cDNA clone)	MC206371, OriGene Technologies
pCMV6-Entry-mmTigit-Myc-DDK-tag	pCMV6-Entry expressing Tigit (Myc-DDK-tagged) - Mouse T cell immunoreceptor with Ig and ITIM domains (Tigit)	MR213712, OriGene Technologies

Plastic consumables

Product	Supplier	Catalogue number
10µl Graduated tips	Starlab	S1111-3800
1000µl Blue graduated tips	Starlab	S1111-2821
10ml Disposable Polystyrene Serological Pipet	Corning (Falcon)	356551
15ml Tube PP, sterile (cellstar)	Greiner Bio One	188271
200µl Yellow tips	Starlab	S1111-0806
250mL Vacuum Filter/Storage Bottle System, 0.22µm Pore	Sigma (Corning)	430756
25ml Disposable Polystyrene Serological Pipet	Corning (Falcon)	356535
300 µM Nylon mesh (Polyamid Monofil)	Neolab	4-1411
50ml Disposable Polystyrene Serological Pipet	Corning (Falcon)	356550
50 ml Syringe	BD Biosciences (Falcon)	1404297
50ml Tube PP, sterile (cellstar)	Greiner Bio One	227261
5ml Disposable Polystyrene Serological Pipet	Corning (Falcon)	356543
70µM Cell strainer nylon	BD Biosciences (Falcon)	352350
96 Well Black with Clear Flat Bottom	Corning (Falcon)	353219
96-Well Microplates, clear, flat bottom (MicroWell)	Thermo Scientific (Nunc)	95029780
Bench liner (Labmat)	VWR	246750000
Cell counting chamber slides (Countess)	Life Technologies (Invitrogen)	C10228
Cell Culture Dishes 100x20 mm	Corning (Falcon)	353003
Cell Culture Dishes 150x25 mm	Corning (Falcon)	353025
Cell Scrapers	Sigma (Corning)	CLS3010
Combitips advanced, 10 mL	Eppendorf	30089464
Combitips advanced, 5 mL	Eppendorf	30089456
Cover Slips	Carl Roth	H878.2
Cryo Cardboard Box, White	Neolab	Feb 01
Cryogenic vials, 1.8ml	Starlab	E3110-6122
Delicate Task Wipes	Kimberley Clark	7216
Dialysis tubing Cellulose Ester	Spectrum Laboratories	131270
Disposable Scalpels	Feather	EF7281 (2975-10)
Disposal bags (Sekuroka)	Carl Roth	E706.1
FPLC column (Superose 6, 10/300 GL)	GE Healthcare Life Sciences	17-5172-01
Gas cartridge	Campingaz	Z00059581
Gloves, Powder Free Textured Latex Exam	blossom	BM 11226-PF-AV
Glucose test strips (Acco-Chek Inform II)	Roche	473360
Grid insert for cryoboxes, 10x10	Neolab	Feb 03
Histology Mega-Cassette System (Tissue-Tek)	Sakura	4173
Insulin syringes (Micro-fine 1ml U-40, 0.33 mm x 12.7 mm)	Becton Dickinson	320801
large volume centrifuge tubes	Sigma (Corning)	CLS431123

(500ml)		
Liquidator96 LTS tips	Steinbrenner	SL-LT-L20
MicroAmp® Fast Optical 96-Well Reaction Plate	Life Technologies	4346906
MicroAmp® Optical 8-Cap Strips	Life Technologies	4323032
MicroAmp® Optical Adhesive Film	Life Technologies	4311971
Micro-osmotic pump (model 1002)	Alzet	4317
Microscopy Slides	Carl Roth	0656.1
Mouse Genome 430 2.0 Array (GeneChip)	Affymetrix	900496
MS Columns	Miltenyi Biotec	130-042-201
needles (Neolus 27G,40 x 20 mm)	Terumo	NN-2719R
Nitril Gloves, Safeskin Purple	Kimberley Clark	52001M
Nitrocellulose membrane (Protran 0.45 N)	GE healthcare (Amersham)	10600002
Nuclease free SafeSeal Tubes (MµIti)	Carl Roth	7080.1
Octo MACS Separator Starter Kit	Miltenyi Biotec	130-042-108
Paper towels comfort	Wepa	277200
Parafilm M	Sigma	P7793
Pasteur capillary pipetts long	Brand	747720
Petri dishes, 94x16 mm	Greiner Bio One	632 180
Pre-Separation Filters	Miltenyi Biotec	130-041-407
Prot/Elec Tips (gel loading)	Biorad	223-9916
Rodent Diet with 10% kcal% fat (low fat diet, LFD)	Research Diets	D12450J
Rodent Diet with 60% kcal% fat (low fat diet, LFD)	Research Diets	D12492
Round Bottom Polypropylene Tube with snap cap 14ml	BD Biosciences (Falcon)	352059
Safe-Lock Tubes 1.5 mL	Eppendorf	22363204
Safe-Lock Tubes 2.0 mL	Eppendorf	22363352
Safe-Lock Tubes, 1.5 ml	Eppendorf	0030 120.086
Safe-Lock Tubes, 2.0 ml	Eppendorf	0030 120.094
scintillation tubes, 5ml PP tube, PE cap	VWR	720-0495
Scintillation vials mini with screwcap	Carl Roth	5404.1
Soft-Ject Disposable Syringes 1ml	Henke Sass Wolf	5010.200V0
Syringe Filter Unit, 0.45 µm (Millex-HV)	Millipore	SLHV033RS
TipOne graduated filtertips, 10µl	Starlab	S1121-3810
TipOne graduated filtertips, 100µl	Starlab	S1120-1840
TipOne graduated filtertips, 1000µl	Starlab	S1126-7810
TipOne graduated filtertips, 20µl	Starlab	S1120-1810
TipOne graduated filtertips, 200µl	Starlab	S1120-8810
Tissue Culture Plates 24 well	Corning (Falcon)	353047
Tissue Culture Plates 48 well	Corning (Falcon)	353078
Tissue Culture Plates 96 well	Corning (Falcon)	353077
Transponder (implantable thermometer) (model IPTT-300)	BioMedic Data Systems	-
Whatman cellulose blotting paper	Sigma (Whatman)	Z763187
XF96 FluxPak	Seahorse Bioscience	102310-001
XF96 Polystyrene Cell Culture Microplates	Seahorse Bioscience	101085-004

Primers and oligonucleotides

Name	Sequence (5’ to 3’)	Description
Itih4_shrna_381_top	AAAAGCGGATCTATGTCAGGCAAGATTCGTCTTGCCTGA CATAGATCCGC	shRNA oligos for Adenoviral vector production.
Itih4_shrna_381_bottom	CACCGCAGGCAGATGACACCTTATGCGAACATA AGGTGTCATCTGCCTGC	shRNA oligos for Adenoviral vector production.
Itih4_shrna_611_top	AAAAGCAGGCAGATGACACCTTATGTTCGCATAAGGTGT CATCTGCCTGC	shRNA oligos for Adenoviral vector production.
Itih4_shrna_611_bottom	TGCTGTTGACTGACACTTCAAACTTCGTTTTGGCCACTGA CTGACGAAGTTTGGTGTCAGTCAA	shRNA oligos for Adenoviral vector production.
Itih4_shrna_861_top	CCTGTTGACTGACACCAAACTTCGTCAGTCAGTGGCCAAA ACGAAGTTTGAAGTGTCAGTCAAC	shRNA oligos for Adenoviral vector production.
Itih4_shrna_861_bottom	TGCTGAGATGTAGATGTCCATCTGAAGTTTTGGCCACTGA CTGACTTCAGATGCATCTACATCT	shRNA oligos for Adenoviral vector production.
Itih4_shrna_2884_top	CCTGAGATGTAGATGCATCTGAAGTCAGTCAGTGGCCAA AACTTCAGATGGACATCTACATCTC	shRNA oligos for Adenoviral vector production.
Itih4_shrna_2884_bottom	TGCTGAACTCAATGAGGTTGAACTGGGTTTTGGCCACTG ACTGACCCAGTTCACTCATTGAGTT	shRNA oligos for Adenoviral vector production.
Itih4_miRNA_394_top	CCTGAACTCAATGAGTGAACTGGGTCAGTCAGTGGCCAA AACCCAGTTCAACCTCATTGAGTTC	miRNA oligos for Adeno-associated virus production.
Itih4_miRNA_394_bottom	TGCTGATAAGGTGTCATCTGCCTGCGGTTTTGGCCACTGA CTGACCGCAGGCATGACACCTTAT	miRNA oligos for Adeno-associated virus production.
Itih4_miRNA_531_top	CCTGATAAGGTGTCATGCCTGCGGTCAGTCAGTGGCCAA AACCGCAGGCAGATGACACCTTATC	miRNA oligos for Adeno-associated virus production.
Itih4_miRNA_531_bottom	AAAAGCGGATCTATGTCAGGCAAGATTCGTCTTGCCTGA CATAGATCCGC	miRNA oligos for Adeno-associated virus production.

Itih4_miRNA_940_top	CACCGCAGGCAGATGACACCTTATGCGAACATAAGGTGTCATCTGCCTGC	miRNA oligos for Adeno-associated virus production.
Itih4_miRNA_940_bottom	AAAAGCAGGCAGATGACACCTTATGTTCGCATAAGGTGTCATCTGCCTGC	miRNA oligos for Adeno-associated virus production.
Itih4_miRNA_2883_top	TGCTGTTGACTGACACTTCAAACTTCGTTTTGGCCACTGACTGACGAAGTTTGGTGTCAGTCAA	miRNA oligos for Adeno-associated virus production.
Itih4_miRNA_2883_bottom	CCTGTTGACTGACACCAAACTTCGTCAGTCAGTGGCCAAAACGAAGTTTGAAGTGTCAGTCAAC	miRNA oligos for Adeno-associated virus production.
mItih4_NheI_Fwd	TGCTGAGATGTAGATGTCCATCTGAAGTTTTGGCCACTGACTGACTTCAGATGCATCTACATCT	For cloning Itih4 cDNA in to pEGFP-N2.
mItih4_KpnI_Rev	CCTGAGATGTAGATGCATCTGAAGTCAGTCAGTGGCCAAAACTTCAGATGGACATCTACATCTC	For cloning Itih4 cDNA in to pEGFP-N2.
mItih4_AsiSI_Fwd	TGCTGAACTCAATGAGGTTGAACTGGGTTTTGGCCACTGACTGACCCAGTTCACTCATTGAGTT	For cloning the Itih4 cDNA in to pCMV6-Entry-mmTigit-Myc-DDK-tag.
mItih4_MluI_Rev	CCTGAACTCAATGAGTGAACTGGGTCAGTCAGTGGCCAAAACCCAGTTCAACCTCATTGAGTTC	For cloning the Itih4 cDNA in to pCMV6-Entry-mmTigit-Myc-DDK-tag.

Restriction digestion enzymes

Restriction enzyme	Supplier and catalogue number
SalI	New England Biolabs, R0138S
XbaI	New England Biolabs, R0145L
MluI	Fermentas, ER0561
NheI	New England Biolabs, R0131L

KpnI	New England Biolabs, R0142S
AsiSI	New England Biolabs, R0630S

Software and programs

Software	Source/supplier
A plasmid Editor (APE)	http://biologylabs.utah.edu/jorgensen/wayned/ape/
AxioVision	Zeiss
Cytoscape (version: 2.8.3)	http://www.cytoscape.org/
Finch TV	Geospiza
GraphPad Prism 5	GraphPad
Illustrator	Adobe
Image Lab	Biorad
Intas-Capture-Software	Intas
ND-1000	Nanodrop
Office	Microsoft
Photoshop	Adobe
UCSC Genome Browser	http://genome.ucsc.edu

Appendices

Abbreviations

2-DE 2-dimenstional electrophoresis
Abd. Abdominal
AHA Azidohomoalanine
Ahsg Alpha-2-HS-glycoprotein
AICAR 5-Aminoimidazole-4-carboxamide ribonucleotide
AMPK Adenosine Monophosphate-Activated Protein Kinase
ANOVA Analysis of Variance
APR Acute Phase Response
Arg Arginine
Arxes1 Adipocyte-related X-chromosome expressed sequence 1
Atgl Adipose Triglyceride Lipase
ATP Adenosine Triphosphate
AAV Adeno-Associated Virus
BA Brown adipocytes
BAT Brown adipose tissue
BBS Borate Buffered Saline
BCA Bicinchoninic Acid
BMI Body Mass Index
BMP Bone morphogenic protein
bp Base pair
BFA Brefeldin A
BSA Bovine Serum Albumin
cAMP Cyclic Adenosine Monophosphate
CD36 Cluster of Differentiation 36
cDNA Complementary DNA
Cebpb CCAAT/enhancer-binding protein beta
Cidea Cell death activator CIDE-A
CLS Crown-Like Structures
CM Conditioned Media
CoA Coenzyme A
Conc. Concentration
$cPGI_2$ Carbaprostacyclin
CREB cAMP responsive element binding protein
cRNA Complementary RNA
CRP C-Reactive Protein

Ctrl Control
Depp Decidual protein induced by progesterone
Diff Difference
dH_2O Distilled H_2O
dl Deciliter
DMEM Dulbecco's Modified Eagle's Medium
DMSO Dimethylsulfoxide
DNA Deoxyribonucleic Acid
dNTP Deoxyribonucleotide Triphosphate
DPBS Dulbecco's Phosphate-Buffered Saline
ECL Enhanced Chemiluminescence
E.coli Eschericha coli
EDTA Ethylenediaminetetraacetic Acid
ELISA Enzyme-linked Immunosorbent Assay
EMT Epithelial-Mesenchymal Transition
FA Fatty Acid
Fabp4 fatty acid binding protein 4
FBS Fetal Bovine Serum
FDR False Discovery Rate
FFA Free Fatty Acid
FGF21 Fibroblast growth factor 21
Fig Fasting-induced gene
FITC Fluorescein isothiocyanate
GC Gastrocnemius Muscle
GI Gastrointestinal
Glut Glucose Transporter
GO-BP Gene Ontology Biological Processes
GSEA Gene Set Enrichment Analysis®
GSIS Glucose Stimulated Insulin Secretion
HEK293 A Human Embryonic Kidney 293 A cell line
HFD High Fat Diet
HRP Horseradish Peroxidase
hrs Hours
Hsl Hormone Sensitive Lipase
Hz Hertz
IFN Interferon-gamma
IGF-1 Insulin-like Growth Factor-1
IgG Immunoglobulin G
iNAMPT Nicotinamide phosphoribosyltransferase
IL-1 Interleukin-1
IL-6 Interleukin-6

IL-8 Interleukin-8
ITI Inter-α-trypsin inhibitors
ITIH4 Inter-alpha-trypsin inhibitor heavy chain H4
iWA Inguinal white adipocytes
iWAT Inguinal white adipose tissue
kb Kilobase
KEGG Kyoto Encyclopedia of Genes and Genomes
LB Ludmilla Broth
LC-MS/MS Liquid Chromatography Tandem Mass Spectrometry
Lpl Lipoprotein Lipase
LPS Lipopolysaccharide
LTQ Linear Trap Quadrupole
Lys Lysine
MCP-1 Monocyte Chemotactic Protein-1
Met Methionine
mRNA Messenger RNA
mTOR Mammalian Target of Rapamycin
MYC V-Myc Avian Myelocytomatosis viral oncogene homolog
NaAc Sodium Acetate
NC Negative control
NCI National Cancer Institute
NE Norepinephrine
NF-κB Nuclear Factor-kappa B
NIH National Institutes for Health
No. Number
OCR Oxygen Consumption Rate
PBS Phosphate-Buffered Saline
PCR Polymerase Chain Reaction
PEI Polyethyleneimine
PenStrep Penicillin-Streptomycin
pg Picogram
Pgc1a Peroxisome proliferator-activated receptor gamma coactivator 1-alpha
PI3K Phosphatidylinositol 3 Kinase
Prdm16 PR domain containing 16
Prkaca Protein Kinase, CAMP-Dependent, Catalytic, Alpha
PRR Proline-Rich Region
PPARα Peroxisomal Proliferator Activated Receptor alpha
pSILAC pulsed- Stable Isotope Label with Amino Acids in Cell Culture
qPCR Quantitative PCR
Rel. Relative
RNA Ribonucleic Acid

ROS Reactive Oxygen Species
Rpm Revolutions per minute
SDS Sodium Dodecyl Sulfate
siRNA Small Interfering RNA
SILAC Stable Isotope Label with Amino Acids in Cell Culture
SNS Sympathetic Nervous System
STAT3 Signal Transducer and Activator of Transcription 3
SVF Stromal Vascular Fraction
T_3 Triiodinthyronine
Taq Thermus aquaticus
TBE Tris-Borat-EDTA
TBS Tris-Buffered Saline
TBS-T TBS-Tween
TEMED Tetramethylethylendiamin
TG Triglyceride
TGF-β Transforming Growth Factor-beta
TNF-α Tumor Necrosis Factor-alpha
TP53 Tumor Protein 53
TX Triton™ X-100
U Units
UCP Uncoupling Protein
UV Ultraviolet
VCP Valosin Containing Protein
VLDL Very-Low Density Lipoprotein
Vol. Volume
vWA von Willebrand type-A
WAT White adipose tissue
WHO World Health Organization

Supplementary figures

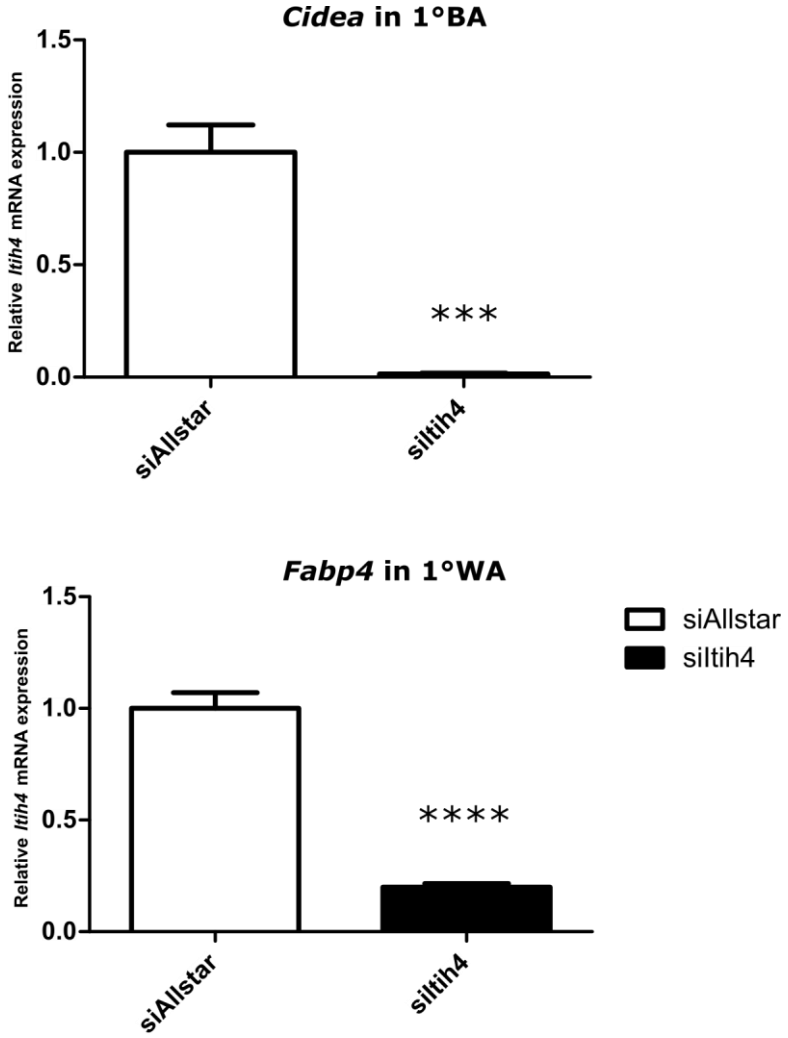

Supplementary figure 1: *Cidea* and *Fabp4* expression in primary adipocytes after ITIH4 knockdown. Brown and inguinal white preadipocytes from the SVF of C57BL/6J 8 weeks old male mice were transfected with siItih4 (20 nM) and negative control (siAllstar) and mRNA expression was measured after 8 days of differentiation. n=3, means ±SEM, * indicates significance to siAllstar (negative control) according to student's t-test.

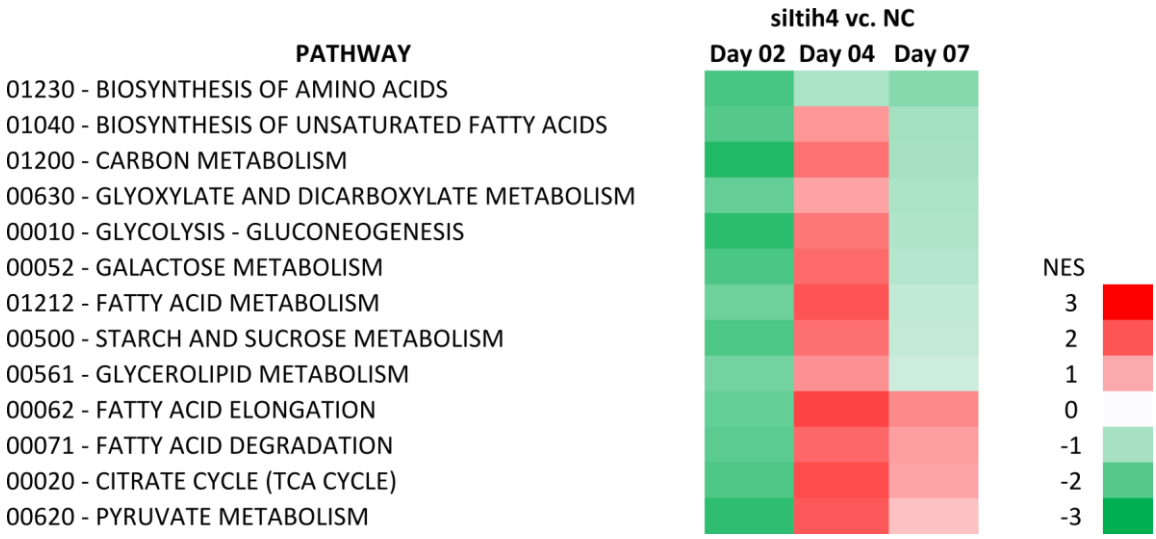

Supplementary figure 2: Metabolic pathways modified with ITIH4 knockdown. PreBAT cells were transfected with siltih4 (20 nM) and siAllstar (depicted here as NC, 20 nM) 2 days before induction of differentiation. Cells were harvested at day 02, 04 and 07 of differentiation and microarray analysis was carried out on GeneChip® Mouse Transcriptome Assay 1.0 chips. The list of genes obtained from the transcriptome analysis was first annotated using entrez-IDs. GSEA was performed on this dataset using the KEGG pathway database by Dr. Carsten Sticht from the Center of Medical Research, University of Heidelberg.

A)

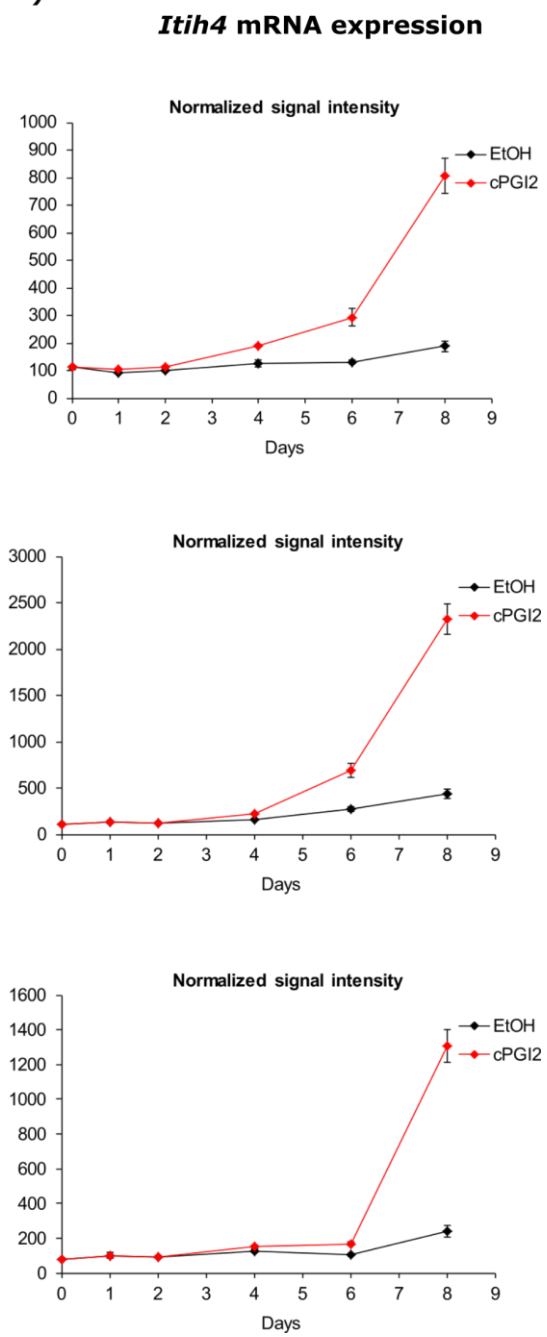
Itih4 mRNA expression
Normalized signal intensity
1000
900
800
700
600
500
400
300
200
100
0
0 1 2 3 4 5 6 7 8 9
Days
EtOH
cPGI2
Normalized signal intensity
3000
2500
2000
1500
1000
500
0
0 1 2 3 4 5 6 7 8 9
Days
EtOH
cPGI2
Normalized signal intensity
1600
1400
1200
1000
800
600
400
200
0
0 1 2 3 4 5 6 7 8 9
Days
EtOH
cPGI2

B)

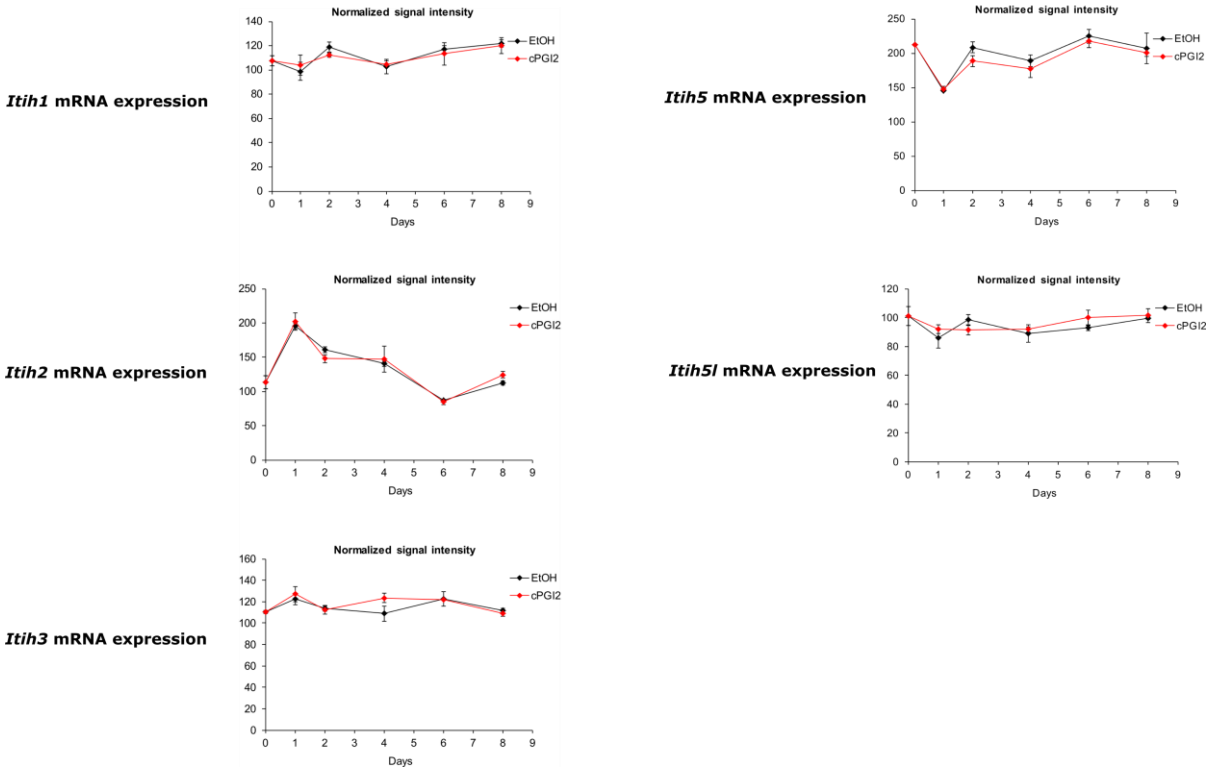

Supplementary figure 3: mRNA expression of inter-α-trypsin inhibitor (IαI) family members during the differentiation of inguinal white adipocyte progenitors. $Lin^{-}CD29^{+}CD34^{+}Sca\text{-}1^{+}$ cells from posterior subcutaneous fat from 7-week old female NMRI mice were cultured and differentiated in adipogenic media ± $cPGI_2$ for 8 days. Expression levels of the inter-α-trypsin inhibitor (IαI) family members: *Itih1*, *Itih2*, *Itih3*, *Itih4*, *Itih5* and *Itih5l* were retrieved from the transcriptome data. Experiment carried out by Bayindir, Babaeikelishomi et al. (2015).

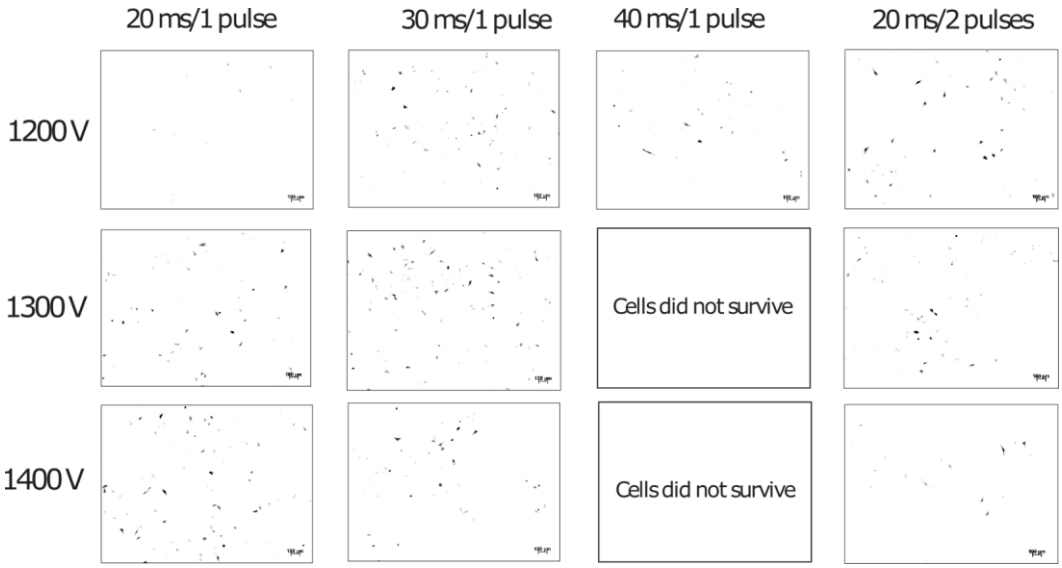

Supplementary figure 4: Optimization of electroporation conditions for PreBAT cells. PreBAT cells were electroporated with pEGFP-N1 (100 ng) using the Neon® transfection system. Different pulse voltages (V), pulse duration (ms) and number of pulses were tested for maximum number of EGFP-positive cells. Images were taken 2 days after electroporation and were converted to grayscale and inverted in Adobe Photoshop.

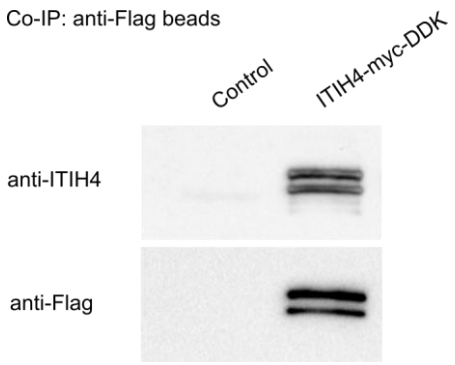

Supplementary figure 5: Immunoblotting of ITIH4-my-DDK protein after co-immunoprecipitation. HEK 293A cells were transfected with 0.5 µg/well of pCMV6-Entry-mmItih4-Myc-DDK-tag vector (untransfected cells were controls) in a 6-well plate. Cells were harvested in RIPA buffer 48 hours after transfection and protein samples were co-immunoprecipitated using ANTI-FLAG® M2 affinity gel beads and immunoblotted using either anti-ITIH4 or anti-Flag antibodies.

Figures

Tables

References

Alberti, K. G., P. Zimmet and J. Shaw (2006). "Metabolic syndrome--a new world-wide definition. A Consensus Statement from the International Diabetes Federation." Diabet Med **23**(5): 469-480.

Alvarez-Llamas, G., E. Szalowska, M. P. de Vries, D. Weening, K. Landman, A. Hoek, B. H. Wolffenbuttel, H. Roelofsen and R. J. Vonk (2007). "Characterization of the human visceral adipose tissue secretome." Mol Cell Proteomics **6**(4): 589-600.

Anveden, A., K. Sjoholm, P. Jacobson, V. Palsdottir, A. J. Walley, P. Froguel, N. Al-Daghri, P. G. McTernan, N. Mejhert, P. Arner, L. Sjostrom, L. M. Carlsson and P. A. Svensson (2012). "ITIH-5 expression in human adipose tissue is increased in obesity." Obesity (Silver Spring) **20**(4): 708-714.

Bartelt, A., O. T. Bruns, R. Reimer, H. Hohenberg, H. Ittrich, K. Peldschus, M. G. Kaul, U. I. Tromsdorf, H. Weller, C. Waurisch, A. Eychmuller, P. L. Gordts, F. Rinninger, K. Bruegelmann, B. Freund, P. Nielsen, M. Merkel and J. Heeren (2011). "Brown adipose tissue activity controls triglyceride clearance." Nat Med **17**(2): 200-205.

Bayindir, I., R. Babaeikelishomi, S. Kocanova, I. S. Sousa, S. Lerch, O. Hardt, S. Wild, A. Bosio, K. Bystricky, S. Herzig and A. Vegiopoulos (2015). "Transcriptional Pathways in cPGI2-Induced Adipocyte Progenitor Activation for Browning." Front Endocrinol (Lausanne) **6**: 129.

Betz, M. J. and S. Enerback (2015). "Human Brown Adipose Tissue: What We Have Learned So Far." Diabetes **64**(7): 2352-2360.

Bhanumathy, C. D., Y. Tang, S. P. Monga, V. Katuri, J. A. Cox, B. Mishra and L. Mishra (2002). "Itih-4, a serine protease inhibitor regulated in interleukin-6-dependent liver formation: role in liver development and regeneration." Dev Dyn **223**(1): 59-69.

Bluher, M. (2013). "Adipose tissue dysfunction contributes to obesity related metabolic diseases." Best Pract Res Clin Endocrinol Metab **27**(2): 163-177.

Bost, F., M. Diarra-Mehrpour and J. P. Martin (1998). "Inter-alpha-trypsin inhibitor proteoglycan family--a group of proteins binding and stabilizing the extracellular matrix." Eur J Biochem **252**(3): 339-346.

Bruun, J. M., A. S. Lihn, C. Verdich, S. B. Pedersen, S. Toubro, A. Astrup and B. Richelsen (2003). "Regulation of adiponectin by adipose tissue-derived cytokines: in vivo and in vitro investigations in humans." Am J Physiol Endocrinol Metab **285**(3): E527-533.

Bukowiecki, L. J. (1989). "Energy balance and diabetes. The effects of cold exposure, exercise training, and diet composition on glucose tolerance and glucose metabolism in rat peripheral tissues." Can J Physiol Pharmacol **67**(4): 382-393.

Campfield, L. A. (2000). "Central mechanisms responsible for the actions of OB protein (leptin) on food intake, metabolism and body energy storage." Front Horm Res **26**: 12-20.

Chandler, K. B., Z. Brnakova, M. Sanda, S. Wang, S. H. Stalnaker, R. Bridger, P. Zhao, L. Wells, N. J. Edwards and R. Goldman (2014). "Site-specific glycan microheterogeneity of inter-alpha-trypsin inhibitor heavy chain H4." J Proteome Res **13**(7): 3314-3329.

Chiellini, C., O. Cochet, L. Negroni, M. Samson, M. Poggi, G. Ailhaud, M. C. Alessi, C. Dani and E. Z. Amri (2008). "Characterization of human mesenchymal stem cell secretome at early steps of adipocyte and osteoblast differentiation." BMC Mol Biol **9**: 26.

Christiaens, V., M. Van Hul, H. R. Lijnen and I. Scroyen (2012). "CD36 promotes adipocyte differentiation and adipogenesis." Biochim Biophys Acta **1820**(7): 949-956.

Cinti, S. (2002). "Adipocyte differentiation and transdifferentiation: plasticity of the adipose organ." J Endocrinol Invest **25**(10): 823-835.

Cornier, M. A., D. Dabelea, T. L. Hernandez, R. C. Lindstrom, A. J. Steig, N. R. Stob, R. E. Van Pelt, H. Wang and R. H. Eckel (2008). "The metabolic syndrome." Endocr Rev **29**(7): 777-822.

Cypess, A. M., S. Lehman, G. Williams, I. Tal, D. Rodman, A. B. Goldfine, F. C. Kuo, E. L. Palmer, Y. Tseng, A. Doria, G. M. Kolodny and C. R. Kahn (2009). "Identification and Importance of Brown Adipose Tissue in Adult Humans." New England Journal of Medicine **360**(15): 1509-1517.
Daniels, S. R., D. K. Arnett, R. H. Eckel, S. S. Gidding, L. L. Hayman, S. Kumanyika, T. N. Robinson, B. J. Scott, S. St Jeor and C. L. Williams (2005). "Overweight in children and adolescents: pathophysiology, consequences, prevention, and treatment." Circulation **111**(15): 1999-2012.
Davalieva, K., S. Kiprijanovska, S. Komina, G. Petrusevska, N. C. Zografska and M. Polenakovic (2015). "Proteomics analysis of urine reveals acute phase response proteins as candidate diagnostic biomarkers for prostate cancer." Proteome Sci **13**(1): 2.
Dietze-Schroeder, D., H. Sell, M. Uhlig, M. Koenen and J. Eckel (2005). "Autocrine action of adiponectin on human fat cells prevents the release of insulin resistance-inducing factors." Diabetes **54**(7): 2003-2011.
Eichelbaum, K., M. Winter, M. Berriel Diaz, S. Herzig and J. Krijgsveld (2012). "Selective enrichment of newly synthesized proteins for quantitative secretome analysis." Nat Biotechnol **30**(10): 984-990.
Enerback, S., A. Jacobsson, E. M. Simpson, C. Guerra, H. Yamashita, M. E. Harper and L. P. Kozak (1997). "Mice lacking mitochondrial uncoupling protein are cold-sensitive but not obese." Nature **387**(6628): 90-94.
Farmer, S. R. (2006). "Transcriptional control of adipocyte formation." Cell Metab **4**(4): 263-273.
Farooqi, S. and S. O'Rahilly (2006). "Genetics of obesity in humans." Endocr Rev **27**(7): 710-718.
Fietta, P. (2005). "Focus on leptin, a pleiotropic hormone." Minerva Med **96**(2): 65-75.
Forner, F., C. Kumar, C. A. Luber, T. Fromme, M. Klingenspor and M. Mann (2009). "Proteome differences between brown and white fat mitochondria reveal specialized metabolic functions." Cell Metab **10**(4): 324-335.
Freedman, D. S., Z. Mei, S. R. Srinivasan, G. S. Berenson and W. H. Dietz (2007). "Cardiovascular risk factors and excess adiposity among overweight children and adolescents: the Bogalusa Heart Study." J Pediatr **150**(1): 12-17 e12.
Fruhbeck, G. (2002). "Peripheral actions of leptin and its involvement in disease." Nutr Rev **60**(10 Pt 2): S47-55; discussion S68-84, 85-47.
Fruhbeck, G. (2006). "Intracellular signalling pathways activated by leptin." Biochem J **393**(Pt 1): 7-20.
Gabriely, I., X. H. Ma, X. M. Yang, L. Rossetti and N. Barzilai (2002). "Leptin resistance during aging is independent of fat mass." Diabetes **51**(4): 1016-1021.
Gangadharan, B., R. Antrobus, R. A. Dwek and N. Zitzmann (2007). "Novel serum biomarker candidates for liver fibrosis in hepatitis C patients." Clin Chem **53**(10): 1792-1799.
Gasparetti, A. L., C. T. de Souza, M. Pereira-da-Silva, R. L. Oliveira, M. J. Saad, E. M. Carneiro and L. A. Velloso (2003). "Cold exposure induces tissue-specific modulation of the insulin-signalling pathway in Rattus norvegicus." J Physiol **552**(Pt 1): 149-162.
Gavrilova, O., B. Marcus-Samuels, D. Graham, J. K. Kim, G. I. Shulman, A. L. Castle, C. Vinson, M. Eckhaus and M. L. Reitman (2000). "Surgical implantation of adipose tissue reverses diabetes in lipoatrophic mice." Journal of Clinical Investigation **105**(3): 271-278.
Goossens, G. H. (2008). "The role of adipose tissue dysfunction in the pathogenesis of obesity-related insulin resistance." Physiol Behav **94**(2): 206-218.
Guerra, C., R. A. Koza, H. Yamashita, K. Walsh and L. P. Kozak (1998). "Emergence of brown adipocytes in white fat in mice is under genetic control. Effects on body weight and adiposity." J Clin Invest **102**(2): 412-420.
Guh, D. P., W. Zhang, N. Bansback, Z. Amarsi, C. L. Birmingham and A. H. Anis (2009). "The incidence of co-morbidities related to obesity and overweight: a systematic review and meta-analysis." BMC Public Health **9**: 88.
Hoda, M. R., S. J. Keely, L. S. Bertelsen, W. G. Junger, D. Dharmasena and K. E. Barrett (2007). "Leptin acts as a mitogenic and antiapoptotic factor for colonic cancer cells." Br J Surg **94**(3): 346-354.

Hondares, E., R. Iglesias, A. Giralt, F. J. Gonzalez, M. Giralt, T. Mampel and F. Villarroya (2011). "Thermogenic activation induces FGF21 expression and release in brown adipose tissue." J Biol Chem **286**(15): 12983-12990.
Hoppmann, J., N. Perwitz, B. Meier, M. Fasshauer, D. Hadaschik, H. Lehnert and J. Klein (2010). "The balance between gluco- and mineralo-corticoid action critically determines inflammatory adipocyte responses." J Endocrinol **204**(2): 153-164.
Hotamisligil, G. S., N. S. Shargill and B. M. Spiegelman (1993). "Adipose expression of tumor necrosis factor-alpha: direct role in obesity-linked insulin resistance." Science **259**(5091): 87-91.
Hu, V. W., D. S. Heikka, P. B. Dieffenbach and L. Ha (2001). "Metabolic radiolabeling: experimental tool or Trojan horse? (35)S-Methionine induces DNA fragmentation and p53-dependent ROS production." FASEB J **15**(9): 1562-1568.
Kadowaki, T. and T. Yamauchi (2005). "Adiponectin and adiponectin receptors." Endocr Rev **26**(3): 439-451.
Kato, A., O. Okamoto, K. Ishikawa, H. Sumiyoshi, N. Matsuo, H. Yoshioka, M. Nomizu, T. Shimada and S. Fujiwara (2011). "Dermatopontin interacts with fibronectin, promotes fibronectin fibril formation, and enhances cell adhesion." J Biol Chem **286**(17): 14861-14869.
Keller, P., C. Keller, A. L. Carey, S. Jauffred, C. P. Fischer, A. Steensberg and B. K. Pedersen (2003). "Interleukin-6 production by contracting human skeletal muscle: autocrine regulation by IL-6." Biochem Biophys Res Commun **310**(2): 550-554.
Kern, P. A., S. Ranganathan, C. Li, L. Wood and G. Ranganathan (2001). "Adipose tissue tumor necrosis factor and interleukin-6 expression in human obesity and insulin resistance." Am J Physiol Endocrinol Metab **280**(5): E745-751.
Kiefer, F. W., M. Zeyda, K. Gollinger, B. Pfau, A. Neuhofer, T. Weichhart, M. D. Saemann, R. Geyeregger, M. Schlederer, L. Kenner and T. M. Stulnig (2010). "Neutralization of osteopontin inhibits obesity-induced inflammation and insulin resistance." Diabetes **59**(4): 935-946.
Klover, P. J., T. A. Zimmers, L. G. Koniaris and R. A. Mooney (2003). "Chronic exposure to interleukin-6 causes hepatic insulin resistance in mice." Diabetes **52**(11): 2784-2789.
Kuroda, Y., H. Kuriyama, S. Kihara, K. Kishida, N. Maeda, T. Hibuse, H. Nishizawa, M. Matsuda, T. Funahashi and I. Shimomura (2010). "Insulin-mediated regulation of decidual protein induced by progesterone (DEPP) in adipose tissue and liver." Horm Metab Res **42**(3): 173-177.
Lazar, M. A. (2007). "Resistin- and Obesity-associated metabolic diseases." Horm Metab Res **39**(10): 710-716.
Lee, P., C. D. Werner, E. Kebebew and F. S. Celi (2014). "Functional thermogenic beige adipogenesis is inducible in human neck fat." Int J Obes (Lond) **38**(2): 170-176.
Li, C., E. S. Ford, G. Zhao and A. H. Mokdad (2009). "Prevalence of pre-diabetes and its association with clustering of cardiometabolic risk factors and hyperinsulinemia among U.S. adolescents: National Health and Nutrition Examination Survey 2005-2006." Diabetes Care **32**(2): 342-347.
Lin, J., C. Handschin and B. M. Spiegelman (2005). "Metabolic control through the PGC-1 family of transcription coactivators." Cell Metab **1**(6): 361-370.
Lo, K. A. and L. Sun (2013). "Turning WAT into BAT: a review on regulators controlling the browning of white adipocytes." Biosci Rep **33**(5).
Loncar, D. (1991). "Convertible adipose tissue in mice." Cell Tissue Res **266**(1): 149-161.
Lowell, B. B., S. S. V, A. Hamann, J. A. Lawitts, J. Himms-Hagen, B. B. Boyer, L. P. Kozak and J. S. Flier (1993). "Development of obesity in transgenic mice after genetic ablation of brown adipose tissue." Nature **366**(6457): 740-742.
Ma, X. H., R. Muzumdar, X. M. Yang, I. Gabriely, R. Berger and N. Barzilai (2002). "Aging is associated with resistance to effects of leptin on fat distribution and insulin action." J Gerontol A Biol Sci Med Sci **57**(6): B225-231.
Mariman, E. C. and P. Wang (2010). "Adipocyte extracellular matrix composition, dynamics and role in obesity." Cell Mol Life Sci **67**(8): 1277-1292.

Mark, A. L., M. L. Correia, K. Rahmouni and W. G. Haynes (2002). "Selective leptin resistance: a new concept in leptin physiology with cardiovascular implications." J Hypertens **20**(7): 1245-1250.
Maurer, S., T. Fromme and M. Klingenspor (2012). "The function of Cox7a1 for brown fat thermogenesis (S14 terminal oxidases)." Biochimica Et Biophysica Acta-Bioenergetics **1817**: S110-S110.
Medrikova, D., T. P. Sijmonsma, K. Sowodniok, D. M. Richards, M. Delacher, C. Sticht, N. Gretz, T. Schafmeier, M. Feuerer and S. Herzig (2015). "Brown adipose tissue harbors a distinct sub-population of regulatory T cells." PLoS One **10**(2): e0118534.
Messerli, F. H., H. O. Ventura, E. Reisin, G. R. Dreslinski, F. G. Dunn, A. A. MacPhee and E. D. Frohlich (1982). "Borderline hypertension and obesity: two prehypertensive states with elevated cardiac output." Circulation **66**(1): 55-60.
Mohamed, E., P. S. Abdul-Rahman, S. R. Doustjalali, Y. Chen, B. K. Lim, S. Z. Omar, A. Z. Bustam, V. A. Singh, N. A. Mohd-Taib, C. H. Yip and O. H. Hashim (2008). "Lectin-based electrophoretic analysis of the expression of the 35 kDa inter-alpha-trypsin inhibitor heavy chain H4 fragment in sera of patients with five different malignancies." Electrophoresis **29**(12): 2645-2650.
Murano, I., G. Barbatelli, V. Parisani, C. Latini, G. Muzzonigro, M. Castellucci and S. Cinti (2008). "Dead adipocytes, detected as crown-like structures, are prevalent in visceral fat depots of genetically obese mice." J Lipid Res **49**(7): 1562-1568.
Muse, E. D., S. Obici, S. Bhanot, B. P. Monia, R. A. McKay, M. W. Rajala, P. E. Scherer and L. Rossetti (2004). "Role of resistin in diet-induced hepatic insulin resistance." J Clin Invest **114**(2): 232-239.
Nayak, A. R., R. S. Kashyap, D. Kabra, H. J. Purohit, G. M. Taori and H. F. Daginawala (2012). "Time course of inflammatory cytokines in acute ischemic stroke patients and their relation to inter-alfa trypsin inhibitor heavy chain 4 and outcome." Ann Indian Acad Neurol **15**(3): 181-185.
Nedergaard, J., T. Bengtsson and B. Cannon (2007). "Unexpected evidence for active brown adipose tissue in adult humans." Am J Physiol Endocrinol Metab **293**(2): E444-452.
Nishimura, H., I. Kakizaki, T. Muta, N. Sasaki, P. X. Pu, T. Yamashita and S. Nagasawa (1995). "cDNA and deduced amino acid sequence of human PK-120, a plasma kallikrein-sensitive glycoprotein." FEBS Lett **357**(2): 207-211.
Nishimura, S., M. Nagasaki, S. Okudaira, J. Aoki, T. Ohmori, R. Ohkawa, K. Nakamura, K. Igarashi, H. Yamashita, K. Eto, K. Uno, N. Hayashi, T. Kadowaki, I. Komuro, Y. Yatomi and R. Nagai (2014). "ENPP2 contributes to adipose tissue expansion and insulin resistance in diet-induced obesity." Diabetes **63**(12): 4154-4164.
Nomiyama, T., D. Perez-Tilve, D. Ogawa, F. Gizard, Y. Zhao, E. B. Heywood, K. L. Jones, R. Kawamori, L. A. Cassis, M. H. Tschop and D. Bruemmer (2007). "Osteopontin mediates obesity-induced adipose tissue macrophage infiltration and insulin resistance in mice." J Clin Invest **117**(10): 2877-2888.
Okamoto, Y., S. Kihara, N. Ouchi, M. Nishida, Y. Arita, M. Kumada, K. Ohashi, N. Sakai, I. Shimomura, H. Kobayashi, N. Terasaka, T. Inaba, T. Funahashi and Y. Matsuzawa (2002). "Adiponectin reduces atherosclerosis in apolipoprotein E-deficient mice." Circulation **106**(22): 2767-2770.
Orava, J., P. Nuutila, M. E. Lidell, V. Oikonen, T. Noponen, T. Viljanen, M. Scheinin, M. Taittonen, T. Niemi, S. Enerback and K. A. Virtanen (2011). "Different Metabolic Responses of Human Brown Adipose Tissue to Activation by Cold and Insulin." Cell Metabolism **14**(2): 272-279.
Pardo, M., A. Roca-Rivada, L. M. Seoane and F. F. Casanueva (2012). "Obesidomics: contribution of adipose tissue secretome analysis to obesity research." Endocrine **41**(3): 374-383.
Patane, G., N. Caporarello, P. Marchetti, C. Parrino, D. Sudano, L. Marselli, R. Vigneri and L. Frittitta (2013). "Adiponectin increases glucose-induced insulin secretion through the activation of lipid oxidation." Acta Diabetol **50**(6): 851-857.
Patel, L., A. C. Buckels, I. J. Kinghorn, P. R. Murdock, J. D. Holbrook, C. Plumpton, C. H. Macphee and S. A. Smith (2003). "Resistin is expressed in human macrophages and directly regulated by PPAR gamma activators." Biochem Biophys Res Commun **300**(2): 472-476.
Peng, Y., S. Yu, H. Li, H. Xiang, J. Peng and S. Jiang (2014). "MicroRNAs: emerging roles in adipogenesis and obesity." Cell Signal **26**(9): 1888-1896.

Pineiro, M., M. A. Alava, N. Gonzalez-Ramon, J. Osada, P. Lasierra, L. Larrad, A. Pineiro and F. Lampreave (1999). "ITIH4 serum concentration increases during acute-phase processes in human patients and is up-regulated by interleukin-6 in hepatocarcinoma HepG2 cells." Biochem Biophys Res Commun **263**(1): 224-229.

Pineiro, M., M. Andres, M. Iturralde, S. Carmona, J. Hirvonen, S. Pyorala, P. M. Heegaard, K. Tjornehoj, F. Lampreave, A. Pineiro and M. A. Alava (2004). "ITIH4 (inter-alpha-trypsin inhibitor heavy chain 4) is a new acute-phase protein isolated from cattle during experimental infection." Infect Immun **72**(7): 3777-3782.

Pollak, M. N., E. S. Schernhammer and S. E. Hankinson (2004). "Insulin-like growth factors and neoplasia." Nat Rev Cancer **4**(7): 505-518.

Prokesch, A., J. G. Bogner-Strauss, H. Hackl, D. Rieder, C. Neuhold, E. Walenta, A. Krogsdam, M. Scheideler, C. Papak, W. C. Wong, C. Vinson, F. Eisenhaber and Z. Trajanoski (2011). "Arxes: retrotransposed genes required for adipogenesis." Nucleic Acids Res **39**(8): 3224-3239.

Pu, X. P., A. Iwamoto, H. Nishimura and S. Nagasawa (1994). "Purification and characterization of a novel substrate for plasma kallikrein (PK-120) in human plasma." Biochim Biophys Acta **1208**(2): 338-343.

Puigserver, P., Z. Wu, C. W. Park, R. Graves, M. Wright and B. M. Spiegelman (1998). "A cold-inducible coactivator of nuclear receptors linked to adaptive thermogenesis." Cell **92**(6): 829-839.

Roca-Rivada, A., J. Alonso, O. Al-Massadi, C. Castelao, J. R. Peinado, L. M. Seoane, F. F. Casanueva and M. Pardo (2011). "Secretome analysis of rat adipose tissues shows location-specific roles for each depot type." J Proteomics **74**(7): 1068-1079.

Rosen, E. D. and B. M. Spiegelman (2006). "Adipocytes as regulators of energy balance and glucose homeostasis." Nature **444**(7121): 847-853.

Saely, C. H., K. Geiger and H. Drexel (2012). "Brown versus white adipose tissue: a mini-review." Gerontology **58**(1): 15-23.

Samad, F., K. Yamamoto, M. Pandey and D. J. Loskutoff (1997). "Elevated expression of transforming growth factor-beta in adipose tissue from obese mice." Mol Med **3**(1): 37-48.

Sarruf, D. A., J. P. Thaler, G. J. Morton, J. German, J. D. Fischer, K. Ogimoto and M. W. Schwartz (2010). "Fibroblast growth factor 21 action in the brain increases energy expenditure and insulin sensitivity in obese rats." Diabetes **59**(7): 1817-1824.

Sartipy, P. and D. J. Loskutoff (2003). "Monocyte chemoattractant protein 1 in obesity and insulin resistance." Proc Natl Acad Sci U S A **100**(12): 7265-7270.

Seale, P., B. Bjork, W. Yang, S. Kajimura, S. Chin, S. Kuang, A. Scime, S. Devarakonda, H. M. Conroe, H. Erdjument-Bromage, P. Tempst, M. A. Rudnicki, D. R. Beier and B. M. Spiegelman (2008). "PRDM16 controls a brown fat/skeletal muscle switch." Nature **454**(7207): 961-967.

Seale, P., S. Kajimura, W. Yang, S. Chin, L. M. Rohas, M. Uldry, G. Tavernier, D. Langin and B. M. Spiegelman (2007). "Transcriptional control of brown fat determination by PRDM16." Cell Metab **6**(1): 38-54.

Sethi, J. K. and A. J. Vidal-Puig (2007). "Thematic review series: adipocyte biology. Adipose tissue function and plasticity orchestrate nutritional adaptation." J Lipid Res **48**(6): 1253-1262.

Silva, J. E. and P. R. Larsen (1983). "Adrenergic activation of triiodothyronine production in brown adipose tissue." Nature **305**(5936): 712-713.

Silva, J. E. and P. R. Larsen (1985). "Potential of brown adipose tissue type II thyroxine 5'-deiodinase as a local and systemic source of triiodothyronine in rats." J Clin Invest **76**(6): 2296-2305.

Song, J., M. Patel, C. N. Rosenzweig, Y. Chan-Li, L. J. Sokoll, E. T. Fung, N. H. Choi-Miura, M. Goggins, D. W. Chan and Z. Zhang (2006). "Quantification of fragments of human serum inter-alpha-trypsin inhibitor heavy chain 4 by a surface-enhanced laser desorption/ionization-based immunoassay." Clin Chem **52**(6): 1045-1053.

Sowers, M. R. and C. A. Karvonen-Gutierrez (2010). "The evolving role of obesity in knee osteoarthritis." Curr Opin Rheumatol **22**(5): 533-537.

Stanford, K. I., R. J. Middelbeek, K. L. Townsend, D. An, E. B. Nygaard, K. M. Hitchcox, K. R. Markan, K. Nakano, M. F. Hirshman, Y. H. Tseng and L. J. Goodyear (2013). "Brown adipose tissue regulates glucose homeostasis and insulin sensitivity." J Clin Invest **123**(1): 215-223.
Steppan, C. M., S. T. Bailey, S. Bhat, E. J. Brown, R. R. Banerjee, C. M. Wright, H. R. Patel, R. S. Ahima and M. A. Lazar (2001). "The hormone resistin links obesity to diabetes." Nature **409**(6818): 307-312.
Steppan, C. M., J. Wang, E. L. Whiteman, M. J. Birnbaum and M. A. Lazar (2005). "Activation of SOCS-3 by resistin." Mol Cell Biol **25**(4): 1569-1575.
Stock, M. J. and N. J. Rothwell (1983). "Role of brown adipose tissue thermogenesis in overfeeding: a review." J R Soc Med **76**(1): 71-73.
Takemura, Y., N. Ouchi, R. Shibata, T. Aprahamian, M. T. Kirber, R. S. Summer, S. Kihara and K. Walsh (2007). "Adiponectin modulates inflammatory reactions via calreticulin receptor-dependent clearance of early apoptotic bodies." J Clin Invest **117**(2): 375-386.
Tan, K. C., A. Xu, W. S. Chow, M. C. Lam, V. H. Ai, S. C. Tam and K. S. Lam (2004). "Hypoadiponectinemia is associated with impaired endothelium-dependent vasodilation." J Clin Endocrinol Metab **89**(2): 765-769.
Tanaka, H., M. Shimazawa, M. Takata, H. Kaneko, K. Tsuruma, T. Ikeda, H. Warita, M. Aoki, M. Yamada, H. Takahashi, I. Hozumi, H. Minatsu, T. Inuzuka and H. Hara (2013). "ITIH4 and Gpx3 are potential biomarkers for amyotrophic lateral sclerosis." J Neurol **260**(7): 1782-1797.
Tschritter, O., A. Fritsche, C. Thamer, M. Haap, F. Shirkavand, S. Rahe, H. Staiger, E. Maerker, H. Haring and M. Stumvoll (2003). "Plasma adiponectin concentrations predict insulin sensitivity of both glucose and lipid metabolism." Diabetes **52**(2): 239-243.
Villarroya, F. and A. Vidal-Puig (2013). "Beyond the sympathetic tone: the new brown fat activators." Cell Metab **17**(5): 638-643.
Villarroya, J., R. Cereijo and F. Villarroya (2013). "An endocrine role for brown adipose tissue?" Am J Physiol Endocrinol Metab **305**(5): E567-572.
Wang, G. X., X. Y. Zhao and J. D. Lin (2015). "The brown fat secretome: metabolic functions beyond thermogenesis." Trends Endocrinol Metab **26**(5): 231-237.
Wang, G. X., X. Y. Zhao, Z. X. Meng, M. Kern, A. Dietrich, Z. Chen, Z. Cozacov, D. Zhou, A. L. Okunade, X. Su, S. Li, M. Bluher and J. D. Lin (2014). "The brown fat-enriched secreted factor Nrg4 preserves metabolic homeostasis through attenuation of hepatic lipogenesis." Nat Med **20**(12): 1436-1443.
Wong, C. and T. H. Marwick (2007). "Obesity cardiomyopathy: pathogenesis and pathophysiology." Nat Clin Pract Cardiovasc Med **4**(8): 436-443.
Wu, J., P. Bostrom, L. M. Sparks, L. Ye, J. H. Choi, A. H. Giang, M. Khandekar, K. A. Virtanen, P. Nuutila, G. Schaart, K. X. Huang, H. Tu, W. D. V. Lichtenbelt, J. Hoeks, S. Enerback, P. Schrauwen and B. M. Spiegelman (2012). "Beige Adipocytes Are a Distinct Type of Thermogenic Fat Cell in Mouse and Human." Cell **150**(2): 366-376.
Wu, J., P. Cohen and B. M. Spiegelman (2013). "Adaptive thermogenesis in adipocytes: is beige the new brown?" Genes Dev **27**(3): 234-250.
Xu, H., G. T. Barnes, Q. Yang, G. Tan, D. Yang, C. J. Chou, J. Sole, A. Nichols, J. S. Ross, L. A. Tartaglia and H. Chen (2003). "Chronic inflammation in fat plays a crucial role in the development of obesity-related insulin resistance." J Clin Invest **112**(12): 1821-1830.
Yadav, H., C. Quijano, A. K. Kamaraju, O. Gavrilova, R. Malek, W. Chen, P. Zerfas, D. Zhigang, E. C. Wright, C. Stuelten, P. Sun, S. Lonning, M. Skarulis, A. E. Sumner, T. Finkel and S. G. Rane (2011). "Protection from obesity and diabetes by blockade of TGF-beta/Smad3 signaling." Cell Metab **14**(1): 67-79.
Yadav, H. and S. G. Rane (2012). "TGF-beta/Smad3 Signaling Regulates Brown Adipocyte Induction in White Adipose Tissue." Front Endocrinol (Lausanne) **3**: 35.
Yamauchi, T., J. Kamon, H. Waki, Y. Terauchi, N. Kubota, K. Hara, Y. Mori, T. Ide, K. Murakami, N. Tsuboyama-Kasaoka, O. Ezaki, Y. Akanuma, O. Gavrilova, C. Vinson, M. L. Reitman, H. Kagechika, K. Shudo, M. Yoda, Y. Nakano, K. Tobe, R. Nagai, S. Kimura, M. Tomita, P. Froguel and T. Kadowaki

(2001). "The fat-derived hormone adiponectin reverses insulin resistance associated with both lipoatrophy and obesity." Nature Medicine **7**(8): 941-946.